國立臺灣大學理學院地質科學系暨研究所

碩士論文

Department of Geosciences

College of Science

National Taiwan University

Master's Thesis

# 蘭陽溪流域河水的化學組成與其可能之地質控制

# River chemistry of Lanyang River and its possible geological controls

高秉辰

Wallace Kao

指導教授：徐澔德 博士、王興麟 博士

Advisor: J. Bruce H. Shyu Ph.D., Shing-Lin Wang Ph.D.

中華民國 114 年 2 月

February 2025

doi:10.6342/NTU202500428

# 國立臺灣大學碩士學位論文
# 口試委員會審定書
## MASTER'S THESIS ACCEPTANCE CERTIFICATE
## NATIONAL TAIWAN UNIVERSITY

蘭陽溪流域河水的化學組成與其可能之地質控制

River chemistry of Lanyang River and its possible geological controls

本論文係高秉辰 R10224213 在國立臺灣大學地質科學系完成之碩士學位論文，於民國 114 年 1 月 20 日承下列考試委員審查通過及口試及格，特此證明。

The undersigned, appointed by the Department of Geosciences, National Taiwan University on 20th January 2025 have examined a Master's Thesis entitled above presented by Wallace Kao R10224213 candidate and hereby certify that it is worthy of acceptance.

口試委員 Oral examination committee:

（指導教授 Advisor）

系（所、學位學程）主管 Director: _____

# 致謝

非常感謝徐澔德老師從我的大學時期至就讀碩士的期間給予指導與研究思考的訓練，並且接受我跟著老師學習。在碩士論文的寫作期間，老師細心與嚴謹地與我討論、指導並幫助我在寫作上的邏輯做出相當大的進步。學術以外，老師亦在生活、職涯方面的小細節處，給予我許多建議與關照。非常感謝王興麟老師在碩士論文的研究上與我經歷大大小小學習的路程。謝謝興麟老師一步一步帶我從地質化學的門外漢到能夠完成今日這本論文。興麟老師在無數的場合與討論中給予我重要的鼓勵，成為我努力與邁進的重要動力。

謝謝各位口委老師，王珮玲老師、朱美妃老師以及林玉詩老師給我把論文改善的建議，並且引導我去思考我在研究與寫作論文的路上尚未解決的問題。另外感謝珮玲老師與美妃老師在我學習化學分析的過程充分的教學與指導，幫助我學習地質化學的基礎。同時感謝地質系與海研所的各位老師，從大學至研究生期間在科學研究的各個專業領域的授業，使我受益良多。

我也要謝謝研究的路上幫助過我克服大大小小困難與挑戰的學長姐、學弟妹與研究助理。首先謝謝陳承鴻學長，在大四的時候引導我成為實驗室的一員。謝謝陳柏宇學長在儀器操作上的指導與解決儀器相關的疑難雜症。謝謝宜蘭高中的林清正老師以及老師所帶領的科展同學團隊幫助我採集與水樣本。謝謝玉秀扮演研究室運作重要的成員，也不時關心我和研究室同仁的狀況。謝謝胡力夫陪我出我所有的野外並在研究工作中給予我很多幫助。謝謝林子游與諸多同期進入地質研究所共患難的好同學們。很感謝研究室裡的同仁，劉司捷學長、廖治豪學長、謝品寬學長、蔡加洛學長、李岳洋學長、許柏沅學長、何艾玲學姊、周海寧學姊、黃巧慈學姊、何安、王紹瑜、戴于芯、陳俊錤在每次大小咪、至生活大小事都給予我很多建議與快樂。就讀地質系所的期間還需要感謝很多人，都是因為認識大家，成就此時的我。

在學校外面，我要謝謝我爸媽，讓我豐衣足食，支持我完成我的學業。謝謝我的弟弟、阿姨、姑姑們、表哥表姊們以及眾多家人，讓我的生活精彩、充實。謝謝我的另一伴張瑀宸，作為我完成論文最後階段最重要的支柱。



doi:10.6342/NTU202500428

# 中文摘要

河流系統是沉積物由造山帶輸送至海洋的主要管道，因此河水的化學組成對於自然界的物質循環具有重要的意義。近年有研究指出臺灣地區受到高侵蝕與風化速率影響，河流中具有相當高的硫酸根濃度，可能與變質岩岩層中硫化鐵礦物的溶解有關。然而河流流經不同之岩層是否的確會出現不同的化學組成，過去並沒有系統性的研究。因此本研究嘗試採集流經不同岩層的河水樣本，藉由分析河水中的陰陽離子組成，探討河水的化學組成與其可能的地質控制。

本研究以蘭陽溪的上游數個主要支流作為研究區域，河水採樣點根據支流所流經的地層差異挑選。其中西北側源自雪山山脈的支流主要流經四稜砂岩、乾溝層與西村層，岩性以砂岩、硬頁岩、變質砂岩為主。東南側中央山脈發源的支流流過以硬頁岩、板岩、千枚岩為主的廬山層，其中武荖坑溪更流經變質程度較高的大南澳片岩。另一方面，雨水及溫泉水的注入亦影響河水的離子變化，因此我們亦採集分析雨水與溫泉水，以推算來自岩層之離子貢獻。

本研究共採集 11 條支流的河水樣本，並收集蘭陽平原雨水與芃芃溫泉、天狗溪噴泉的溫泉水進行分析。於 2022 年至 2023 年間進行六次採樣，水樣經過處理後利用離子層析儀（IC）與感應耦合電漿質譜儀（ICP-MS）分別獲得陰離子與陽離子濃度數據。根據前人建立的端成分模型，蘭陽溪流域河水的陽離子成分均來自矽酸鹽岩與碳酸鹽岩的化學風化及混合，證明此處沒有蒸發鹽礦的影響。硫酸根濃度較高的樣本幾乎都臨近或流經溫泉露頭，暗示硫酸根受到溫泉的影響可能較大。唯在保養溪，除潛在未發現的溫泉影響外，現地的觀察顯示其高濃度之硫酸根亦可能來自四稜砂岩中硫化鐵礦物的風化。武荖坑溪之陽離子組成與其他溪流相差甚遠，可能與其流經之大南澳片岩中的大理岩有關。基於得到的結果，在蘭陽溪流域，只有當河床底岩差異夠明顯且流域不受溫泉影響時，受到底岩岩性影響之河水離子組成差異才會比較明顯。

關鍵詞：蘭陽溪、化學風化、河水化學、硫酸根、硫化礦物。



doi:10.6342/NTU202500428

# Abstract

River systems play a crucial role in various natural cycles, thus the chemical compositions of river water are important to understanding the circulations of matter in nature. Some previous studies reported high sulfate concentrations in rivers in southern Taiwan, and suggest the weathering of sulfide minerals as the cause. Despite this, no systematic research has been conducted to examine any links between rivers and the rock formations they run through. This study analyzes samples from rivers of basins with varying lithology, and aims to discuss the possible geological controls of the chemical compositions with major ions analysis.

The study area focuses on upstream tributaries along the Lanyang River in northeastern Taiwan. The basins of these tributaries spread across the Hsuehshan Range and the Central Range. These ranges differ in lithology, with the Central Range consisting of higher-grade and older metamorphic rocks.

We sampled 11 rivers and 2 hot springs from 2022 to 2023. In addition, rainwater samples were collected to represent atmospheric input for calibration. We obtained anion and cation concentrations using Ion Chromatography (IC) and Induced Coupled Plasma Mass Spectrometer (ICP-MS) respectively. Based on the cation end-member model, riverine cations originate from a mixture of silicate and carbonate weathering, while evaporite weathering is absent in this region. Anion results show a potential correlation between high sulfate concentrations and hot springs. At Baoyang River, however, apart



doi:10.6342/NTU202500428

from the possible influence of an unknown hot spring, field observations suggest that its high sulfate concentrations may be contributed by the weathering of sulfides in the Szeleng Sandstone. The cation characteristics of WRK stand out from the other rivers, which is likely due to marbles in the Tananao Schist in its drainage basin. Based on the results, in the Lanyang River region, the influence of bedrock lithology on the chemical composition of river waters is only more obvious when the bedrock is distinctive enough, and there is no hot spring influence in the drainage basin.

Keywords: Lanyang River, chemical weathering, river chemistry, sulfate, sulfide.



doi:10.6342/NTU202500428

# Table of Contents





doi:10.6342/NTU202500428

doi:10.6342/NTU202500428

**doi:10.6342/NTU202500428**

# List of Figures





doi:10.6342/NTU202500428

doi:10.6342/NTU202500428

# List of Tables





doi:10.6342/NTU202500428

# Chapter 1 Introduction

## 1.1 Motives

### 1.1.1 Chemical weathering of rocks and minerals

Chemical weathering of rocks and minerals affects the balances of elements such as hydrogen, oxygen, carbon in the hydrosphere, lithosphere. Chemical weathering is discussed in terms of the mineralogy of the weathered materials and the weathering acid. For the mineralogy of the materials, much effort has been put into studying the weathering of carbonates and silicates as they are the main constituents of most rocks in the crust (Li, 2000; Lerman et al., 2007).

Chemical weathering of carbonates and silicates influences even the balance of gases in the atmosphere. The atmospheric steady state model is one of the early models that proposed the weathering of carbonate and silicate acts as a buffer to maintain the constant partial pressure of carbon dioxide ($CO_2$) (Siever, 1968). In the steady state model, a combination of weathering, sedimentation, reconstitution, and diagenesis form a system as a whole to create the atmospheric equilibrium. This model emphasizes the fixing and freeing of hydrogen ion ($H^+$) to maintain the $CO_2$ equilibrium. Weathering of carbonates and silicates absorbs $H^+$, which is mainly supplied by carbonic acid ($H_2CO_3$) created through the reaction between water and $CO_2$, and limitedly by HCl from volcanic emissions. Silicate weathering by acids involves a two-step reaction, which ultimately transforms feldspar into kaolinite. Silicate weathering would result in the absorption of



doi:10.6342/NTU202500428

$H^+$, and release of $SiO_2$ and alkali metals. Carbonate weathering adsorbs $H^+$ and releases bicarbonate ($HCO_3^-$) and alkaline earth metals such as magnesium (Mg) and calcium (Ca). $HCO_3^-$ is transported to the ocean with alkaline earth metals, where the sedimentation of limestone and reconstitution of silicates in the ocean return $CO_2$ into the atmosphere. The steady state model was built as a conserve system where $CO_2$ in the atmosphere is kept at a constant partial pressure. In this model, weathering of carbonates and silicates on land plays the crucial role of removing $CO_2$ from the atmosphere.

In their study on silicate weathering, Walker and others (1981) proposed that the consumption rate of $CO_2$ in the weathering of silicates regulates its partial pressure in the atmosphere. The basic process involves several steps similar to Siever's steady state model. First, the atmospheric or bio-generated $CO_2$ is dissolved in water, where it is transformed into dissolved inorganic carbon (DIC). DIC includes aqueous $CO_2$, $HCO_3^-$, and carbonate ($CO_3^{2-}$). Secondly, the DIC is transported along with other materials, such as other ions produced from the weathering of silicates, to the ocean via rivers. Lastly, DIC precipitates with the cations such as Mg and Ca as carbonate sediments in the ocean. Carbonic acid as the major weathering agent against carbonate and silicate minerals would result in the consumption of atmospheric carbon, acting as a carbon sink (Lerman et al., 2007).

Like the steady state model, the above process highlights the importance of rivers acting as a conduit for dissolved weathered materials to travel from land to ocean.



doi:10.6342/NTU202500428

Through analyzing riverine water, the weathering rate of surface materials and the consumption rate of $CO_2$ in a river system can be estimated. Garrels and Mackenzie (1967) were among the first to conclude that the dissolved chemical compositions in natural waters were the result of mineral weathering. They analyzed water from the springs and lakes in Sierra Nevada, USA, and determined that the dissolved silica (Si) was the product of the weathering of silicates. In another study, Meybeck (1987) analyzed river data based on the mineral and rock characteristics in the catchments. The data came from unpolluted, monolithic French watersheds, including 25 rock types from granite to evaporite (Meybeck, 1986). The elements in dissolved river loads derived from the weathering of surface rocks. Among the elements analyzed from rivers, Si and potassium (K) essentially derived from silicate weathering, meanwhile 55% of sodium (Na) came from halite. Riverine Ca mainly originated from carbonate weathering, whereas dolomites and silicates contributed approximately the same amount of Mg. Thus, looking into riverine waters may help us describe and analyze the chemical weathering mechanism of surface rocks and minerals.

In early discussions, most studies consider $H_2CO_3$ as the major acid in the chemical weathering of silicates and carbonates. However, the role of sulfuric acid ($H_2SO_4$) in the weathering of rocks has gained increasing attention in recent years. One of the earlier example is the anthropogenic $H_2SO_4$ in the New England region. Pollution derived $H_2SO_4$ was determined to be the dominant chemical weathering agent in the New England region



doi:10.6342/NTU202500428

(Johnson et al., 1972). Aside from the $H_2SO_4$ create by human activities, natural sulfur is another source for sulfuric acid. Recent studies argue sulfur in the form of $H_2SO_4$ is a significant agent in the weathering of silicates and carbonates. Contrary to the consumption of $CO_2$ in the carbonic acid driven chemical weathering, the attack of $H_2SO_4$ on carbonates releases $CO_2$ into the atmosphere (Lerman et al., 2007). Although the degree of weathering driven by sulfuric acid is not comparable to that by carbonic acid, it could well be underestimated (Calmels et al., 2007; Burke et al., 2018).

Non-anthropogenic riverine sulfate related to chemical weathering of minerals and rocks can be traced back to two sources, sulfate evaporites and sulfide minerals. In the average sedimentary rocks, sulfates take up 2.2% and sulfides take up 1.7% (Lerman et al., 2007). Various studies had analyzed river chemistry data and attributed the sulfate content in river water to the oxidation of sulfide minerals such as pyrite. For example, in some rivers in the southern flank of the Nepal Himalayas, dissolved sulfate is primarily derived from sulfide oxidation (Galy and France-Lanord, 1999), based on the presence of sulfide and lack of anhydrite and gypsum in the High Himalaya Crystalline and the Lesser Himalaya regions. In North America, high sulfate concentration was detected in the Makenzie River in Canada (Calmels et al., 2007). By plotting the sulfur isotope ($\delta^{34}S$) against the oxygen isotope ($\delta^{18}O$), the results demonstrated that pyrite oxidation contributes 85% (±5%) of riverine sulfate. These cases have shown that sulfide minerals like pyrite are a major contributor to riverine sulfate when evaporite deposits are absent.



doi:10.6342/NTU202500428

### 1.1.2 Sulfate and chemical weathering in Taiwanese riverine waters

As the role of sulfate is increasingly noticed in terms of chemical weathering, more studies have been conducted in rivers where high sulfate concentrations are found. There have been multiple accounts of high sulfate concentrations in rivers and tributaries outflowing from the Central Range, Taiwan. For example, in Gaoping (Kaoping) River, the second largest river of Taiwan measured by discharge, sulfate concentrations in its tributaries were measured with a range of 561 ~ 931 μM (Chung et al., 2009; Das et al., 2012) and an average of 900 ± 400 μM (Blattmann et al., 2019). For rivers flowing eastward out of the Central Range, sulfate concentrations are found to be ranging from 526 to 1383 μM at Liwu River (Calmels et al., 2011). In the Beinan River region, sulfate concentration was measured to be on average 1560 ± 926 μM (Wang, 2019), or range from 360 to 3400 μM (Wang et al., 2024). The cases above show that riverine sulfate content in Taiwan may be up to 16 times higher than the world average, which was estimated to be 116.6 μM (Livingstone, 1963) or 300 μM (Burke, 2018). More data are included Table 1.1.



doi:10.6342/NTU202500428

Table. 1.1 Sulfate fluxes and concentrations in rivers in Taiwan, compared to estimated world average.

| **Location** | **Sulfate flux ($10^6$ mole/yr/km$^2$)** | **$SO_4^{2-}$ (μM)** |
|---|---|---|
| Beinan | 2.7 ~ 11.8[1] | 500 ~ 4800[1], 360 ~ 3400[2] |
| Choshui | - | 1805 ~ 1810[3] |
| Gaoping | 2.5 ~ 2.9[4] | 561 ~ 931[5], 900 ± 400[6] |
| Liwu | 2.14[7] | 526 ~ 1383[7], 313.35 ~ 800.5[8] |
| Taimali river and Hengchun Peninsular | - | 22 ~ 3758[9] |
| World average | 0.005 ~ 0.007[10] | 300[10], 116.6[11] |

All concentrations that are presented have been converted to μM.

(Data source: 1. Wang, 2019; 2. Wang et al., 2024; 3. Meyer et al., 2017; 4. Das et al., 2012; 5. Chung et al., 2009; 6. Blattman et al., 2019; 7. Calmels et al., 2011; 8. Yoshimura et al., 2001; 9. Bufe et al., 2021;10. Burke et al., 2018; 11. Livingstone, 1963.)

Due to the lack of documented evaporite outcrops in Taiwan, sulfide minerals such as pyrite are proposed to be the main source for riverine sulfate. For example, Yoshimura and other (2001) found high sulfate concentrations even in the tributaries at high altitudes in the Taroko Gorge region. The high sulfate concentrations found in higher altitudes were suspected to originate most likely from pyrite oxidation in the metamorphosed marine sedimentary rocks in the Taroko area. Additionally, the $\delta^{13}C$ values from the carbon in dissolved inorganic carbon (DIC) indicate that the carbon was supplied from the chemical weathering of carbonate minerals in the rocks. Lastly, the sulfate concentrations are well related to the high $\delta^{13}C$ values, which indicates that sulfuric acid is a major weathering agent for dissolving carbonates in the region. In the Gaoping region,



doi:10.6342/NTU202500428

sulfide oxidation accounts for 85 ± 7% of dissolved sulfate (Das et al., 2012). According to Blattmann and others (2019), in the Gaoping River, sulfuric acid-driven weathering is responsible for approximately two-thirds of total mineral dissolution, with carbonates almost entirely dissolved by sulfuric acid.

However, the extent of sulfuric acid driven process in Taiwan is debatable. Previous studies focused on the Central Range; but no similar analyses had been extended to other lithological units, such as the lower-grade metamorphic rocks of the Hsuehshan Range. Based on their results, Blattmann and others (2019) argued that the entire Taiwan Island is a net source of carbon dioxide for the carbon cycle. This assumption does provoke the question whether or not the findings from tributaries in the Central Range can represent the entire Taiwan Island.



doi:10.6342/NTU202500428

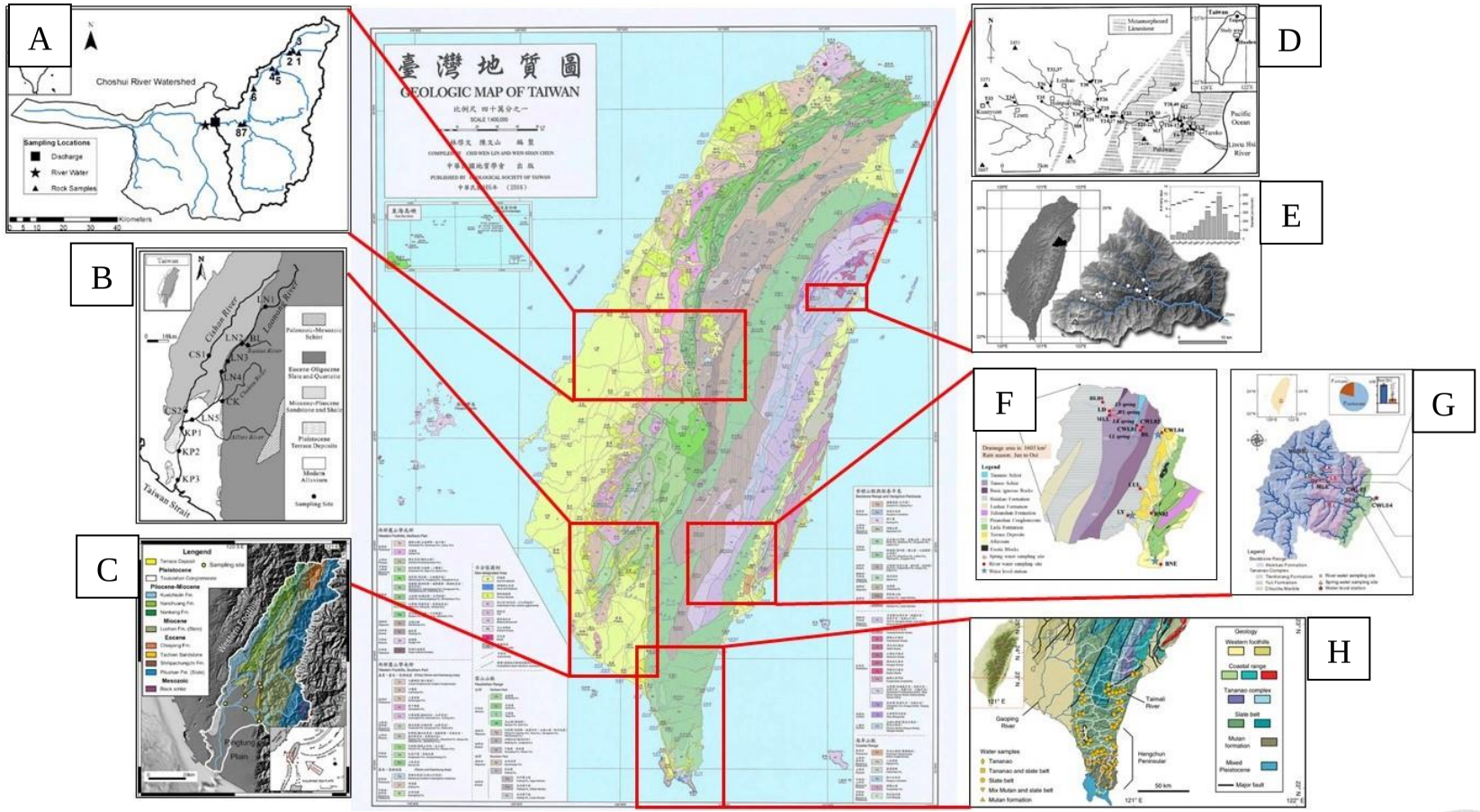


Figure 1.1 Previous chemical weathering study areas in Taiwan. (A) Choshui river, Meyer et al., 2017; (B) Gaoping river, Chung et al., 2009; (C) Gaoping river, Blattmann et al., 2019; (D) Liwu river, Yoshimura et al., 2001; (E) Liwu river, Calmels et al., 2011; (F) Beinan river, Wang, 2019; (G) Beinan river, Wang et al., 2024; (H) Taimali river and Hengchun Peninsular, Bufe et al., 2021.



doi:10.6342/NTU202500428

## 1.2 Purpose

This study intends to examine systematically the composition of major ions from riverine water in the metamorphic belts of Taiwan, to help deduce some of the questions related to chemical weathering in Taiwan.

Previous studies in Taiwan were focused on the rivers outflowing from the Central Range, for instance Gaoping River (Das et al., 2012; Blattmann et al., 2019), Liwu River (Yoshimura et al., 2001; Calmels et al., 2011), and Beinan River (Wang, 2019; Wang et al., 2024). These rivers flow through higher-grade metamorphic sedimentary rocks, in a region with higher erosion, weathering, deposition, and sedimentation rates. However, similar studies have yet to be conducted in the northern part of Taiwan Island. Therefore, the first question this study aims to answer is whether high riverine sulfate content can be found in other parts of Taiwan.

Secondly, pyrite has been argued as the main non-anthropogenic source for riverine sulfate. Although studies attributed riverine sulfate to pyrite oxidation in the Central Range region, it is unclear if that is the case for the river systems elsewhere. It is reasonable to consider pyrite oxidation in the Central Range region. Pyrite appears abundantly in the rocks of the Central Range (Yen, 1959; Horng et al., 2012). However, there has been reports of pyrite appearing in other rock formations or units that are not



doi:10.6342/NTU202500428

part of the Central Range. In the Hsuehshan Range for example, pyrite has been found in metasandstones in Szeleng Sandstone (Yui et al., 1997). Thus, it is possible that rivers in the Hsuehshan Range may also draw sulfate from pyrite oxidation in the rocks they flow through.

As metamorphic rocks make up the majority of the Taiwan orogeny, the third question this study targets is whether the metamorphic grades of surface rocks influences the chemical characteristics of the rivers. If so, since there are two main mountain ranges in Taiwan, which greatly differ in age and metamorphic grades, we would expect to find a systematic differentiation in the chemical composition of riverine waters.



doi:10.6342/NTU202500428

# Chapter 2 Background

## 2.1 Sources for major ions

### 2.1.1 Surface runoff

In this study, we take samples of river water for analysis. River is an essential surface component of the water cycle. The natural circulation of water on Earth is represented in the water cycle (Figure 2.1). The water cycle is composed of several processes including evaporation, transpiration, condensation, precipitation, and runoff (Water cycle, Encyclopaedia Britannica, https://www.britannica.com/science/water-cycle). Runoff is formed by the accumulation of rain or snow in drainage basins. Runoff flows across the surface, and it can seep through soil and rock fissures into underground aquifers, or converge to form rivers and lakes on the surface (Water Education Foundation, https://www.watereducation.org/). Rivers play an important role in the water cycle, acting as the conduit transporting materials from land to the ocean. Groundwater is another source of input for riverine waters. Groundwater water fills a saturated zone in soil and rocks underground known as aquifers. Due to changes in topography and levels of water saturation in the lithosphere, deep groundwater could reach the surface and mix with surface bodies of water. Human activities contribute much into runoff as well, including various anthropogenic sources such as industrial or agricultural wastes.



doi:10.6342/NTU202500428

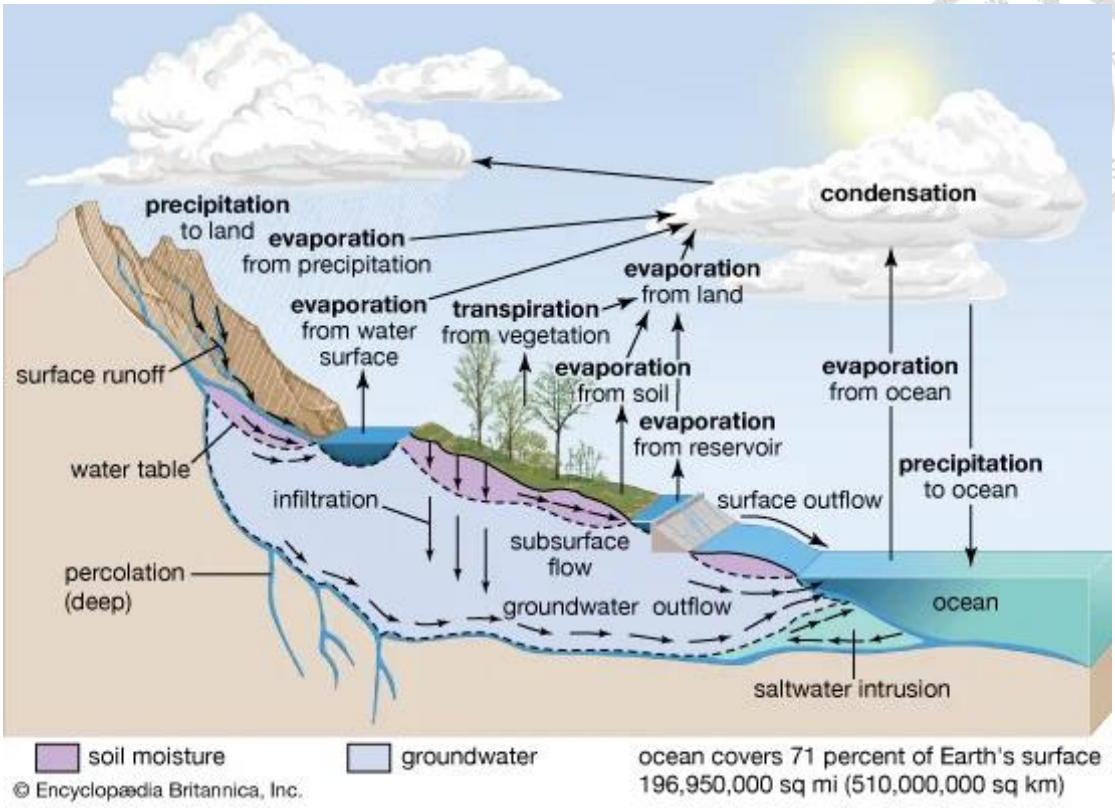


Figure 2.1 Diagram of water cycle (Encyclopaedia Britannica).

### 2.1.2 Chemical weathering of silicates and carbonates

Based on data collected from 60 major world rivers, Gaillardet and others (1999) concluded that the main control of riverine dissolved loads is lithology. Moreover, chemical weathering of carbonates and evaporites from sedimentary rocks provides dissolved cations to the rivers and influences the chemical compositions of all rivers.

In the lithosphere, the average sedimentary rock consists of shale, carbonates, sandstone, and evaporites (Li, 2000). In sedimentary rocks, silicates and carbonates are the most prominent minerals, taking up around 94 % of the minerals per one gram of rock (Figure 2.2). Na, Mg, K, and Ca are the cations commonly found in silicate minerals. Mg



doi:10.6342/NTU202500428

and Ca are the major cations found in carbonate minerals, such as calcite or aragonite. The dissolved solids released in global rivers and groundwater through mineral-water weathering reactions consist of major cations, Na, Mg, K, and Ca, and anions such as bicarbonate ($HCO_3^-$), sulfate ($SO_4^{2-}$), and chloride ($Cl^-$), and dissolved silica (Lerman et al., 2007).

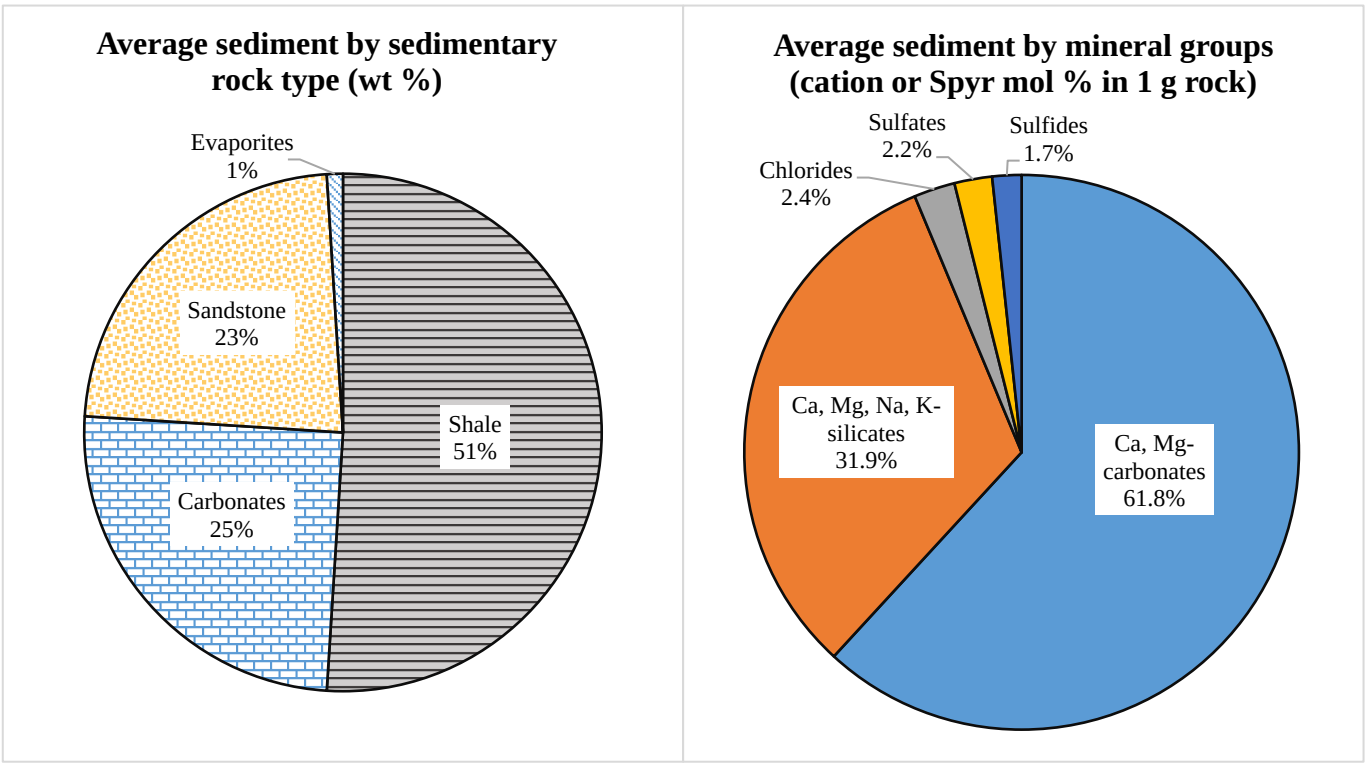


Figure 2.2 Composition of average sediment by sedimentary rock types (left) and by mineral groups based on chemical composition (right). (Lerman et al., 2007).



doi:10.6342/NTU202500428

Chemical weathering of carbonates and silicates is generally described with four reactions (Reactions 2-1, 2-2, 2-3, and 2-4). These reactions involve two major weathering acids, carbonic acid ($H_2CO_3$) or sulfuric acid ($H_2SO_4$), and carbonates or silicates as the weathered material.

**Carbonic acid weathering**

$$Carbonates_{(s)} + H_2O_{(l)} + CO_{2(g)} \rightarrow (0.66\ Ca^{2+}, 0.33\ Mg^{2+}, 0.011\ Na^{+})_{(aq)} + 2\ HCO_3^-{}_{(aq)} \quad (2\text{-}1)$$

$$Silicates_{(s)} + H_2O_{(l)} + 2\ CO_{2(g)} \rightarrow (0.32\ Ca^{2+}, 0.22\ Mg^{2+}, 0.9\ Na^{+})_{(aq)} + 2\ HCO_3^-{}_{(aq)} + SiO_{2(s)} \quad (2\text{-}2)$$

**Sulfuric acid weathering**

$$Carbonates_{(s)} + H_2SO_{4(aq)} \rightarrow (0.66\ Ca^{2+}, 0.33\ Mg^{2+}, 0.011\ Na^{+})_{(aq)} + SO_4^{2-}{}_{(aq)} + H_2O_{(l)} + CO_{2(g)} \quad (2\text{-}3)$$

$$Silicates_{(s)} + H_2SO_{4(aq)} \rightarrow (0.32\ Ca^{2+}, 0.22\ Mg^{2+}, 0.9\ Na^{+})_{(aq)} + SO_4^{2-}{}_{(aq)} + H_2O_{(l)} + SiO_{2(s)} \quad (2\text{-}4)$$

In reactions 2-1 and 2-2, atmospheric $CO_2$ is dissolved in water, forming carbonic acid. When 1 mole of carbonate reacts with the carbonic acid, 1 mole of $CO_2$ is consumed, and 2 moles of $HCO_3^-$ are produced. In the case of silicate weathering by carbonic acid, 1 mole of $CO_2$ is needed for each mole of $HCO_3^-$ created. In a hypothetical scenario, when carbonic acid reacts



doi:10.6342/NTU202500428

with a bulk of material composed of equal portions of carbonates and silicates, reactions 2-1 and 2-2 is combined into Reaction 2-5 (Lerman et al., 2007).

$$CaCO_3 + H_2O + CO_2 \rightarrow Ca^{2+} + 2\,HCO_3^-$$

$$+) \quad CaSiO_3 + H_2O + 2\,CO_2 \rightarrow Ca^{2+} + 2\,HCO_3^- + SiO_2$$

$$CaCO_3 + CaSiO_3 + 2\,H_2O + 3\,CO_2 \rightarrow 2\,Ca^{2+} + SiO_2 + 4\,HCO_3^- \quad (2\text{-}5)$$

For a sedimentary rock with equal amounts of carbonate and silicate minerals reacting with carbonic acid, 3 moles of $CO_2$ is consumed to produce 4 moles $HCO_3^-$. Rivers transport the produced $HCO_3^-$ to the ocean, where Ca and Mg could react with $HCO_3^-$ and lead to inorganic carbonate precipitation (Garrels and Mackenzie, 1971).

$$Ca^{2+} + 2\,HCO_3^- \rightarrow CaCO_3 + CO_2 + H_2O \quad (2\text{-}6)$$

Although the precipitation of every two moles of bicarbonate releases one mole of $CO_2$, one mole of $CO_2$ is consumed for every mole of carbonate weathered, and two moles of $CO_2$ are consumed for every mole of silicate weathered. Therefore the total weathering process of silicates and carbonates acts as a carbon sink.

This carbonic acid driven weathering pathway had been considered as the dominant chemical weathering process, regulating the partial pressure of $CO_2$ in the atmosphere (Siever, 1968).

The sulfuric acid weathering pathway is demonstrated in Reactions 2-3 and 2-4. In



doi:10.6342/NTU202500428

Reaction 2-3, sulfuric acid reacts with carbonate, and releases $CO_2$ from carbonates. The process of silicates reacting with sulfuric acid does not involve carbon (Reaction 2-4), thus having no effect on the atmospheric carbon budget.

However, the reaction between sulfuric acid and carbonate minerals does not always release gaseous $CO_2$ immediately. Reaction 2-7 presents another carbonate-weathering pathway. In this reaction, the ratio of $CaCO_3$ to $H_2SO_4$ is 2:1, resulting in the production of $HCO_3^-$ instead of a prompt release of $CO_2$. Nevertheless this reaction still leads to the release of $CO_2$ through the carbonate precipitation in the ocean (Torres et al., 2014).

$$2\ CaCO_3 + H_2SO_4 \rightarrow 2\ Ca^{2+} + 2\ HCO_3^- + SO_4^{2-} \quad (2\text{-}7)$$

### 2.1.3 Sources of riverine sulfate

The dissolution of sedimentary evaporites such as anhydrite ($CaSO_4$) and gypsum ($CaSO_4 \cdot 2H_2O$), and the oxidative weathering of sulfide minerals such as pyrite ($FeS_2$) are the natural sources of riverine sulfate (Meybeck, 1987; Relph et al., 2021). Due to the lack of reports of evaporites in Taiwan (Ho, 1975; Li et al., 1997), this section focuses on the weathering of pyrite.

Oxidative weathering of pyrite (OWP) is an important source of natural sulfuric acid. For instance, in various river systems of France, 34 % of riverine sulfate is produced from



doi:10.6342/NTU202500428

pyrite weathering (Meybeck et al., 1987). In earlier studies, the estimates of global OWP fluxes range from 0.5 to 0.65 Tmol/y (Francois and Walker, 1992; Lerman et al., 2007). However, recent estimates put OWP contribution to riverine sulfate at 1.3 (± 0.2) Tmol S/y (Burke et al., 2018). This shows that previous estimations of OWP may have been too low, and thus the effect of sulfuric acid weathering could have been underestimated as well. Two reactions describe oxidation of pyrite into sulfuric acid, demonstrated under laboratory condition (Taylor et al., 1984).

$$4\ FeS_2 + 15\ O_2 + 14\ H_2O \rightarrow 4\ Fe(OH)_3 + 8\ SO_4^{2-} + 8\ H^+_{(aq)} \quad (2\text{-}8)$$

$$FeS_2 + 14\ Fe^{3+}_{(aq)} + 8\ H_2O_{(aq)} \rightarrow 15\ Fe^{2+}_{(aq)} + 2\ SO_4^{2-}{}_{(aq)} + 16\ H^+_{(aq)} \quad (2\text{-}9)$$

In reaction 2-8, oxygen directly reacts with pyrite ($FeS_2$), which produces 8 moles of sulfuric acid from 4 moles of pyrite. A second oxidation pathway of pyrite involves ferric iron, which produces 2 moles of sulfuric acid from 1 mole of pyrite (Reaction 2-9).

In Taiwan, due to the exposure of sulfide minerals and high weathering rates, chemical weathering driven by sulfuric acid has been proposed to be prominent in Taiwan (Das et al., 2012; Blattmann et al., 2019).



doi:10.6342/NTU202500428

## 2.2 Study Area

### 2.2.1 Geological Background

This study focuses on the tributaries of the Lanyang River. The Lanyang River is a northeastward flowing major river in northeastern Taiwan. It originates from the northern summit of Mt. Nanhu. The main stream is estimated to be 73 kilometers long. The drainage basin of the Lanyang River is around 978 $km^2$ (Water Resources Agency, Ministry of Economics).

The Lanyang River was selected for its location. The Hsuehshan Range and the Central Range, two distinct mountain ranges with different metamorphic rocks, are situated alongside the banks of the Lanyang River. The drainage basins of its tributaries span across these two major mountain ranges of Taiwan. Figure 2.3 shows the geological map of this region.

The Hsuehshan Range is on the left bank of the Lanyang River. The northern part of the Hsuehshan Range consists mainly of sedimentary rocks, which had undergone low-grade metamorphism. In the study area, the main formations in Hsuehshan Range are Hsichun Formation, Szeleng Sandstone, and Kankou Formation. The Hsichun Formation consists of alterations of silty argillite and fine-grained metasandstone, thick-bedded argillite or slate interbedded with thin metasandstone. It is Eocene or early Oligocene in



doi:10.6342/NTU202500428

age (Ho, 1975). The Szeleng Sandstone is made up of mostly thick-bedded grey to white metasandstone. It is probably Eocene or Oligocene in age (Ho, 1975). The Kankou Formation is comprised mostly of slate, occasionally interbedded with thin fine-grained sandstone. It is late Oligocene to early Miocene in age (Ho, 1975).

The southeastern tributaries of the Lanyang River flow through the Central Range. The Lushan Formation is the major formation in the northern Central Range (Ho, 1975). It consists mostly of dark colored slate and argillite, and is middle Miocene in age (Chang, 1974). Apart from the Lushan Formation, there is the Tananao Schist (Yen, 1960; Tsan, 1977) in this region. The Tananao Schist is a loosely defined unit, with a collection of complex metamorphic rock formations with ages from late Paleozoic to early Mesozoic (Yen, 1953). The Tananao Schist is mainly composed of various types of schist, including mica schist, quartz-mica schist, and thin interbedded green schist. Metachert and marble are also present in this unit.



doi:10.6342/NTU202500428

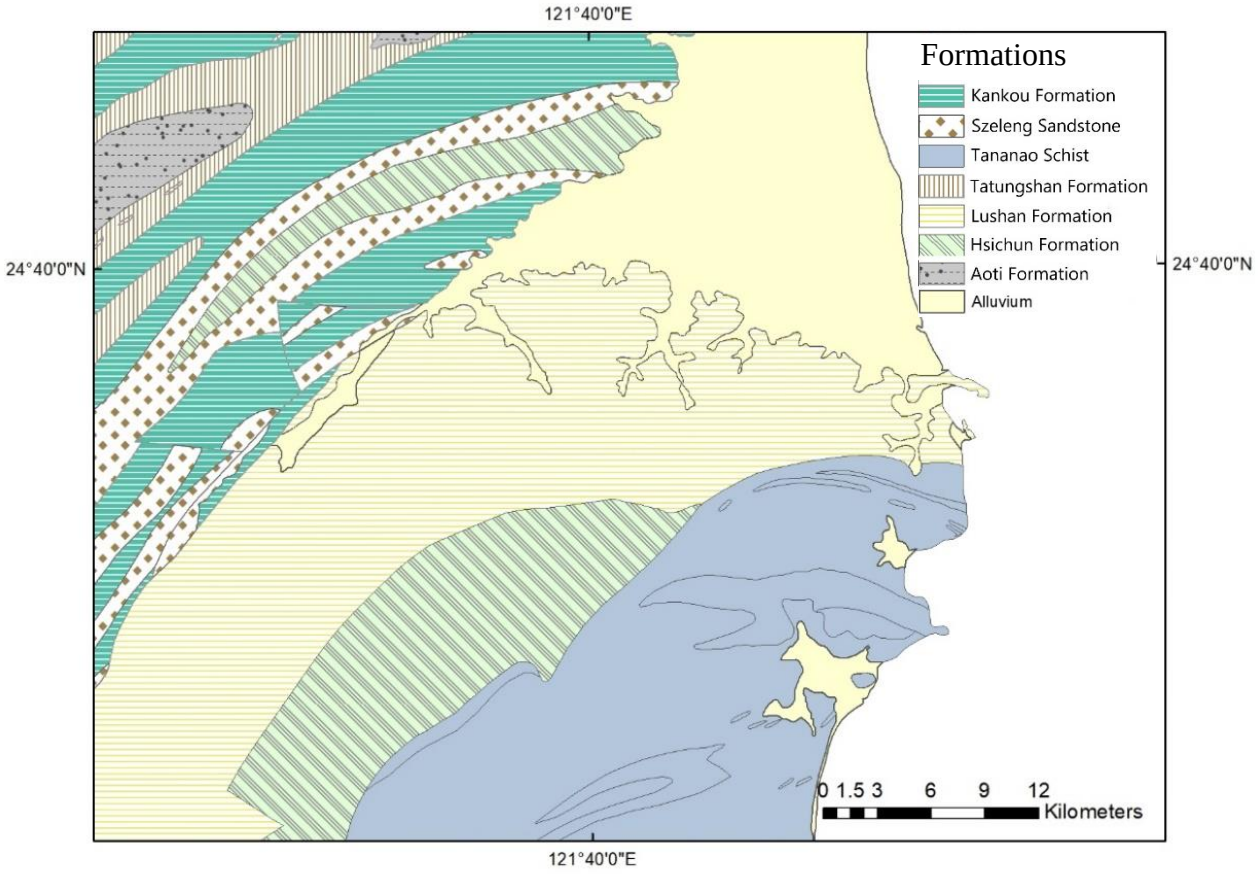


Figure 2.3 Geological map of the region (CGS).

Silicates such as quartz, feldspar, and clay minerals are the main minerals forming the sedimentary rocks in both the Hsuehshan Range and the Central Range. In addition, there are older and higher-grade metamorphic rocks in the Tananao Schist. Mica, chlorite, and biotite form the various types of schist in the Tananao Schist, and carbonate minerals mainly form the marble in this unit.

Sulfide minerals are common in the rocks in Taiwan. Horng and others (2012) reported findings of pyrrhotite in the Eocene-Oligocene metamorphic formations (the



doi:10.6342/NTU202500428

Hsichun Formation in this study) and the Pre-Tertiary metamorphic complex (the Tananao Schist in this study). One sample was reported in the Hsichun Formation in the Hsuehshan Range, while several samples were found in the Hsichun formation and the Tanaoao Schist in the Central Range. However, pyrrhotite was not reported in the other formations in the Hsuehshan Range nor in the Lushan Formation in the Central Range. There had been other reports of the sulfides in the Hsuehshan Range as well, in quartz veins in Szeleng Sandstone (Yui et al., 1997). Moreover, cupriferous pyrite had been reported in southern Yilan County in the Tananao Schist since the early 20$^{th}$ century (Yen, 1959).

### 2.2.2 Sample sites

The sample sites of this study were selected across the two mountain belts with difference in age, metamorphic grade, and variety of rock formations (Figure 2.4). The sample sites are located in rivers with drainage basins of various sizes and different surface lithology. There are documented hot springs in the drainage basins at three sites. This study selected these sites to compare local and regional differences in terms of river chemistry.

Five sample sites were selected in the northwest side of Lanyang River in the



doi:10.6342/NTU202500428

Hsuehshan Range. They are located at the Cukeng River (CK), Jiuliao River (JL), Songluo River (SL), Bonbon River (BB), and Baoyang River (BY). These rivers flow through the Hsichun Formation, Szeleng Sandstone, and Kankou Formation.

Six sites were selected in the southern side of the Lanyang River in the Central Range. These sites are located in the Wulaokeng River (WRK), Xinliao River (XL), Dagou River (DG), Malun River (ML), Tiangou River (TG), and Siji River (SJ). The Lushan Formation is the most prominent formation in this region. Apart from the Lushan Formation, rocks from the mid to high-grade metamorphic rocks of the Tananao schist can also be found in the basin of WRK.

Hot springs are present in several drainage basins of the rivers in this study. The hot spring influence should be taken into account, thus we took hot springs samples to compare their chemical results with riverine water. In the Hsuehshan Range, the Bonbon River directly flows through the Bonbon hot spring. In the Central Range, there were reports of hot spring outcrops in the upstream of Tiangou River and Siji River. Due to accessibility, we have only taken hot spring samples in Bonbon and Tiangou hot springs.

Finally, agricultural and industrial activities may cause pollution input to the rivers, which should be avoided. Upstream tributaries were picked to keep away from potential sources of contamination, such as farms, settlements, populated townships, and factories.



doi:10.6342/NTU202500428

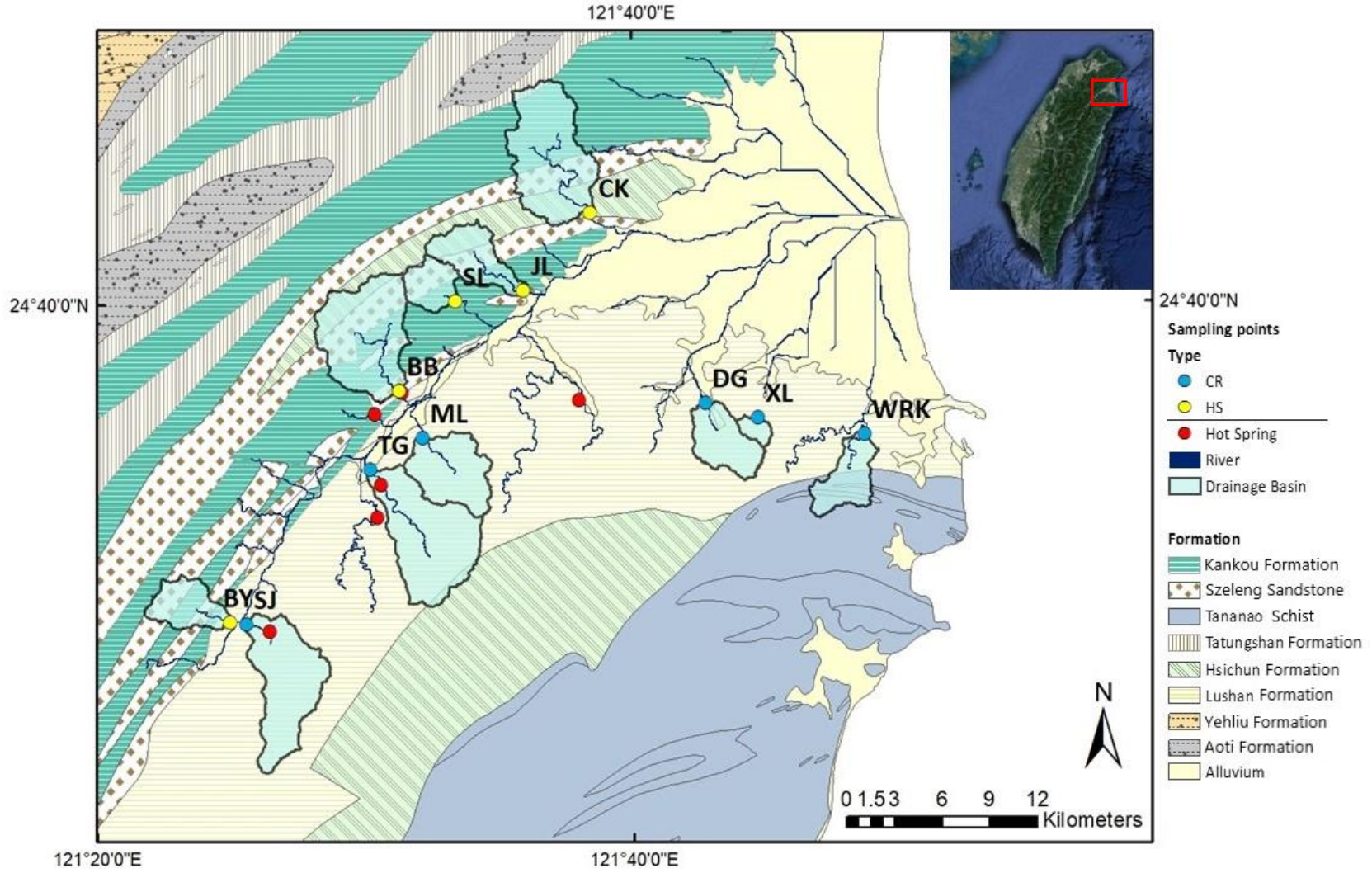


Figure 2.4 Sample siyes of this study, with the tributaries, drainage basins, and known hot springs plotted on the 1/250 k geological map of the region.



doi:10.6342/NTU202500428

Table 2.1 List of sample sites, the tributaries they are on, and the lithology of drainage basins of those tributaries

| Sample point | River | Source | Geological formation | Lithology |
|---|---|---|---|---|
| CK | Cukeng | Hsuehshan Range | Hsichun Formation<br>Kankou Formation<br>Szeleng Sandstone | Quartzite, sandstone, argillite, metasandstone |
| JL | Jiuliao | | | |
| SL | Songluo | | | |
| BB | Bonbon | | | |
| BY | Baoyang | | Kankou Formation<br>Szeleng Sandstone | Quartzite, argillite, metasandstone |
| WRK | Wulaokeng | Central Range | Tananao Schist<br>Lushan Formation | Black schist, green schist, siliceous schist, marble, argillite, slate, metasandstone |
| XL | Xinliao | | | |
| DG | Dagou | | Lushan Formation | Argillite, slate, metasandstone |
| ML | Malun | | | |
| TG | Tiangou | | | |
| SJ | Siji | | | |



doi:10.6342/NTU202500428

# Chapter 3 Methods

The methods of this study can be divided into two major components: fieldwork and chemical analysis. Fieldwork includes rainwater collection, river and hot spring water collection, on-site measurements of water samples, and site observations. In chemical analysis, anions are measured using ion chromatography (IC), and cations are measured using Inductively Coupled Plasma Mass Spectrometer (ICP-MS).

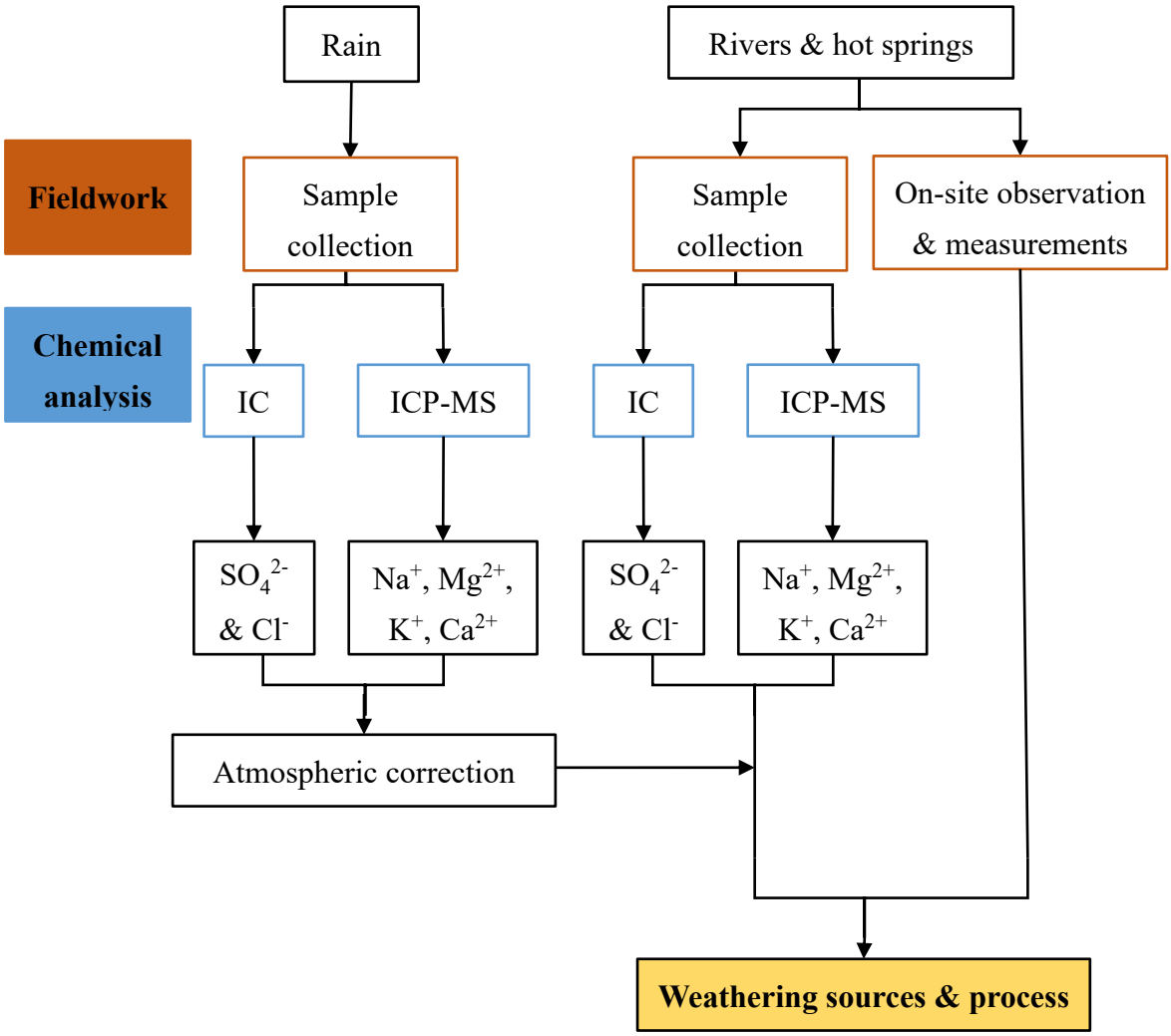


Figure 3.1 Flow chart of study method.



doi:10.6342/NTU202500428

## 3.1 Field work

### 3.1.1 Water collection and storage

The same collection and storage methods were applied to all water samples.

**In lab: bottle preparations.**

I. We washed 1-L PE bottles (Figure 3.2) three times with MilliQ water, and then dried them in an oven at 60 ℃ for 3 days.

II. We used 100 mL Pyrex bottles for storing the water samples. In addition, 20 mL glass vials were used to store water samples for chemical analysis. The Pyrex bottles and vials (Figure 3.2) were completely submerged in 10% neutral detergent for at least 3 days.

III. The 20 mL glass vials used to store samples for cation analysis were completely submerged in 5% nitric acid for at least 3 days additionally.

IV. The bottles and vials were rinsed with MilliQ water until no bubbling from detergent could be observed. Then the bottles and their components were dried in an oven at 60℃ for 3 days.

V. We assembled the dried Pyrex bottles and vials then sealed them in clean zip bags before usage.

**On site: collection.**

I. The PE bottles were rinsed three times with the subject water on site. Then we filled



doi:10.6342/NTU202500428

the PE bottles with subject water.

II. We assembled a disposable, sterile filter unit (Finetech, 500 mL, PES membrane, pore size 0.22 μm), a hand pump, and a Pyrex bottle (Figure 3.2) as a manual filter system (Figure 3.3). We had chosen 0.22 μm pore size to filter out most natural organisms, including bacteria, cells, and large viruses. Organisms were filtered to prevent the continuation of biochemical processes or deterioration, which could alter the original chemical state of the water sample after collection.

III. We poured the subject water through the manual filter system, where filtered water was collected at the bottom in a Pyrex bottle.

IV. After collection, the Pyrex bottles were sealed and labeled (Figure 3.4), and stored in a cooled state before the samples were transported back to the lab.

**In lab: storage.**

I. For anion analysis, 15 mL of each sample was kept it in non-acid cleaned vials.

II. For cation analysis, nitric acid was added to create a 5 mL, 2% nitric acid sample solution to ensure dissolution of cations.

III. Extra sample water was kept in Pyrex bottles until analysis was complete.

IV. All samples are stored at approximately 4°C to suppress biological growth and to avoid alterations before chemical analysis.



doi:10.6342/NTU202500428

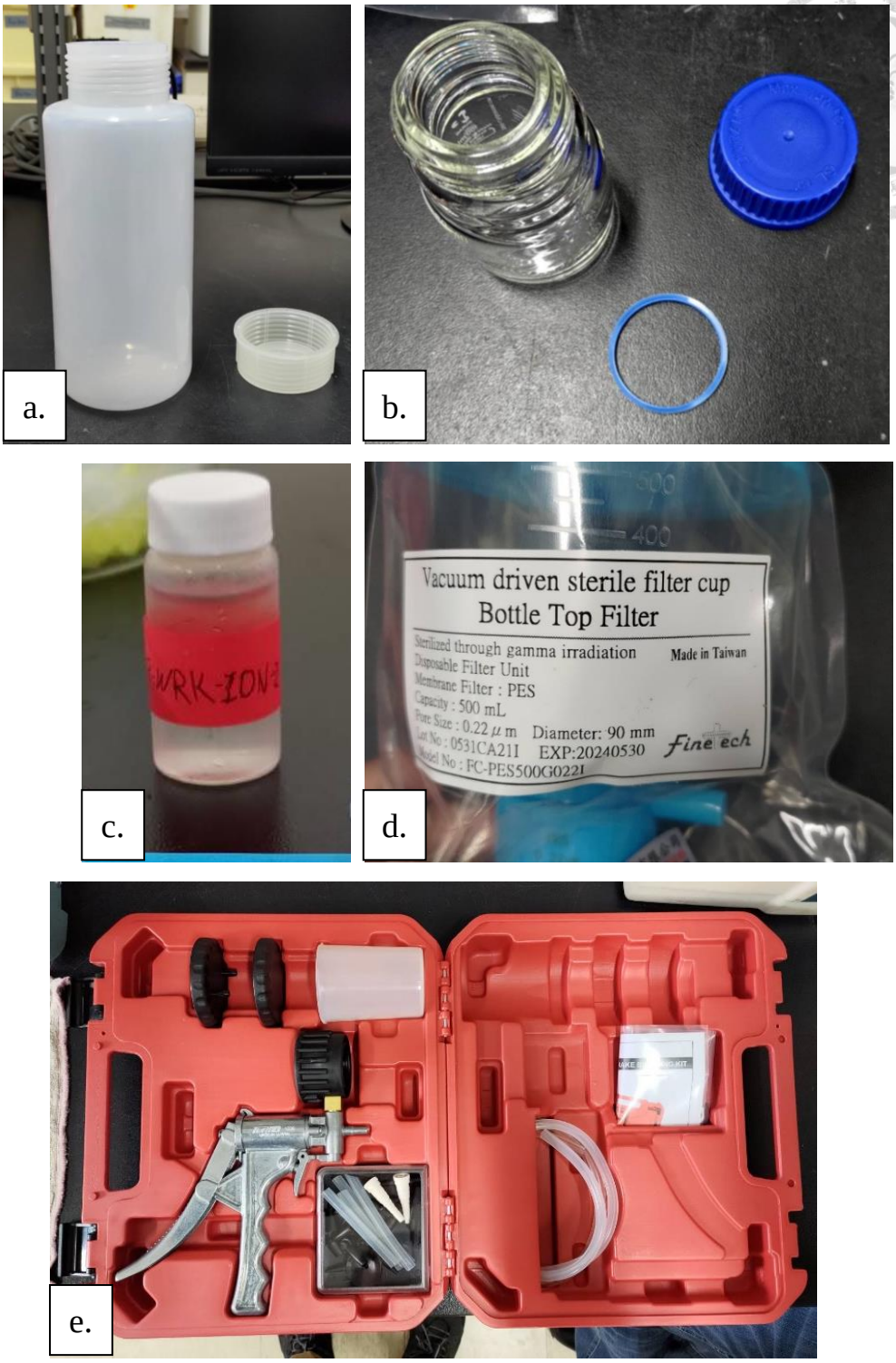


Figure 3.2 Bottles and tools. (a) 1-L PE bottle used for collection. (b) 100 mL Pyrex glass bottle, with cap and seal ring. (c) 20 mL glass vial. (d) Vacuum driven bottle top filter, disposable unit, with 500 mL capacity and pore size of 0.22 μm. (e) Manual vacuum pump.



doi:10.6342/NTU202500428

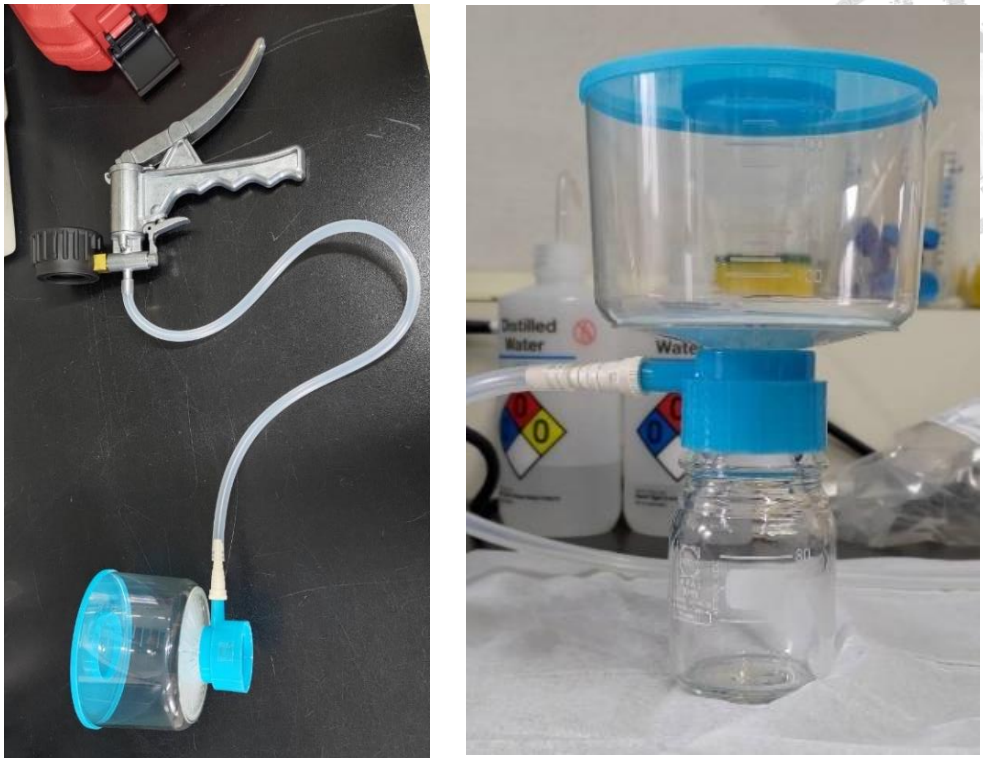


Figure 3.3 Left: Manual filtration system, assembled. Right: filter cup attaching to the Pyrex bottle.

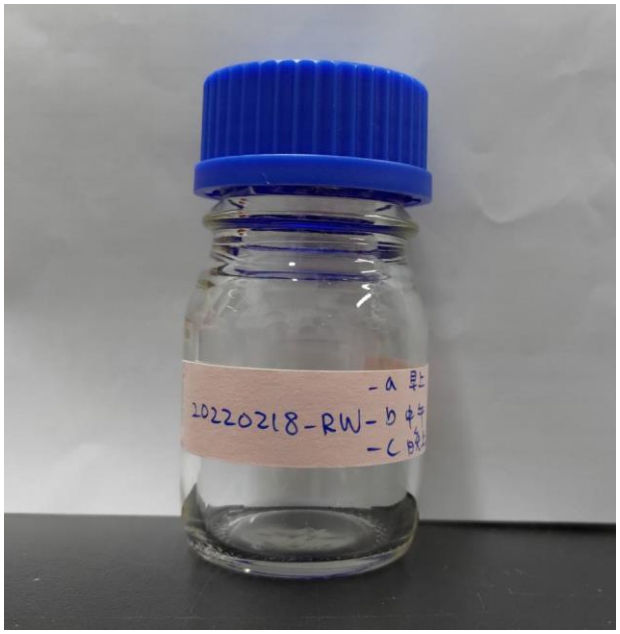


Figure 3.4 Sealed and labeled Pyrex bottle.



doi:10.6342/NTU202500428

### 3.1.2 Rainwater

Rainwater was collected by the student project at National Yilan Senior High School (YLHS), from February 2022 to January 2023. To obtain a valid representation of atmospheric inputs, the first 6 hours of rainfall was neglected to avoid capturing anthropogenic airborne pollutions. We selected three locations for rainwater collection: at Zhuangwei (ZW) for its close proximity to the shore, Yilan high school (YLHS) as the basis for comparison, and finally Niudou (ND) for its remote and mountainside environment (Figure 3.5).

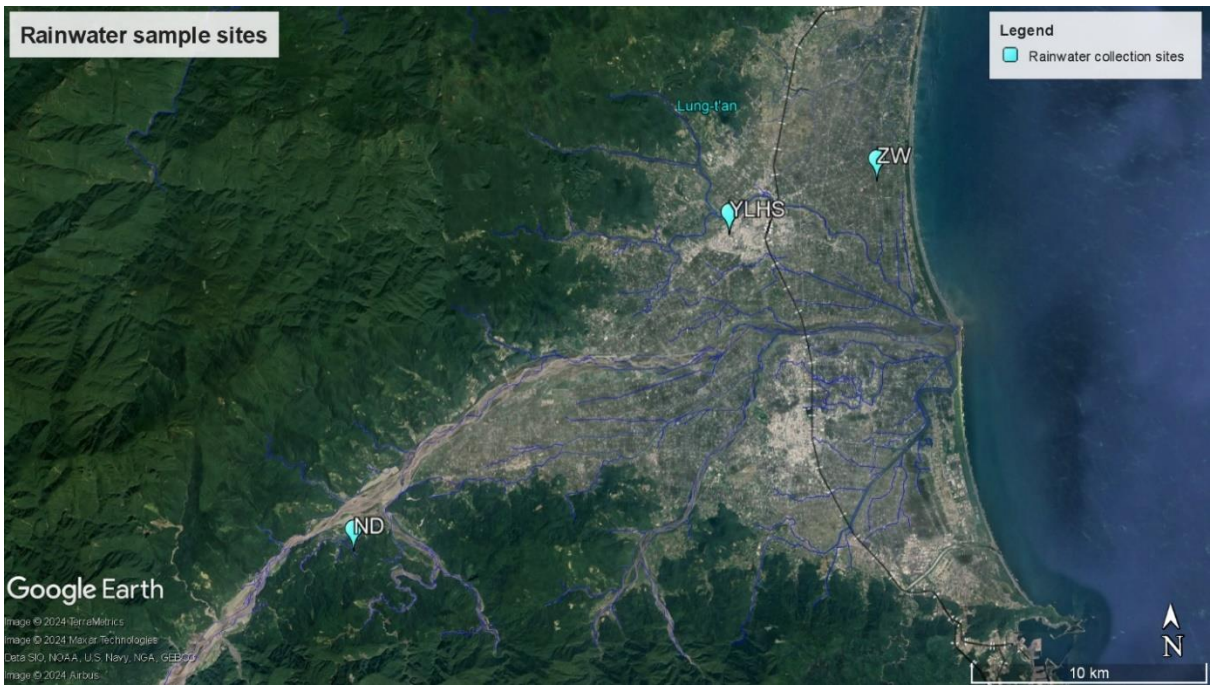


Figure 3.5 Google Earth view of the rainwater collection sites. The sites are Zhuangwei (ZW), Yilan high school (YLHS), and Niudou (ND) from east to west.



doi:10.6342/NTU202500428

### 3.1.3 River water & hot spring

We carried out six sampling campaigns, during 2022/2/7~2/10, 2022/7/5~7/7, 2022/9/25~9/27, 2023/4/9~4/11, 2023/6/26~6/28, 2023/9/11~9/13 respectively. These periods were chosen according to wet and dry seasons of the study area and usually after a period of continuous rainfall to ensure sufficient flow in the rivers.

### 3.1.4 On site observations and measurements

Each sample site was observed and documented, which included descriptions of the amount of flow, turbidity, and the color of the water. At each site, we described the composition of riverbed gravels, documenting their rock type, sizes, and colors. Bedrock lithology of the riverbeds were also documented.

On-site pH, conductivity, and salinity measurements were performed with the Xylem Analytics pH/Cond 3320 SET 2 meter (Figure 3.6 and 3.7). These parameters are used only as reference to compare seasonal changes.



doi:10.6342/NTU202500428


Figure 3.6 Xylem Analytics pH/Cond 3320 SET 2 pH/conductivity meter.

Figure 3.7 Photo showing an on-site measurement at BB, 2023/9/11.



doi:10.6342/NTU202500428

## 3.2 Chemical analysis

### 3.2.1 Anion Analysis

The anions of interest in this study are sulfate ($SO_4^{2-}$), chloride ($Cl^-$), nitrate ($NO_3^-$), and phosphate ($PO_4^{3-}$). We used IC to obtain the absolute concentration of each anion. The instrument used was the Anion System DIONEX ICS-3000 (Figure 3.8) at Global Change Research Center (GCRC, National Taiwan University). Apart from sulfate, chloride, nitrate, and phosphate, the IC also measures the concentrations of fluoride ($F^-$), nitrite ($NO_2^-$), and bromide ($Br^-$).

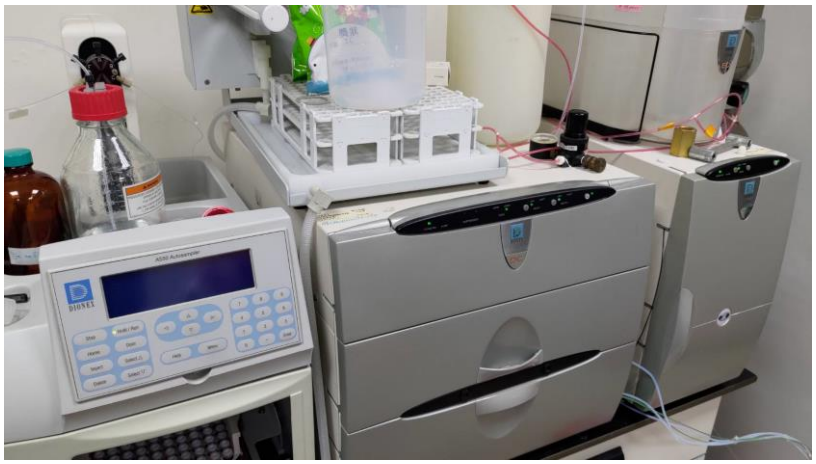

Figure 3.8 DIONEX ICS-3000 at GCRC, National Taiwan University. This is an IC with anion columns, and it measures $F^-$, $Cl^-$, $NO_2^-$, $Br^-$, $NO_3^-$, $SO_4^{2-}$, and $PO_4^{3-}$ in ppm.



doi:10.6342/NTU202500428

In IC analysis, charged ions are separates based on their affinity to the styrene and divinylbenzene materials inside the column. The instrument records the time duration and signal strength of the charged ion, which are translated into the identification of different ions and their amount. The peaks of different ions are calibrated by a set of laboratory prepared external standards. The calibration curves of the tested anions are set between 0.1 to 10 ppm.

Rainwater samples were submitted to the IC in a non-diluted state. River water samples were diluted with MilliQ water to 10 % volume concentrations. Hot spring water samples were diluted with MilliQ water to 1 % volume concentration. Triplicates of each sample were created for each sample to produce 1 mL of sample solution. The IC processes 250 μL of sample fluid from each vial; each vial is sampled once. External standards were inserted between every 10 vials.



doi:10.6342/NTU202500428

### 3.2.2 Cation Analysis

The cations of interest in this study are $Na^{+}$, $Mg^{2+}$, $K^{+}$, and $Ca^{2+}$. The instrument used for cation measurement is the Agilent 7700, Inductively Coupled Plasma Mass Spectrometer (ICP-MS), at the Department of Geosciences, National Taiwan University (Figure 3.9).

The ICP-MS first nebulizes target sample into small aerosol water droplets. The metals in the liquid droplets are ionized into detectable cations, and then transported by the carrier gas (Argon) to the mass spectrometer. At the spectrometer, cations separate according to their charge to mass ratio and subsequently captured at the sensor for qualitative and quantitative measurements.


Figure 3.9 ICP-MS at Department of Geosciences, National Taiwan University.



doi:10.6342/NTU202500428

Two external standards and a reference standard were prepared at several different concentrations for calibration. The first external standard is Multi-Element Calibration standard-4 (ES4) by Agilent Technologies (part number 8500-6942, lot number 11-97YPY2). The matrix of ES4 is water with trace nitric and hydrofluoric acids. ES4 was prepared at 100, 50, and 2 ppb. The second external standard used was the Multi-Element Calibration standard-2A (ES2A) by Agilent Technologies (part number 8500-6940, lot number 1-166MKBY2). The matrix of ES2A is 5% nitric acid. ES2A was prepared at 200, 50, 12.5, and 5 ppb.

The reference standard used for this study was the ICP multi-element standard solution X for surface water testing (product number 1.09493, M10C for short) manufactured by Supelco. The matrix of M10C is 3 - 5% nitric acid. M10C was prepared at 2-, 4-, and 20-time dilutions.

ES4 and ES2A were queued from low to high concentration before sample solutions, while M10C was placed after the sample solutions. The lower calibration concentrations, up to 200 ppm, were set according to external standards ES4 and ES2A. The high concentrations were assigned based on the calculate dilutions of M10C. The calibration curve for $Na^+$ is set between 5 to 4091 ppb, 5 to 17895.5 for $Ca^{2+}$, and 5 to 7599 for $Mg^{2+}$.

Rainwater, river water, and hot spring water samples were prepared in 4-time, 8-



doi:10.6342/NTU202500428

time, and 100-time dilutions respectively. Two percent mass concentration of nitric acid ($HNO_3$) was used as the solvent for the cation samples. Rainwater solutions were prepared under 1-part sample and 3-part solvent; river water solutions were 1-part sample and 7-part solvent; and hot spring water solutions were 1-part sample with 99-part solvent. Rhodium (Rh) and Bismuth (Bi) were added to sample solutions as internal standards (IS) with 2 ppb concentration. All samples were prepared in the clean room at the Global Change Research Center (GCRC), NTU.

### 3.2.3 Data analysis

To obtain valid data and results for discussion, we performed data checks on the uncorrected data produced by the IC and ICP-MS.

For the anion results produced by IC, each sample was processed three times. We calculated an average, a standard deviation (STD), and an RSD (Equation 3-1) with the three results from each sample. For sulfate, the principle for a valid result is an error under 5%. In the case of chloride, due to the naturally lower concentrations and the effect of dilution, the error is allowed to be up to 15%.

$$\text{RSD (\%)} = (\text{STD}/\text{Average}) \times 100\% \quad (3\text{-}1)$$

ICP-MS produces a mean and a STD for each sample. RSD (Equation 3-1) was calculated internally by the ICP-MS. The program uses two modes to calculate the



doi:10.6342/NTU202500428

amount of an element in the sample: pulse mode (P mode) and analogue mode (A mode). The calibration curves were set at lower concentrations. P mode is used for elements with naturally low concentrations, such as trace elements. A mode is used when an element has a large concentration. Due to the sensitivity of ICP-MS, some Na and K data are below the detection limit. If a concentration result of a sample is below the detection limit or calculated to be negative, these invalid data are treated as zero.

In order to obtain accurate ion concentrations, data with extreme values were excluded. Some samples were marked as invalid due to contaminations, mixing, or human error. For unspecified samples that produced questionable results, the following method was implemented.

$$\text{Upper bound} = Q_3 + 1.5 \times (Q_3 - Q_1) \quad (3\text{-}2)$$

$$\text{Lower bound} = Q_1 - 1.5 \times (Q_3 - Q_1) \quad (3\text{-}3)$$

Where $Q_1$ is the first quartile and $Q_3$ is the third quartile. Values that either exceeded the upper bound, or were less than the lower bound were excluded from average calculations.



doi:10.6342/NTU202500428

# Chapter 4 Results

## 4.1 Fieldwork

### 4.1.1 River and hot spring collection

In total, 59 riverine and 8 hot spring samples were taken from 6 campaigns (Table 4.1). We were able to collect samples in each campaign for most sample sites; however, there were exceptions. The stream at CK was dry in April 2023 (Figure 4.1). We only obtained three samples from DG, in February and September 2022, and September 2023. No samples were collected at DG in April and July 2022, and June 2023 due to the dry riverbed (Figure 4.2). The lack of river water was likely due to little rainfall in the dry season. ML was skipped in September 2022 due to inaccessibility following the typhoons Hinnamnor (軒嵐諾) and Muifa (梅花). Only four samples were collected from JL, since this site was added on the third campaign in September 2022 for comparison with other tributaries in the Hsuehshan side.

Hot spring samples were collected starting from the second campaign in June 2022. In September 2023, intense rainfall from typhoon Haikui (海葵) led to a rise of river water, which covered the hot spring outcrops. Therefore, only four samples of hot spring water were retrieved from each of BB and TG sites.



doi:10.6342/NTU202500428

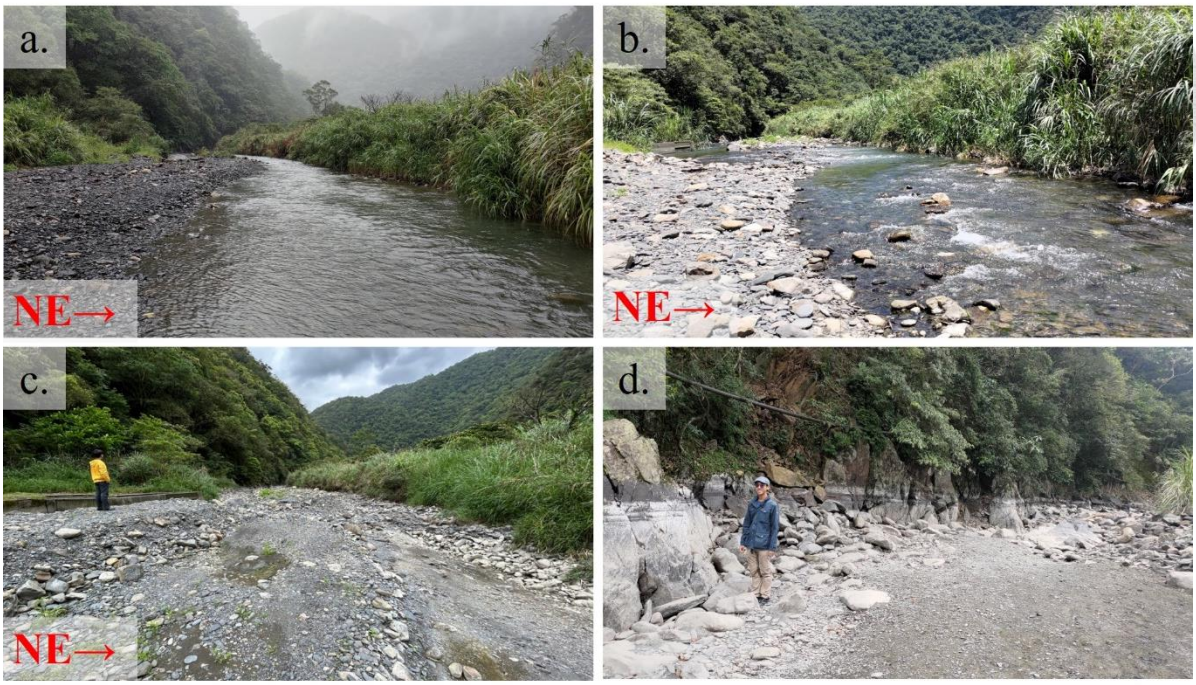


Figure 4.1 Riverbed with surface runoff at CK, taken on (a) 2022/9/25 and (b) 2023/6/26. Dry riverbed taken on 2023/4/9 in (c) and (d). Location at (d) is about 200 meters upstream from (a) to (c).


Figure 4.2 Dry riverbed at DG, picture taken on (a) 2022/7/7, (b) 2023/4/11, and (c) 2023/6/26. (d) DG river with surface runoff, 2023/9/11.



doi:10.6342/NTU202500428

### 4.1.2 On-site observations

On-site observations of the riverbed pebbles and bedrocks at each sample site generally match previous studies and the 1/50k geological map of Taiwan (Central Geological Survey, 2020). Riverbed pebbles and cobbles, and surrounding bedrock outcrops in the tributaries in the Hsuehshan Range mostly consist of sandstone, metasandstone, argillite, or slate. An example is the interbedded sandstone and thin mudstone at BB (Figure 4.3). There are yellow to orange colorations on the surfaces of large, grey metasandstone boulders at BY. This is an indication of weathered iron in the boulders there (Figure 4.4).

In the Central Range, metasandstone and slate are the major rock types. At sites SJ (Figure 4.5), TG, ML, dark colored slates of the Lushan Formation appear to contain weathered iron-containing minerals. At WRK, the rock types are more diverse than other sites in the Central Range. The pebbles and cobbles at WRK include vein quartz, black schist, green schist, marble, and metamorphic mafic rocks (Figure 4.6). These metamorphic rocks are consistent with the presence of the Tananao Schist in the drainage basin of WRK.



doi:10.6342/NTU202500428

Figure 4.3 Clear interbedded sandstone and mudstone outcrop at BB.

Figure 4.4 Yellow to orange coloration indicating weathering of iron on metasandstone boulders at BY.

Figure 4.5 Dark, laminated slate in Lushan Formation with well-developed slaty cleavage, SJ.



doi:10.6342/NTU202500428

Figure 4.6 Pebbles found in the riverbed at WRK. From right to left are black schist, marble, metamorphic mafic rock, siliceous schist, and a vein quartz at the top of the picture.

### 4.1.3 On-site measurements

We took preliminary measurements of temperature, pH, conductivity, and salinity on site during each sample collection; the results are shown in Table 4.1. Individual rivers do not produce drastic changes in pH, conductivity, and salinity between different seasons. The pH of each site among each campaign ranges between 6.5 and 8.6. Conductivities of each site vary from each campaign between 5 % to 16 %. Salinity varies between 0 ppt and 0.2 ppt.

Temperatures of riverine water vary depending on the weather. The high and low temperatures which were measured are consistent with the climate. Temperatures measured in winter and fall are lower than those in summer. The temperatures of hot spring waters are independent to the weather. As hot springs are groundwater bodies



doi:10.6342/NTU202500428

heated by geothermal circumstances, they were expected to be warmer than river waters. Hot spring waters are warmer than riverine waters with two exceptions. These occurred in September 2022 for BB; and in June 2023 for TG. These anomalies will be discussed at the end of this section.

Most riverine pH results were mildly basic, varying between 7.3 and 8.6, but the BB samples range from 6.5 to 7.7. BB samples are acidic in September in 2022, and April, June, and September in 2023. The hot spring waters at BB are acidic and are mostly lower in pH than the riverine waters at BB, ranging from 5.7 to 6.5. All the samples collected from TG hot spring are lower in pH than their riverine counterparts, ranging from 6.6 to 7.2. TG hot spring samples are acidic in July 2022 and April 2023. The pH at BB and TG show a larger seasonal variation. A possible explanation for this could be the influence of mixing between river water and hot spring water.

The conductivities of riverine water range from 54.0 to 596.0 μS/cm. Hot spring waters have significantly higher conductivities, ranging from 237.0 to 1160.0 μS/cm.

Salinity in riverine waters range between 0.0 and 0.2 ppt. Since rivers are fresh water bodies, the low salinities are expected. BY samples show a consistent 0.1 ppt in salinity. SJ and TG riverine waters range from 0.1 to 0.2 ppt, both rivers flow through known hot springs. The salinity of ML is consistently 0.1 ppt. The salinity in BB maintains at 0.0



doi:10.6342/NTU202500428

ppt. The hot spring samples fluctuate dramatically compared to riverine waters, ranging between 0.0 and 0.5 ppt.

In September 2022, BB-HS is cooler than BB. The pH and conductivity readings of the BB and BB-HS samples from this campaign did not display the same level of differences seen in other campaigns. Due to the typhoons that passed through before this campaign, the water level at BB was high and covered up the hot spring outcrops. The sampling was performed at the mainstream of BB, while a heat source was felt underwater. At that time, it was recognized as a potential hot spring output. However, from the measurements, these two samples likely show a mixing of river water and hot spring water. The BB hot spring water from that campaign had a 6.5 pH compared to the 5.7 to 5.8 of other samples, and the conductivity was 237.0 μS/cm, significantly lower than the other samples. The BB river water from that campaign had a pH of 6.5, the lowest of all samples, and the conductivity was 268.0 μS/cm, up to 50 % higher than the other samples. Thus, both samples are deemed invalid representations of respective bodies of water, and they are excluded from further calculations (Table 4.3).

In the June 2023 campaign, a temperature anomaly occurred in the TG and TG-HS samples. However, unlike the BB case in September 2022, the pH, conductivity support the fact that these two samples are distinctive from each other, and are consistent with



doi:10.6342/NTU202500428

previous patterns at the site. Therefore, even though it is unclear why the temperature of the two samples was inverted compared to other campaigns, we consider that they are valid and included them in further calculations.



doi:10.6342/NTU202500428

Table 4.1 On-site measurements by campaign, sites in the Hsuehshan Range.

| Sample site | Sample period | 22-Feb | 22-Jul | 22-Sep | 23-Apr | 23-Jun | 23-Sep |
|---|---|---|---|---|---|---|---|
| BY | Temperature (℃) | 15.3 | 25.9 | 24.3 | 21.8 | 24.9 | 20.7 |
| | pH | 8.3 | 8.3 | 8.2 | 8.1 | 8.2 | 8.0 |
| | Conductivity (μS/cm) | 429.0 | 438.0 | 434.0 | 476.0 | 436.0 | 399.0 |
| | Salinity (ppt) | 0.1 | 0.1 | 0.1 | 0.1 | 0.1 | 0.1 |
| BB | Temperature (℃) | 17.8 | 24.5 | 24.5 | 17.2 | 22.9 | 21.6 |
| | pH | 7.4 | 7.7 | 6.5 | 6.9 | 7.0 | 6.9 |
| | Conductivity (μS/cm) | 178.7 | 195.9 | 268.0 | 222.0 | 191.9 | 177.9 |
| | Salinity (ppt) | 0.0 | 0.0 | 0.0 | 0.0 | 0.0 | 0.0 |
| BB-HS | Temperature (℃) | - | 35.2 | 24.0 | 39.1 | 36.8 | - |
| | pH | - | 5.9 | 6.5 | 5.8 | 5.7 | - |
| | Conductivity (μS/cm) | - | 911.0 | 237.0 | 896.0 | 769.0 | - |
| | Salinity (ppt) | - | 0.4 | 0.0 | 0.4 | 0.3 | - |
| SL | Temperature (℃) | 15.5 | 24.5 | 21.6 | 16.6 | 21.7 | 21.2 |
| | pH | 7.7 | 7.5 | 7.4 | 7.6 | 7.4 | 7.3 |
| | Conductivity (μS/cm) | 69.4 | 77.4 | 54.0 | 80.1 | 82.0 | 74.8 |
| | Salinity (ppt) | 0.0 | 0.0 | 0.0 | 0.0 | 0.0 | 0.0 |
| JL | Temperature (℃) | - | - | 24.1 | 18.6 | 24 | 22.1 |
| | pH | - | - | 7.5 | 7.9 | 7.7 | 7.4 |
| | Conductivity (μS/cm) | - | - | 100.8 | 130.3 | 121.0 | 103.4 |
| | Salinity (ppt) | - | - | 0.0 | 0.0 | 0.0 | 0.0 |
| CK | Temperature (℃) | 18.3 | 27.8 | 22.8 | - | 25.1 | 22.4 |
| | pH | 7.8 | 8.5 | 8.1 | - | 7.8 | 7.4 |
| | Conductivity (μS/cm) | 93.8 | 110.9 | 99.6 | - | 101.6 | 82.9 |
| | Salinity (ppt) | 0.0 | 0.0 | 0.0 | - | 0.0 | 0.0 |



doi:10.6342/NTU202500428

Table 4.1 (Continued) Sites in the Central Range.

| Sample site | Sample period | 22-Feb | 22-Jul | 22-Sep | 23-Apr | 23-Jun | 23-Sep |
|---|---|---|---|---|---|---|---|
| SJ | Temperature (℃) | 15.6 | 23.3 | 22.6 | 16.2 | 21.1 | 19.4 |
| | pH | 8.6 | 8.5 | 8.4 | 8.4 | 8.3 | 8.3 |
| | Conductivity (μS/cm) | 426.0 | 432.0 | 371.0 | 500.0 | 412.0 | 348.0 |
| | Salinity (ppt) | 0.1 | 0.1 | 0.1 | 0.2 | 0.1 | 0.1 |
| TG | Temperature (℃) | 19.2 | 27.0 | 26.4 | 21.7 | 24.7 | 29.8 |
| | pH | 7.7 | 8.0 | 7.7 | 7.8 | 8.0 | 7.4 |
| | Conductivity (μS/cm) | 543.0 | 342.0 | 518.0 | 596.0 | 479.0 | 491.0 |
| | Salinity (ppt) | 0.2 | 0.1 | 0.2 | 0.2 | 0.2 | 0.2 |
| TG-HS | Temperature (℃) | - | 28.2 | 26.9 | 22.7 | 23 | - |
| | pH | - | 6.6 | 7.2 | 6.7 | 7.2 | - |
| | Conductivity (μS/cm) | - | 1160.0 | 704.0 | 869.0 | 573.0 | - |
| | Salinity (ppt) | - | 0.5 | 0.3 | 0.4 | 0.2 | - |
| ML | Temperature (℃) | 16.8 | 24.7 | - | 18.1 | 24.5 | 22.9 |
| | pH | 8.5 | 8.3 | - | 8.3 | 8.2 | 8.1 |
| | Conductivity (μS/cm) | 364 | 315.0 | - | 421.0 | 377.0 | 333.0 |
| | Salinity (ppt) | 0.1 | 0.1 | - | 0.1 | 0.1 | 0.1 |
| DG | Temperature (℃) | 17.7 | - | 26.1 | - | - | 23.3 |
| | pH | 8.1 | - | 7.8 | - | - | 7.5 |
| | Conductivity (μS/cm) | 203.0 | - | 224.0 | - | - | 231.0 |
| | Salinity (ppt) | 0.0 | - | 0.0 | - | - | 0.0 |
| XL | Temperature (℃) | 15.8 | 27.1 | 24.1 | 21.2 | 26.5 | 23.3 |
| | pH | 7.6 | 7.7 | 7.5 | 7.5 | 7.4 | 7.4 |
| | Conductivity (μS/cm) | 66.7 | 89.3 | 61.6 | 86.8 | 85.0 | 71.1 |
| | Salinity (ppt) | 0.0 | 0.0 | 0.0 | 0.0 | 0.0 | 0.0 |
| WRK | Temperature (℃) | 17.1 | 30.7 | 25.5 | 21.7 | 26.6 | 24.6 |
| | pH | 8.1 | 8.2 | 7.9 | 8.0 | 8.0 | 7.8 |
| | Conductivity (μS/cm) | 140.7 | 215.0 | 151.2 | 218.0 | 194.6 | 172.4 |
| | Salinity (ppt) | 0.0 | 0.0 | 0.0 | 0.0 | 0.0 | 0.0 |



doi:10.6342/NTU202500428

## 4.2 Ion results

### 4.2.1 Measured concentration results

The water samples from all sites produced chloride ($Cl^-$), sulfate ($SO_4^{2-}$), sodium (Na), magnesium (Mg), and calcium (Ca) results successfully. Several potassium (K) results were below the detection limit. The sites closer to sea, such as CK, DG, XL, and WRK, have lower K content. Nitrate and phosphate were below the detection limit, showing that anthropogenic pollution is minimal in this region. Anion and cation concentrations before atmospheric correction is listed in Table 4.2. The detailed results of individual samples are listed in appendix Table A.3 and Table A.4.



doi:10.6342/NTU202500428

Table 4.2 Average concentrations of riverine samples (uncorrected).

| Sample site | $Cl^-$ (μM) | $SO_4^{2-}$ (μM) | Na (μM) | Mg (μM) | K (μM) | Ca (μM) |
|---|---|---|---|---|---|---|
| BY | 19.2 ± 5.7 | 1370.9 ± 112.2 | 161.5 ± 28.9 | 859.4 ± 60.9 | 47.8 ± 6.3 | 531.8 ± 73.2 |
| BB | 34.7 ± 11.3 | 467.0 ± 62.2 | 147.8 ± 26.0 | 273.8 ± 26.0 | 15.5 ± 2.8 | 235.2 ± 35.1 |
| SL | 39.5 ± 8.1 | 115.6 ± 18.0 | 92.1 ± 12.8 | 98.0 ± 15.0 | 10.7 ± 1.9 | 77.2 ± 12.4 |
| JL | 54.3 ± 7.4 | 155.2 ± 15.4 | 124.9 ± 18.1 | 150.9 ± 20.4 | 10.9 ± 2.1 | 133.7 ± 24.6 |
| CK | 76.3 ± 11.9 | 102.8 ± 11.4 | 159.0 ± 23.1 | 107.2 ± 15.0 | 9.1 ± 1.7 | 118.0 ± 19.4 |
| SJ | 21.6 ± 5.2 | 590.5 ± 70.6 | 568.5 ± 227.1 | 872.5 ± 66.6 | 23.9 ± 3.9 | 424.2 ± 60.7 |
| TG | 26.3 ± 9.6 | 784.0 ± 70.7 | 490.9 ± 205.5 | 939.2 ± 159.3 | 38.3 ± 14.1 | 604.2 ± 114.1 |
| ML | 33.3 ± 9.4 | 624.8 ± 92.9 | 197.3 ± 37.7 | 714.5 ± 79.7 | 19.8 ± 1.7 | 440.8 ± 68.8 |
| DG | 83.2 ± 7.1 | 337.2 ± 41.0 | 148.8 ± 12.6 | 233.7 ± 12.2 | 10.2 ± 3.0 | 343.9 ± 24.1 |
| XL | 84.6 ± 8.3 | 85.9 ± 13.2 | 171.6 ± 15.1 | 81.7 ± 15.2 | 4.8 ± 1.9 | 75.4 ± 16.2 |
| WRK | 103.7 ± 12.0 | 99.7 ± 15.4 | 167.9 ± 22.6 | 46.8 ± 8.1 | 22.7 ± 3.6 | 332.6 ± 77.5 |



doi:10.6342/NTU202500428

### 4.2.2 Rainwater results

In this study, we collected rainwater samples to represent atmospheric input. In total, 46 rainwater samples were processed. Anion and cation concentrations in rainwater fluctuate vastly. Detailed results for each rainwater sample are listed in appendix Table A.1 and Table A.2.

The precipitation of rain is a primary process for atmospheric substance to deposit on land in Taiwan; thus, rainwater is selected to represent the atmospheric input of ions in rivers. Deposition of airborne particles by rainfall is the main source of riverine chloride due to the lack of evaporites in Taiwan (Ho, 1975). Such particles in the atmosphere may originate from the ocean, a major chlorine reservoir. Seasalt aerosols created by waves leave the ocean surface, and transform to volatile products of chlorine such as hydrogen chloride (HCl) and chlorine ($Cl_2$) in the troposphere. Subsequently, chlorine could deposit over land through rainfall (Graedel and Keene, 1996).

The ion concentrations of rainwater samples are shown in Figure 4.7. The dissolved ions in rainwater display drastic variations in concentration. The fluctuating concentrations could be seasonally dependent, or the result of weather events and pollution. For this study, the rainwater data is used only to calculate a representation of atmospheric input. Hence, we will not discuss rainwater characteristics in depth. However,



doi:10.6342/NTU202500428

to obtain atmospheric representation, it is necessary to rule out obviously contaminated samples. Cation concentrations of sample 20220607 are 3 orders of magnitude greater than other samples (Figure 4.7). After consulting with YLHS, we found that there was a human error during the collecting of this sample, thus it was excluded from further calculations.

To calculate accurate average concentrations, we applied the analytic method in Section 3.2.3. The outliers are values exceeding the upper bound or lower bound. Outliers with extreme concentration values were identified, and were excluded from the calculations for average (appendix Table A.1, outlier data are in *Italic*). Due to natural variations of the ion concentrations, each ion were independently calculated for outliers, as well as the average concentration and standard deviation. The average ion concentrations are presented in Table 4.3.

Table 4.3 The average concentrations of major ions in rainwater.

| | $Cl^-$ | $SO_4^{2-}$ | Na | Mg | K | Ca |
|---|---|---|---|---|---|---|
| Average (μM) | 24.9 | 4.2 | 27.9 | 3.7 | 3.3 | 3.5 |
| STD (μM) | 26.1 | 1.7 | 12.7 | 3.2 | 1.4 | 2.0 |

Data of polluted events and extreme values were excluded from this calculation. Atmospheric correction for riverine data is based on this set of data.



doi:10.6342/NTU202500428

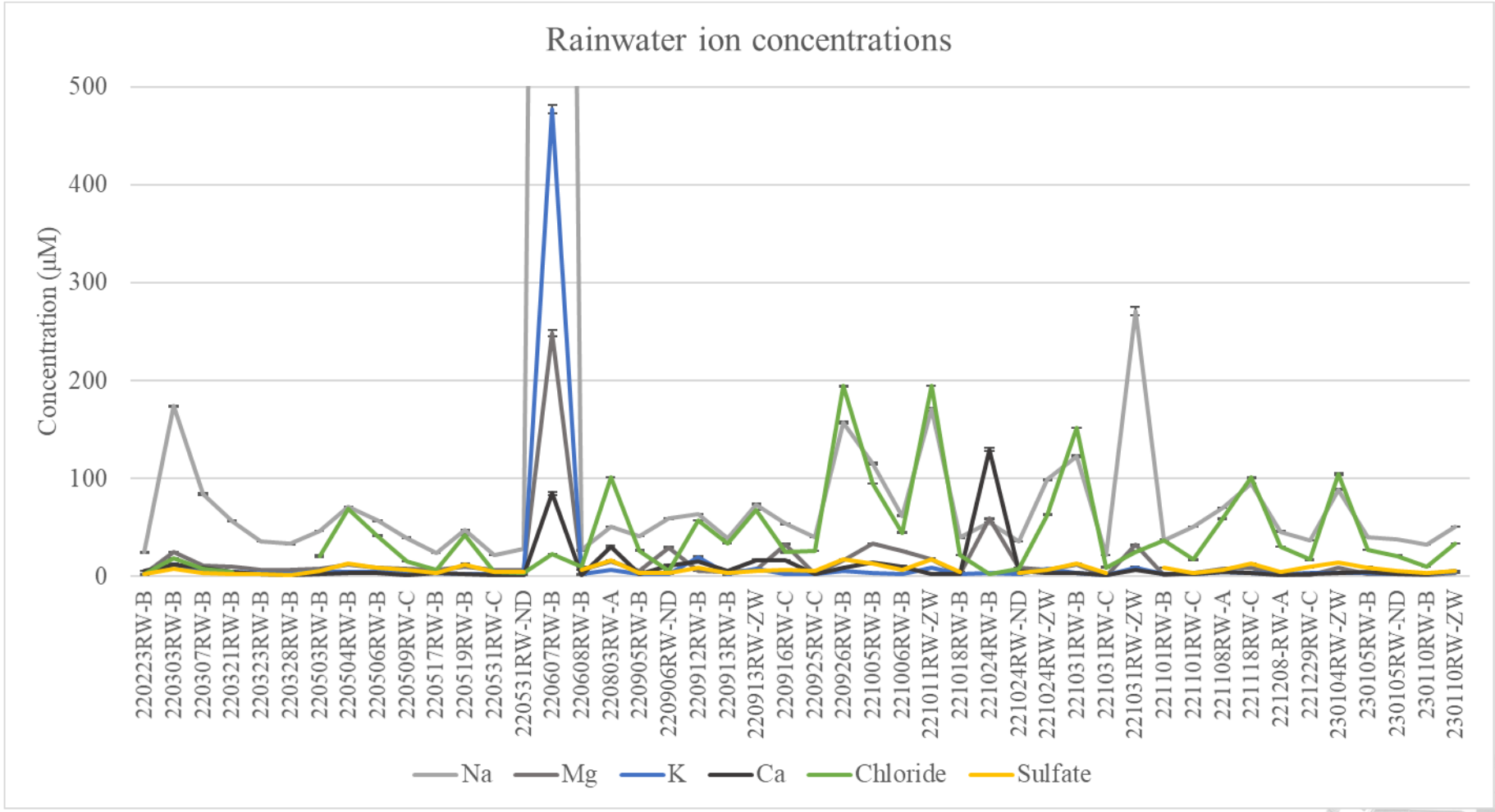


Figure 4.7 Concentrations of Na, Mg, K, Ca, $Cl^-$, and $SO_4^{2-}$ measured from rainwater samples.



doi:10.6342/NTU202500428

### 4.2.3 Atmospheric correction with chloride

Although we obtained the average ion concentrations for rainwater after the analysis, we need additional support for the data to represent atmospheric input accurately. The first evidence is the lack of evaporite in Taiwan (Ho, 1975), which means that riverine chloride should mainly originate from atmospheric deposition.

To further support this argument, we examined the riverine chloride results. Chloride concentrations in river waters ranges between 12 and 130 μM (Figure 4.8, appendix Table A.3), much lower than the world average of 487 μM (calculated from Burke et al., 2018). The world average was calculated from global rivers, including dry in-land rivers and rivers that flow through evaporite deposits. For example, the highest concentration was measured from the Colorado River, at 5114 μM (Burke et al., 2018). However, there are no in-land rivers, nor are there large evaporite deposits in Taiwan. Therefore, it is reasonable that the chloride concentrations in this region are lower than the world average.

It is noteworthy that there is an eastward increase in average riverine chloride concentrations (Figure 4.9). To investigate further, we plotted riverine chloride concentrations against the distances between the sample site and coastline (Figure 4.10). The distances were measured northeastwardly, following the general trend of the river valley and the direction of the seasonal monsoon. The spatial relationship demonstrates



doi:10.6342/NTU202500428

that chloride concentrations in rivers decrease with the increase of distance to the sea. This pattern clearly supports the idea that riverine chloride is provided by the sea, via atmospheric deposition. Therefore, it can be confidently concluded that the chloride in riverine water comes predominantly from the atmosphere, and can be used to correct the riverine sulfate and cation concentrations with Equation 4-1:

$$[X]_{atmos} = [Cl^-]_{river} \times [X/Cl^-]_{rain} \quad (4\text{-}1)$$

Where $[X]_{atmos}$ is the atmospheric contribution of ion X to rivers . $[Cl^-]_{river}$ is the riverine chloride concentration. $[X/Cl^-]_{rain}$ is the average rainwater X to chloride ratio.



doi:10.6342/NTU202500428

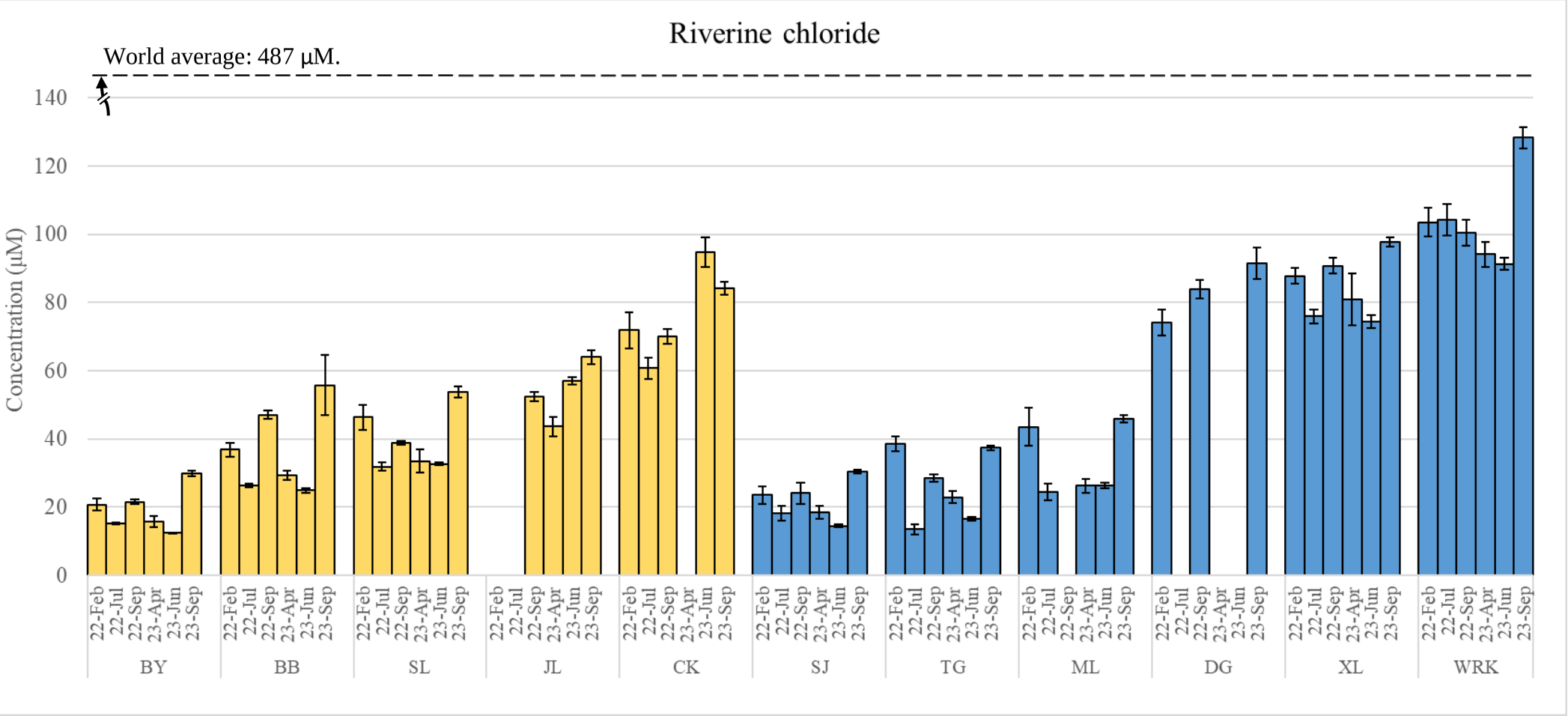


Figure 4.8 Chloride concentration by campaign. Bars in yellow are sample sites located in the Hsuehshan Range, blue bars are samples sites in the Central Range. The world average is calculated from Burke et al., 2018.

doi:10.6342/NTU202504428

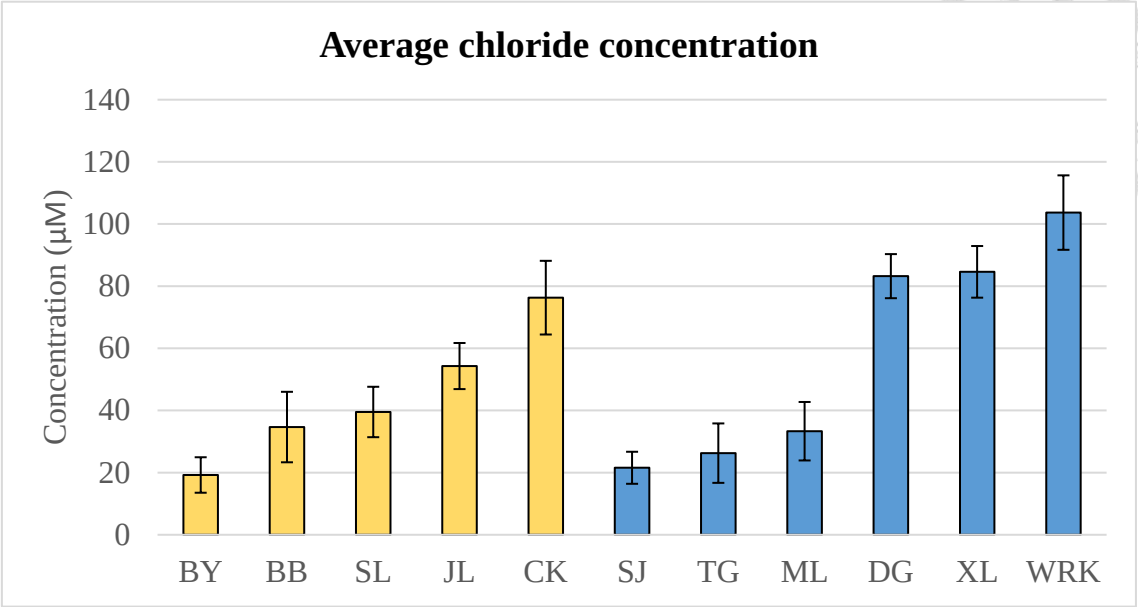


Figure 4.9 Average riverine chloride concentration. Yellow bars are sites located in the Hsuehshan Range; blue bars are sites in the Central range. The bars are arranged in an eastward direction from left to right.

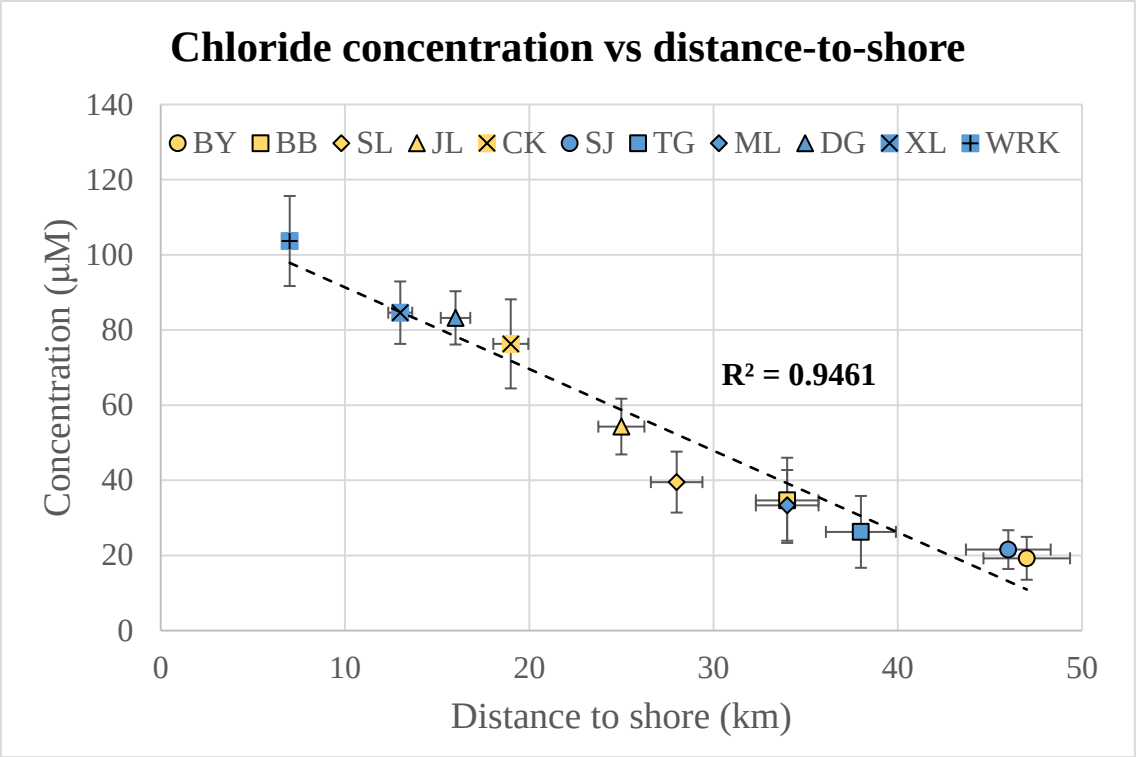


Figure 4.10 Riverine chloride concentrations versus distances between the sample sites and the coastline. Yellow points are in the Hsuehshan Range; blue points are in the Central Range. A negative correlation is clear from the plot. The error for distances is set at 5 %.



doi:10.6342/NTU202500428

### 4.2.4 Corrected riverine concentration results

Using chloride and average rainwater concentrations, we corrected all the riverine concentration results. The average sulfate concentrations range from 71.2 μM to 1404.3 μM (Table 4.4) after atmospheric correction. Anion concentrations from each campaign are shown in appendix Table A.3. After atmospheric correction, the maximum sulfate concentration is 1532.0 ± 39.1 μM, and the minimum is 50.0 ± 2.8 μM. Some sulfate concentrations are higher than world average of 300 μM (Burke et al., 2018), but the average sulfate concentration of 5 sites are below the estimated world average.

Mg and Ca are the main cation constituents in riverine water. The average cation concentrations, with atmospheric correction, are listed in Table 4.4. Cation results for each site are shown in appendix Table A.4 (uncorrected) and Table A.5 (corrected). Mg is more abundant at BY, BB, SL, JL, SJ, TG, and ML. After atmospheric correction, the maximum Mg concentration is 1054.5 ± 7.4 μM, and the minimum is 20.9 ± 3.4 μM. Ca is comparable in concentrations with Mg at several sites. Ca is the second most plentiful riverine cation in 7 out of 11 sites, and is the most prominent cation at CK, DG, and WRK. After atmospheric correction, the maximum Ca concentration is 739.3 ± 1.7 μM, and the minimum is 46.3 ± 3.4 μM.

After atmospheric correction, the maximum Na concentration is 974.7 ± 11.6 μM, and the minimum is 3.0 ± 26.3 μM. Na is the most common cation at XL. At SJ, the Na



doi:10.6342/NTU202500428

concentration is comparable to that of Ca. K is the least common major cation. In some cases, K is below detection limit. After atmospheric correction, the maximum K concentration is 66.1 ± 0.4 μM. At DG and XL, K concentrations are negative after conducting atmospheric correction, and these results are treated as zero. This illustrates the scarcity of geologically supplied K in some regions.



doi:10.6342/NTU202500428

Table 4.4 Average concentrations of riverine samples (corrected).

| Sample site | $SO_4^{2-}$ (μM) | Na (μM) | Mg (μM) | K (μM) | Ca (μM) |
|---|---|---|---|---|---|
| BY | 1367.7 ± 112.9 | 139.9 ± 33.8 | 856.5 ± 61.4 | 45.2 ± 6.8 | 529.1 ± 73.1 |
| BB | 461.1 ± 63.6 | 108.9 ± 29.9 | 268.7 ± 27.4 | 10.9 ± 3.8 | 230.4 ± 35.4 |
| SL | 108.9 ± 17.7 | 47.7 ± 20.9 | 92.2 ± 15.6 | 5.5 ± 2.8 | 71.7 ± 12.4 |
| JL | 146.0 ± 16.1 | 63.9 ± 25.8 | 142.9 ± 21.2 | 3.9 ± 2.8 | 126.2 ± 25.4 |
| CK | 89.9 ± 11.3 | 73.3 ± 25.6 | 95.8 ± 16.0 | 1.6 ± 1.3 | 107.3 ± 20.9 |
| SJ | 586.8 ± 71.1 | 544.3 ± 230.8 | 869.3 ± 67.1 | 21.1 ± 4.4 | 421.2 ± 60.7 |
| TG | 779.6 ± 71.0 | 461.4 ± 199.3 | 935.3 ± 158.5 | 34.8 ± 14.7 | 600.6 ± 113.2 |
| ML | 619.1 ± 93.7 | 159.9 ± 42.9 | 709.6 ± 79.8 | 15.5 ± 2.9 | 436.2 ± 68.7 |
| DG | 323.0 ± 39.8 | 55.3 ± 15.7 | 221.3 ± 12.0 | 1.7 ± 1.7 | 332.3 ± 23.2 |
| XL | 71.5 ± 14.0 | 76.5 ± 23.7 | 69.2 ± 16.2 | 0.0 | 63.6 ± 16.7 |
| WRK | 82.0 ± 15.2 | 52.2 ± 32.3 | 31.5 ± 8.8 | 9.1 ± 3.9 | 318.2 ± 77.7 |

Sulfate and cations are corrected with atmospheric input.



doi:10.6342/NTU202500428

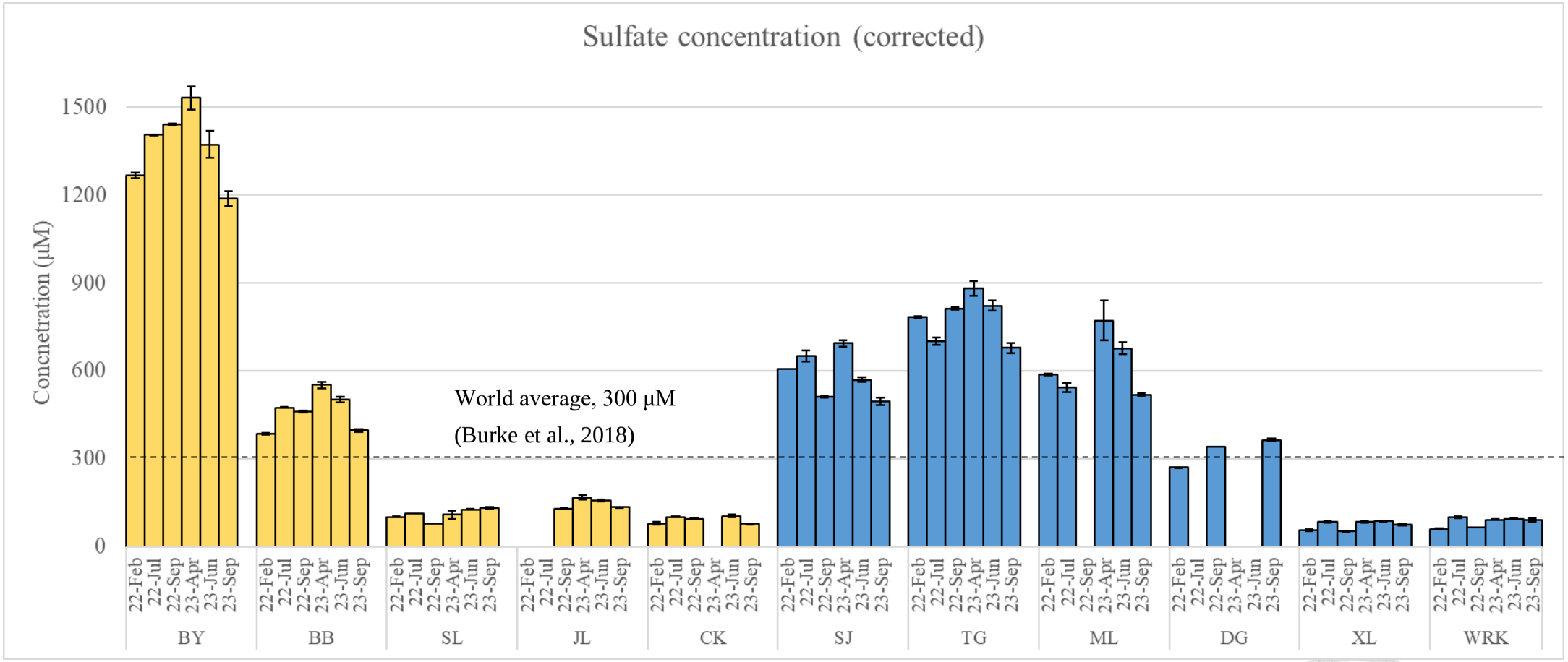


Figure 4.11 Sulfate concentration (corrected) by campaign. Bars in yellow are sample sites located in the Hsuehshan Range, blue bars are samples sites in the Central Range.

doi:10.6342/NTU202504428

### 4.2.5 Hot spring water

There are six documented hot spring outcrops in this study area: Bonbon, Paigu, Cingshuei, Renze, Tiangou, and Siji (water resources department, Yilan County; Water Resources Agency, Minister of Economics). Due to limited accesses, we have only taken direct samples from the suspected hot spring outcrops of BB and TG. Four samples from BB and TG hot springs were taken.

Results from hot spring waters show higher anion and cation concentrations compared to nearby riverine samples. The average concentrations are shown in Table 4.5. The anion results by campaign are shown in appendix Table A.6. Hot spring cation results by campaign are shown in appendix Table A.7.

After atmospheric correction, the chloride concentrations at both BB and TG are just over 100 μM. The average chloride concentration at BB hot spring is 112.0 ± 10.4 μM, almost 4 times greater than the BB riverine concentration. Similarly, the TG-HS concentration, 115.4 ± 36.0 μM, is about 4 times higher than the riverine TG average.

Hot spring sulfate concentrations are higher than their riverine counterparts. The average sulfate concentration of BB-HS is 657.2 μM, compared to 455.0 μM of riverine BB. The average sulfate concentration of TG hot spring is 965.4 μM, compared to 789.3 μM of riverine TG. Na is the most abundant cation in BB hot spring. At TG, Mg is the most abundant cation, followed by Ca.



doi:10.6342/NTU202500428

Table 4.5 Average concentrations for hot spring samples.

| Sample site | Cl (μM) | $SO_4^{2-}$ (μM) | Na (μM) | Mg (μM) | K (μM) | Ca (μM) |
|---|---|---|---|---|---|---|
| BB - HS | 112.0 ± 10.4 | 657.2 ± 46.3 | 5531.4 ± 646.8 | 474.6 ± 51.6 | 291.2 ± 76.3 | 420.2 ± 81.3 |
| TG - HS | 115.4 ± 36.0 | 965.4 ± 76.6 | 2461.9 ± 2161.7 | 1235.4 ± 116.4 | 55.0 ± 33.3 | 875.7 ± 238.0 |



doi:10.6342/NTU202500428

# Chapter 5 Discussion

## 5.1 Water – rock relationship

### 5.1.1 Anthropogenic and atmospheric sources of sulfate

Riverine sulfate originates from various sources. Nitrate and phosphate concentrations are low or undetectable, thus sulfate supplied by anthropogenic pollution is minimal and can be neglected.

Like chloride and other ions, atmospheric deposition could be another source for riverine sulfate. Although we have established the basis for atmospheric correction, we want to further understand the magnitude of atmospheric contribution to sulfate. To achieve this, we plotted average sulfate concentrations against the distances between the sample sites and the coastline (Figure 5.1), following the same process of chloride. There appears to be a relatively positive correlation between sulfate concentrations and the distances to the coast. The trend is opposite to that of chloride, which is negatively correlated to the distances to the coastline. This opposite trend from that of chloride suggests that riverine sulfate may not be mainly contributed by the sea through atmospheric deposition.



doi:10.6342/NTU202500428

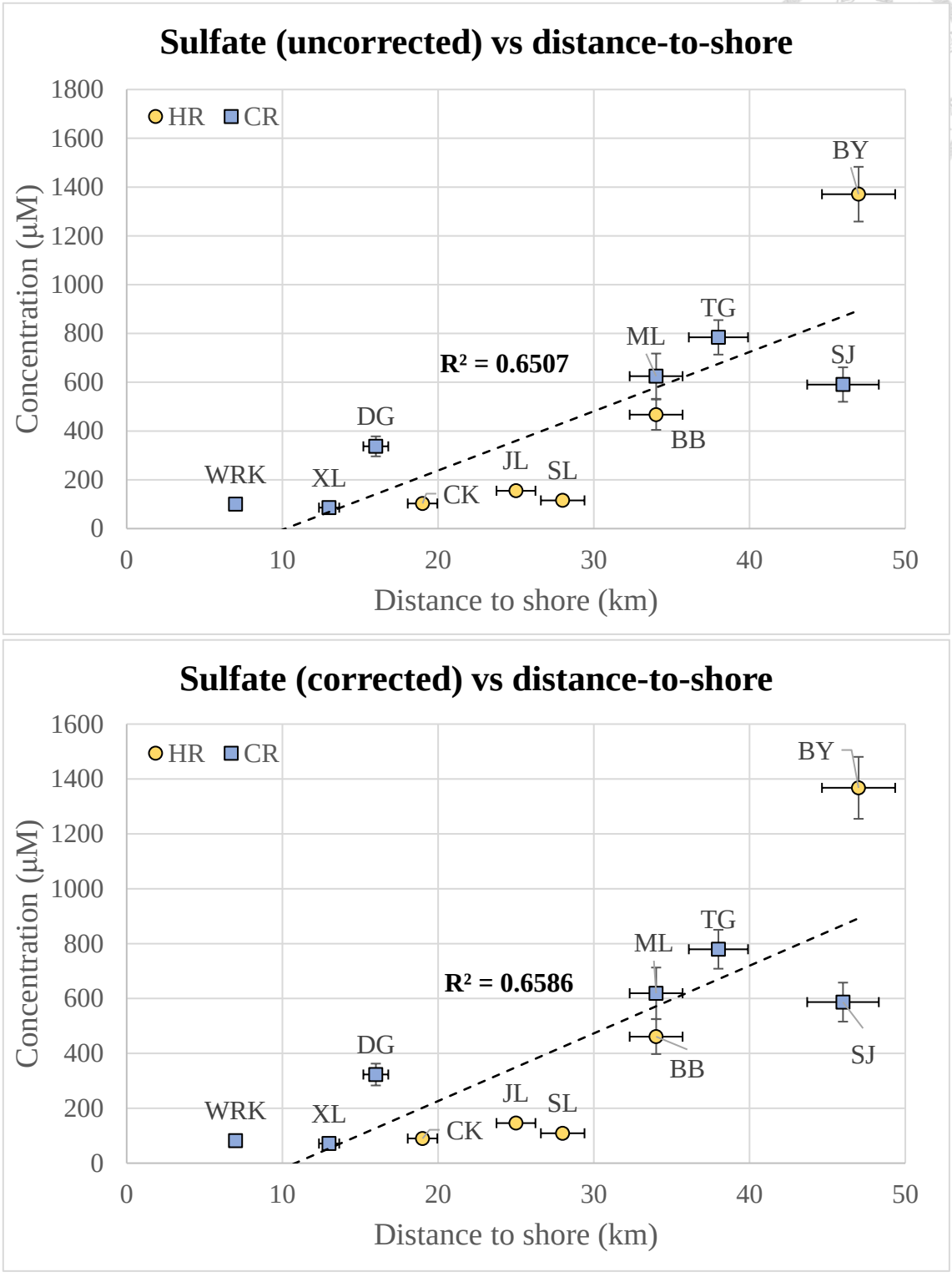


Figure 5.1 Average sulfate concentrations vs distance-to-shore. The top figure is the comparison between uncorrected sulfate data and distance-to-shore. The bottom figure is the comparison with corrected data. The black dashed line are the trend lines of all data.



doi:10.6342/NTU202500428

This is also supported by the differences in average sulfate concentrations before and after correction, which are marginal (Figure 5.2). Hence, although atmospheric deposition may contribute to the sulfate content in rivers in the study area, it is not the main supplier. The positive trend between sulfate concentrations and the distances to the coast, however, suggests that some additional factors may control the amount of riverine sulfate, which will be discussed further.

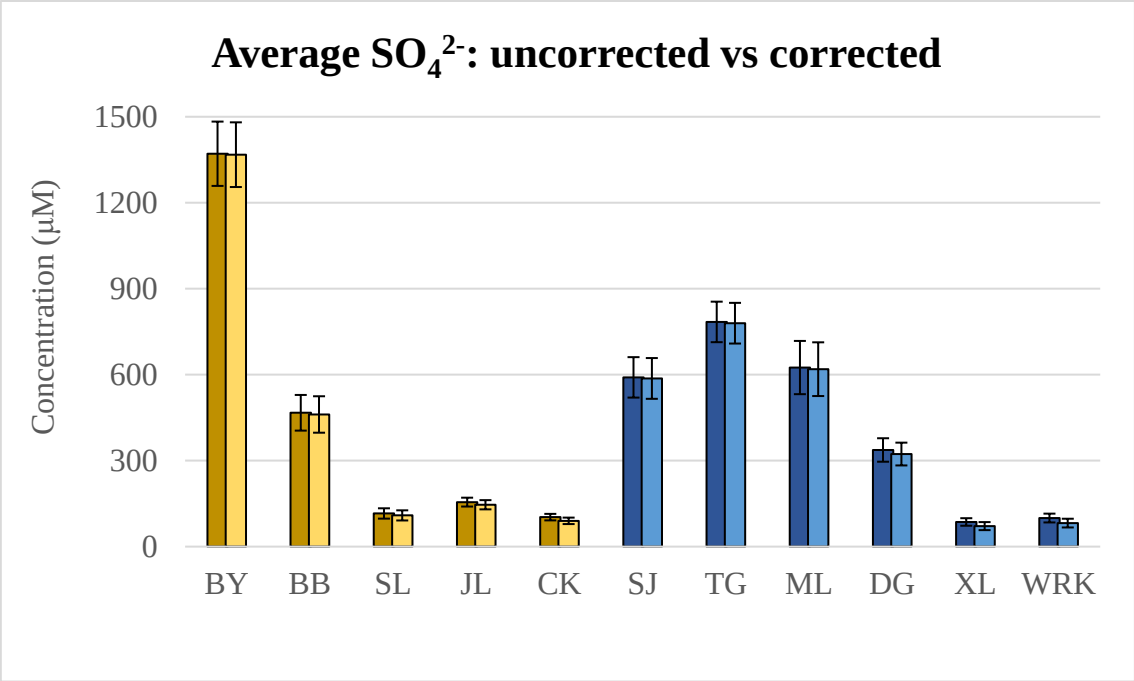


Figure 5.2 Comparison between uncorrected and corrected average sulfate concentrations. Hsuehshan samples are in yellow, Central Range samples are in blue. For each site, the uncorrected data is the left bar, the atmospheric corrected data is the right bar.



doi:10.6342/NTU202500428

### 5.1.2 Cation end-member

Since anthropogenic pollution and atmospheric deposition are not the main contributor to riverine sulfate, we proceed to consider the geological sources of riverine sulfate. The end member model of Mg and Ca provides an insight to the chemical weathering paths of the rocks. Gaillardet and others (1999) calculated the ranges of molar ratio for silicates, carbonates, and evaporites weathering paths based on worldwide large rivers. For a river that flows through a monolithic drainage basin, the Mg/Na and Ca/Na ratios maintain within certain ranges (Table 5.1).

Table 5.1 End-member molar ratio (±2 s.d.) for silicates, carbonates, and evaporites.

| Molar Ratio | Mg/Na | Ca/Na |
|---|---|---|
| Silicate | 0.25 ± 0.20 | 0.35 ± 0.25 |
| Carbonate | 30 ± 15 | 60 ± 30 |
| Evaporite | 0.10 ± 0.08 | 0.50 ± 0.50 |

(Modified from Burke et al., 2018).



doi:10.6342/NTU202500428

The atmospheric corrected molar ratios of riverine data from this study are plotted in the end-member model (Figure 5.3). There is no data in or near the evaporite weathering domain, again consistent with the fact that evaporites are absent in the bedrocks of the region. This is also consistent with geology reports (Ho, 1975) and the chloride results (Section 4.2.2). Sulfate evaporites, such as gypsum, is thus unlikely to be the main source of riverine sulfate. Hence, the major sulfate contributor for rivers would most likely be sulfides, such as pyrite, in the bedrocks that make up the drainage basins.

In the end-member model, almost all of the data points lie on a linear trend between the carbonate and the silicate weathering domains. The distribution of the data in the plot shows a mixture of silicate and carbonate weathering. The Mg/Na ratios are between 0.4 and 10, and Ca/Na ratios are between 0.5 and 10. Since the bedrocks in this area are composed of the sedimentary rocks and low-grade metamorphic rocks, the result is consistent with the local geology. However, there is no clear distinction between the samples from the Hsuehshan Range and the Central Range. Moreover, apart from the WRK samples, which deviates from the rest, there seems to be no pattern related to the diversity of the rock formations in the area.



doi:10.6342/NTU202500428

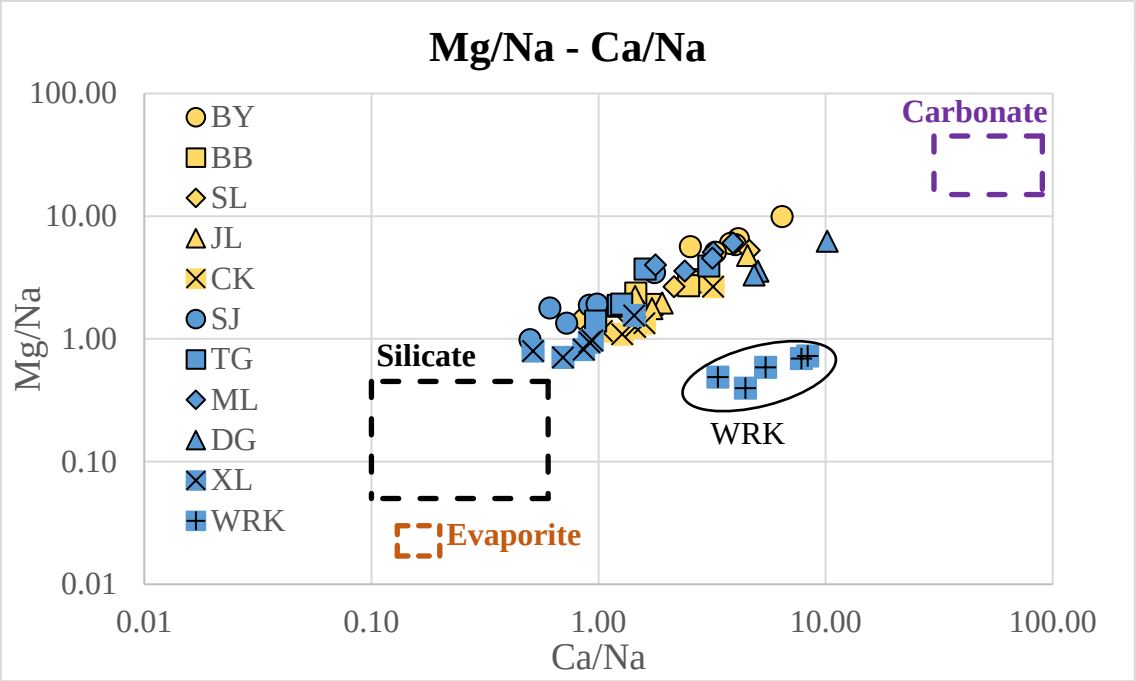


Figure 5.3 End-member weathering model in logarithmic scale. Cations concentrations had been corrected with atmospheric input.

To understand the chemical weathering characteristics on a grander scale, we compared our results with previous studies from Taiwan (Figure 5.4). We chose data from the Gaoping River (Blattman et al., 2019) and the Beinan River (Wang, 2019) for comparison. The Gaoping and the Beinan river systems flow out of the southern Central Range, whereas some of the tributaries in this study originate from the northern Central Range. The distribution of our data in the figure is apparently different from the Gaoping and the Beinan river systems. This could be explained by the differences in lithological composition of the drainage basins. The northern Central Range tributaries in this study predominantly flow through the Lushan Formation. Meanwhile, the Tananao Schist and



doi:10.6342/NTU202500428

the Pilushan Formation are more prominent in the southern Central Range (CGS; Blattmann et al., 2019; Wang, 2019). Interestingly, the WRK samples are from the only drainage basin in this study where the Tananao Schist is also present. This could be the reason why the WRK samples show characteristics closer to the Beinan River and the Gaoping River instead of the other tributaries in this study.

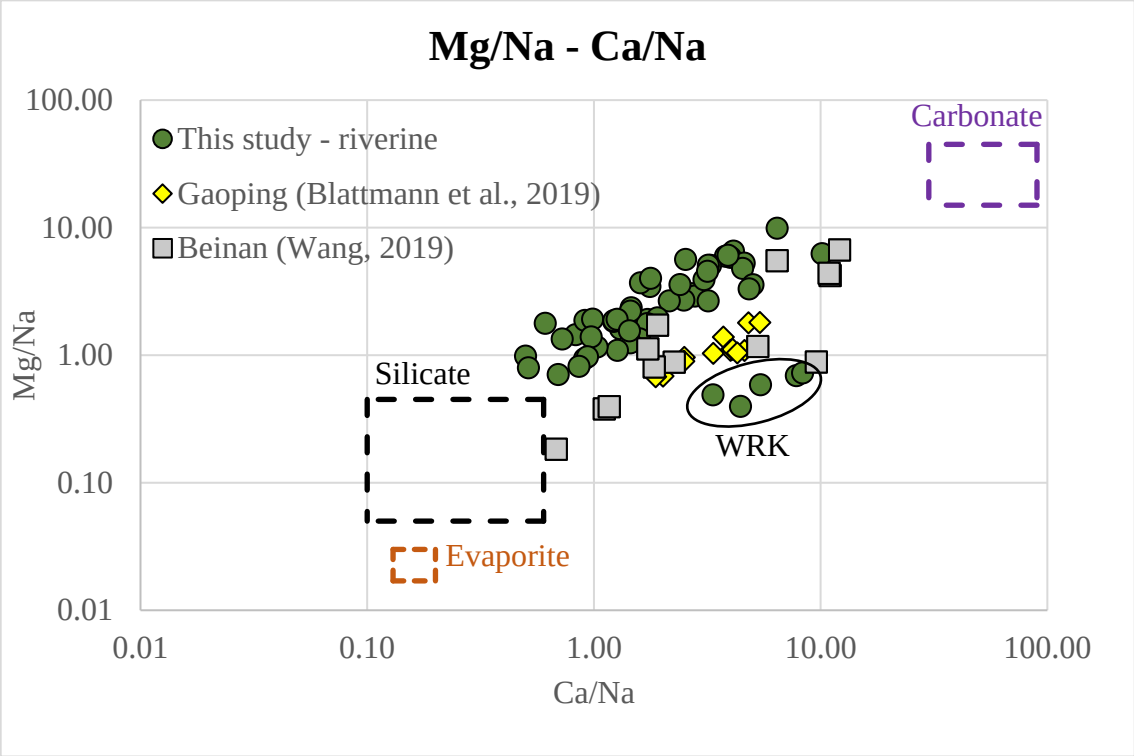


Figure 5.4 End-member model comparison of this study and previous studies.



doi:10.6342/NTU202500428

In this region, apart from WRK, the cation compositions in the tributaries are not different enough to show specific characteristics or differences between the basins in the two ranges or with various rock formations. However, if the degree of difference in lithology is large enough, chemical composition of river waters may begin to show some differences. This is shown by the WRK samples in this study and the differences between the northern and southern Central Range.

### 5.1.3 Characteristics of sulfate concentration

After atmospheric correction, the minimum average sulfate concentration was measured at XL in the Central Range, and the maximum was measured at BY in the Hsuehshan Range (Table 4.4, Figure 5.5). The average concentrations of sites BY, BB, SJ, TG, ML, and DG exceed the world average (300 μM, Burke et al., 2018), ranging between 1 to nearly 5 times higher. However, SL, JL, CK, XL, and WRK samples produced results only around 20 % to 50 % of the world average.



doi:10.6342/NTU202500428

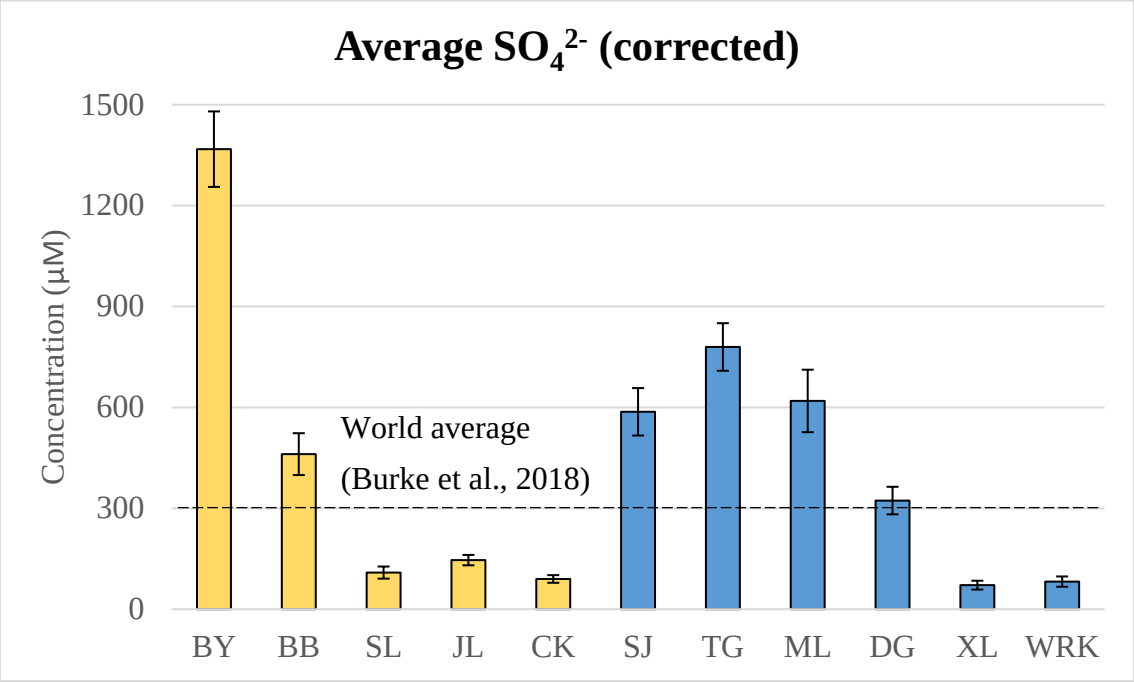


Figure 5.5 Average sulfate concentration, atmospheric corrected. Yellow bars are sites located in the Hsuehshan Range; blue bars are sites in the Central range. The bars are arranged in an eastward direction from left to right.

No distinguishable characteristics or trends in sulfate concentrations can separate the Hsuehshan Range samples from the Central Range ones. The sites with high sulfate concentrations are not collectively located in the same mountain range; instead, they are situated in the upper stream of Lanyang River. The upper stream tributaries are at higher altitudes in the mountains, as shown by the positive trend between sulfate concentrations and the distances to the coastline (Figure 5.1). A possible interpretation for this trend is that the rocks exposed in these basins could come from the deeper part of the rock formations, and may have recorded relatively recent geothermal activities.



doi:10.6342/NTU202500428

### 5.1.4 Sulfate versus cation

Although neither sulfate data nor cation analyses can clearly distinguish the Central Range samples from the Hsuehshan Range ones, interesting patterns are revealed when we plot cations against sulfate.

In Figure 5.6, we plotted the sum of Na and K concentrations against sulfate concentrations. The plot provides us with three groups of distinct behaviors. Group A has a tight distribution, which includes SL, JL, CK, XL, and WRK samples. These sites are in the downstream region, with low sulfate, Na, and K concentrations. Group B includes the scattered distribution of BB, SJ, TG, ML, and DG samples. Additionally, there are known hot spring outcrops in the basins of BB, SJ, and TG. Although there was no hot spring records in ML, this river flows between Chingshui Geothermal Park (清水地熱公園) and Jiuzhize Hot Spring (鳩之澤溫泉). Therefore, there may be some unreported hot spring in the ML basin, or its behavior is the result of geothermal influence nearby. DG is a part of Group B due to the separation of its data from Group A. There is no documented hot spring in the DG basin. Whether DG is under hot spring influence is uncertain. If there is, the effect on its chemical properties may be limited since the DG data is distributed between Group A and the rest of Group B. Finally, the BY samples stand out from the rest with high sulfate concentrations, categorized as Group C.



doi:10.6342/NTU202500428

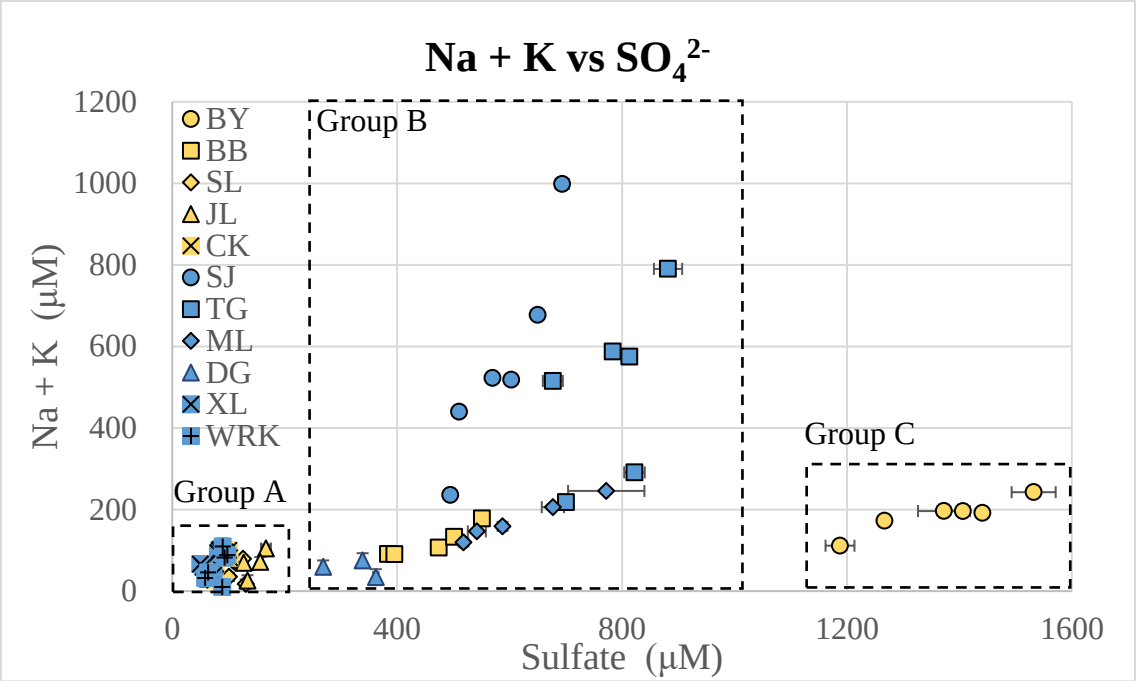


Figure 5.6 The sum of Na and K concentrations versus sulfate concentration.

Figure 5.8 compares the concentrations between sulfate and the sum of Mg and Ca. This comparison shows the different weathering paths of the reactions between sulfuric acid and minerals. The sum of Mg and Ca represents the dissolved materials of carbonates and silicates, and sulfate represents sulfuric acid. When sulfuric acid reacts and dissolves carbonates, the following reactions take place (Torres et al., 2016):

$$\text{Carbonates} + H_2SO_4 \rightarrow (0.66\ Ca^{2+}, 0.33\ Mg^{2+}, 0.011\ Na^{+}) + SO_4^{2-} + CO_2 + H_2O \quad (5\text{-}1)$$

$$\text{Carbonates} + 0.5\ H_2SO_4 \rightarrow (0.66\ Ca^{2+}, 0.33\ Mg^{2+}, 0.011\ Na^{+}) + 0.5\ SO_4^{2-} + HCO_3^{-} \quad (5\text{-}2)$$



doi:10.6342/NTU202500428

In reaction 5-1, the reaction between equal molar ratios of carbonate and sulfuric acid results in the spontaneous release of $CO_2$ from the carbonates. In reaction 5-2, the sulfuric acid to carbonate ratio is 1 to 2. This reaction produces aqueous bicarbonate ($HCO_3^-$) instead. Although the immediate carbon products are in different states, in long-term geological time scale, both reactions would lead to the release of $CO_2$. Since sulfuric acid drives the weathering process, no carbon is absorbed from the atmosphere. The bicarbonate would be transported by rivers in aqueous state to the ocean, where it could lead to precipitation of inorganic carbonates, while also releasing $CO_2$ (Garrels and Mackenzie, 1971).

$$Mg^{2+}/Ca^{2+} + 2\ HCO_3^- \rightarrow (Mg/Ca)CO_3 + CO_2 + H_2O \quad (5\text{-}3)$$

When silicate weathering is driven by sulfuric acid, the following reaction occurs (Torres et al., 2016):

$$Silicates + H_2SO_4 \rightarrow (0.32\ Ca^{2+}, 0.22\ Mg^{2+}, 0.9\ Na^{+}) + SO_4^{2-} + CO_2 + H_2O \quad (5\text{-}4)$$

In reaction 5-4, the sulfate to Mg + Ca ratio would be 2 to 1. The weathering of silicates by sulfuric acid would release $CO_2$ into the atmosphere. However, there is no data from our results close to this weathering path (Figure 5.7). This means in this region, sulfuric acid-driven carbonate weathering is more prominent.



doi:10.6342/NTU202500428

It may be surprising that the weathering of carbonates is dominant in the region where the bedrocks are predominantly made of silicates. However, Blum and others (1998) demonstrated that carbonate weathering is significant in a silicate-dominant region, in the High Himalayan Crystalline Series (HHCS), northern Pakistan. In that study, carbonates accounts for only ~1% of the rocks in the Raikhot watershed, meanwhile quartz, plagioclase, K-feldspar, and biotite form most of the bedrock. Blum and others (1998) suggested that the weathering of carbonates contributed 82% of the $HCO_3^-$ flux in the Raikhot watershed, however, only 18% is derived from silicate weathering. Therefore, our data (Figure 5.7) may implicate a similar result, where carbonate weathering is more significant than silicate weathering in a silicate dominant region.

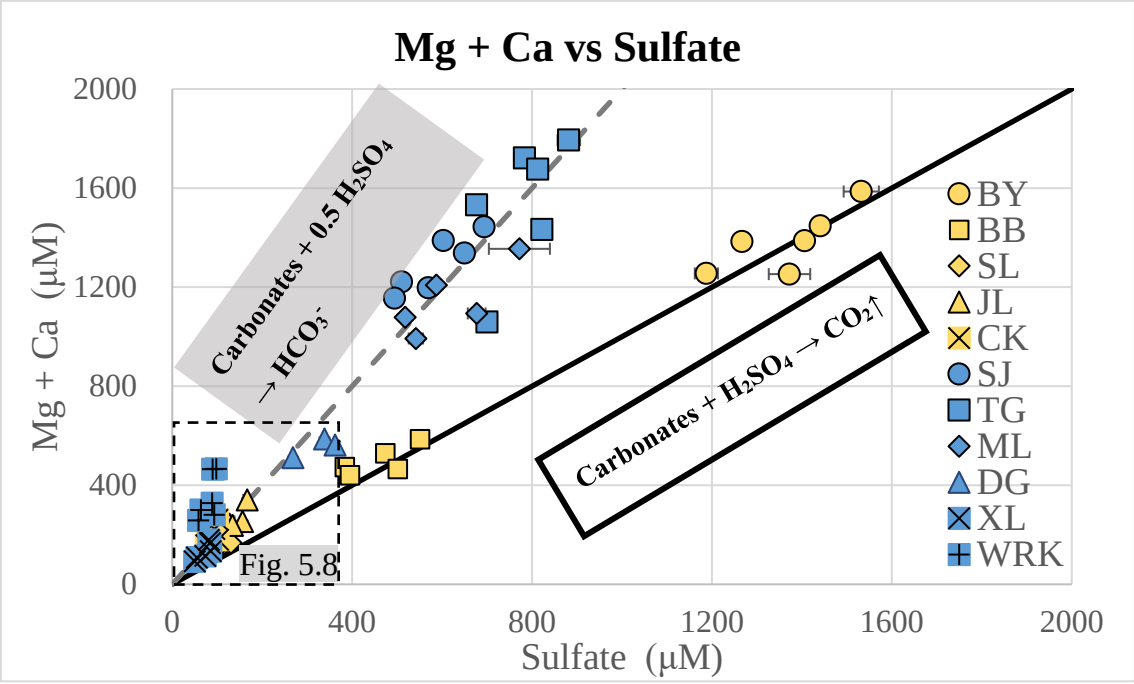


Figure 5.7 The sum of Mg and Ca concentration versus sulfate concentration. The black solid line indicates reaction 5-1. The grey dashed line indicates reaction 5-2.



doi:10.6342/NTU202500428

In Figure 5.7, there is a distinction between the samples from the Central Range and the Hsuehshan Range in the upstream of Lanyang River. Both BY and BB from the Hsuehshan Range fit on the black line. This result indicates that in the upper stream of the Hsuehshan Range, sufficient sulfuric acid reacts with the carbonates in the rocks, producing $CO_2$. Sites SJ, TG, and ML fit on the grey dashed line.

In the downstream (Figure 5.8), the data of sites CK and XL fall generally on the gray line, showing weaker carbonate weathering by sulfuric acid. However, SL, JL, and DG show a mixture of both reactions, lying between the two lines. Finally, WRK again separates from the rest, which indicates the weakest carbonate weathering by sulfuric acid.

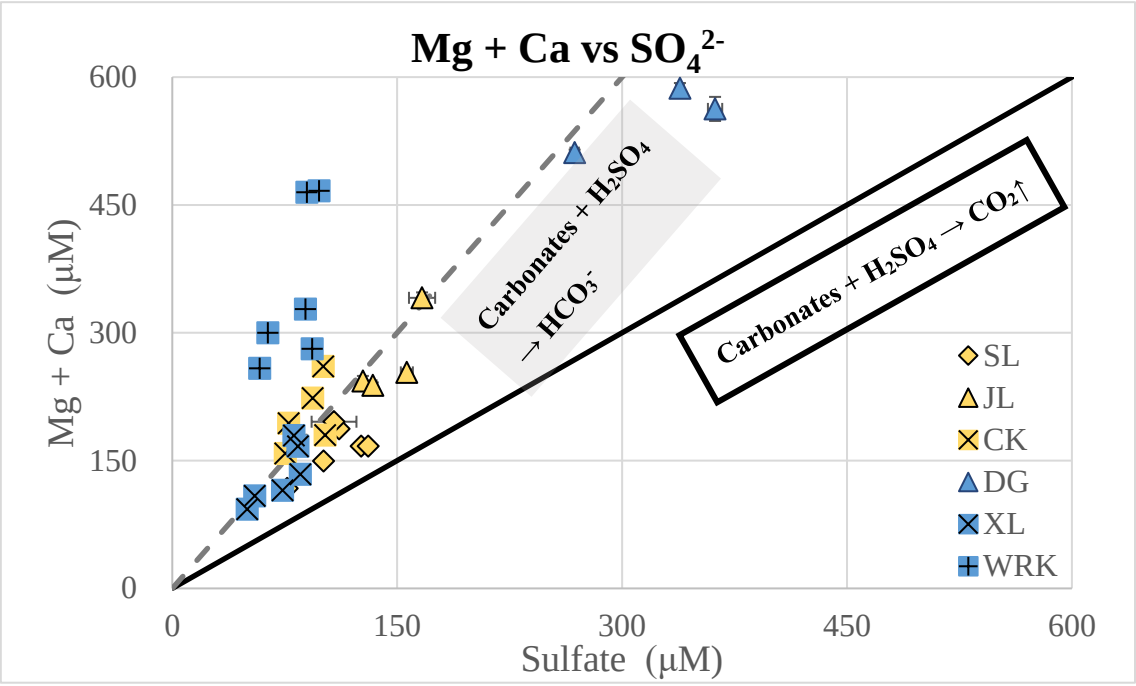


Figure 5.8 The sum of Mg and Ca concentration versus sulfate concentration of downstream sites.



doi:10.6342/NTU202500428

By plotting cations against sulfate, several rivers display distinct characteristics. However, the patterns do not show clear correlation to bedrock lithology. Therefore, other influences could be controlling the chemical compositions of river waters. One such influence is likely the hot spring, which is discussed in the next section.



doi:10.6342/NTU202500428

## 5.2 Hot spring influences

In this study, we noticed that hot springs might contribute to the dissolved materials in riverine waters. Hot spring outcrops are present in the basins of SJ, TG, and BB (Water resource department, Yilan County). Hot spring waters were directly sampled at BB. A suspected outflow of hot spring water was sampled at TG. The hot spring outcrop at SJ was not sampled due to inaccessibility.

We compared hot spring and riverine sulfate data in Figure 5.9. From the results, average sulfate concentrations at BB, SJ, and TG are much higher than the concentrations from SL, JL, CK, DG, XL, and WRK. The average sulfate concentrations of BB and TG hot springs are 36% and 22% higher than that of their riverine counterparts. The average sulfate concentration of ML is comparable to SJ. The high sulfate content at ML can potentially be attributed to hot springs since it flows between TG and the Chingshui River, both of which are renowned for geothermal activities. It is possible that the river water of ML is mixed with hot spring water seeping from an unknown source. Therefore, high sulfate content found at the rivers without known hot springs may be under the influence of undocumented hot springs or geothermal activities close by.



doi:10.6342/NTU202500428

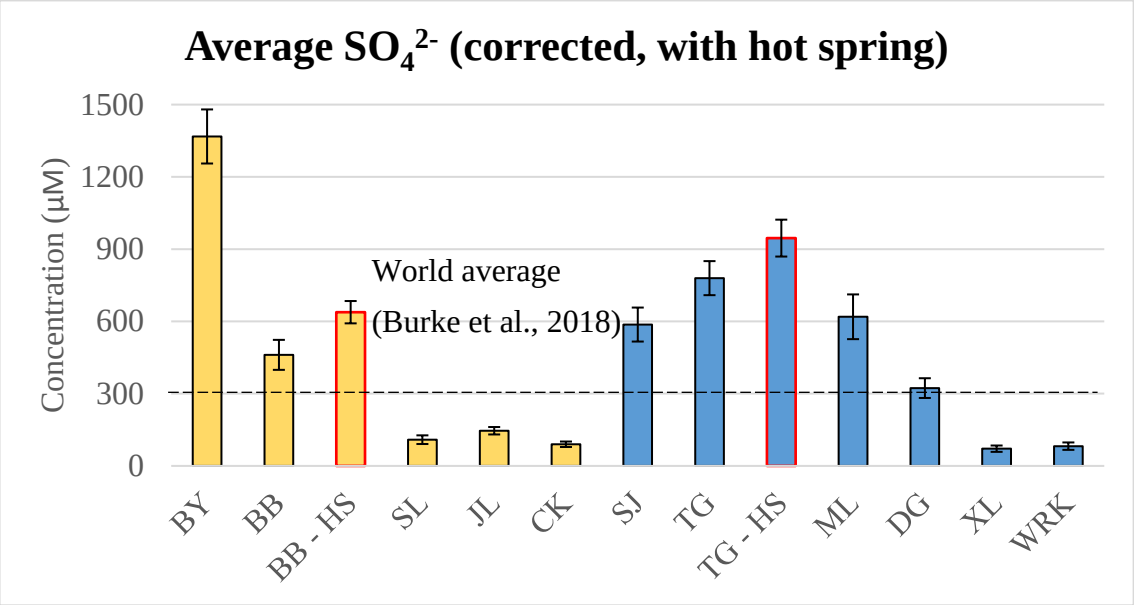


Figure 5.9 Average riverine and hot spring sulfate results. Yellow bars are sites in the Hsuehshan Range; blue bars are sites in the Central range. Hots spring samples are bars with red outlines. The bars are arranged in an eastward direction from left to right.

Hot spring influence can also be observed in the cation concentrations. Hot spring samples produced cation concentrations much higher than riverine waters. This is consistent with the reports of high Na and K in the hot spring waters in the study area (Table 5.2, Figure 5.10), namely the Tuchang and Chingshui region (Chen, 1985). However, Mg and Ca concentrations are much higher than the reported numbers at the Tuchang and Chingshui region. This could be due to the natural variations in chemical properties of different hot springs. Riverine cation concentrations are generally much lower than hot spring samples. This is most likely due to the dilution effect. In their respective mountain ranges, the riverine samples with known hot springs, namely SJ, TG,



doi:10.6342/NTU202500428

and BB, have higher cation concentrations than the rivers without hot springs (Figure 5.11 and 5.12).

Table 5.2 Hot spring cation concentrations compared to previous reports.

| Region | Na (μM) | Mg (μM) | K(μM) | Ca (μM) |
|---|---|---|---|---|
| BB-HS[1] | 5410.2 | 458.6 | 277.0 | 405.2 |
| TG-HS[1] | 2328.8 | 1217.9 | 54.2 | 859.2 |
| Tuchang[2] | 36,277.0 | 49.4 | 447.6 | 69.9 |
| Chingshui[2] | 42,193.0 | <4.1 | 1023.0 | 5.0 |

1: This study, average cation concentrations (corrected). 2: Data from Chen, 1985. Concentrations were converted from mg/L to μM.

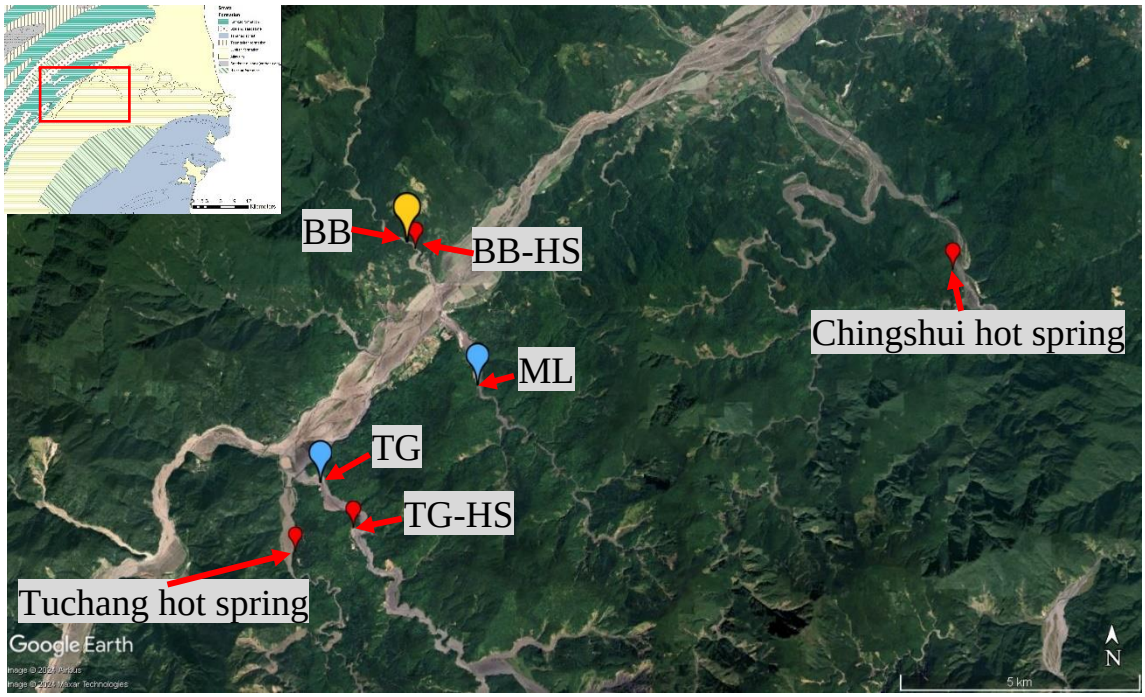


Figure 5.10 Locations of the Tuchang, Chingshui hot springs and nearby sample sites.



doi:10.6342/NTU202500428

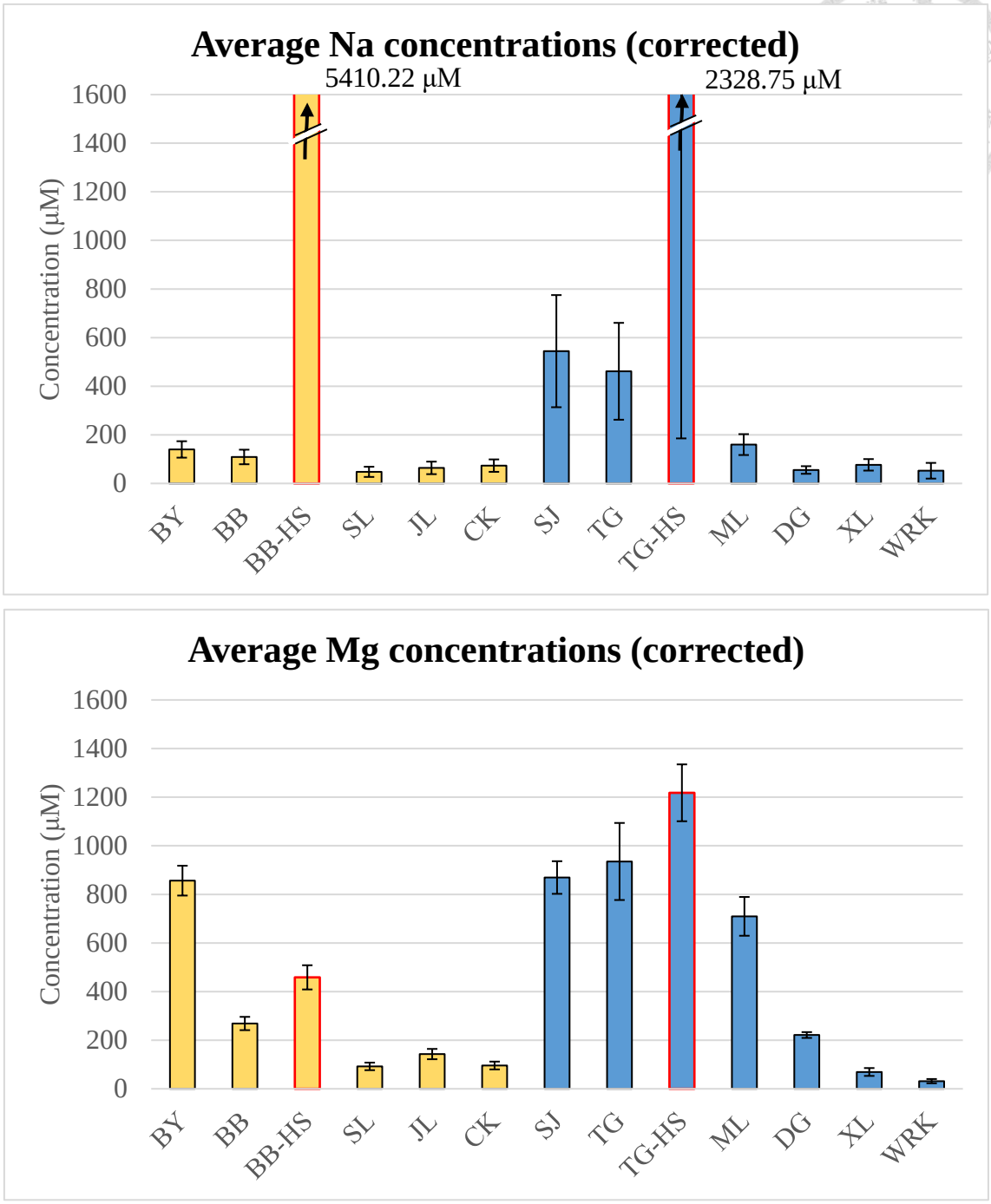


Figure 5.11 Average Na and Mg concentrations of riverine and hot spring samples from this study (corrected). Yellow bars are sites in the Hsuehshan Range; blue bars are sites in the Central range. Hots spring samples are bars with red outlines. The bars are arranged in an eastward direction from left to right



doi:10.6342/NTU202500428

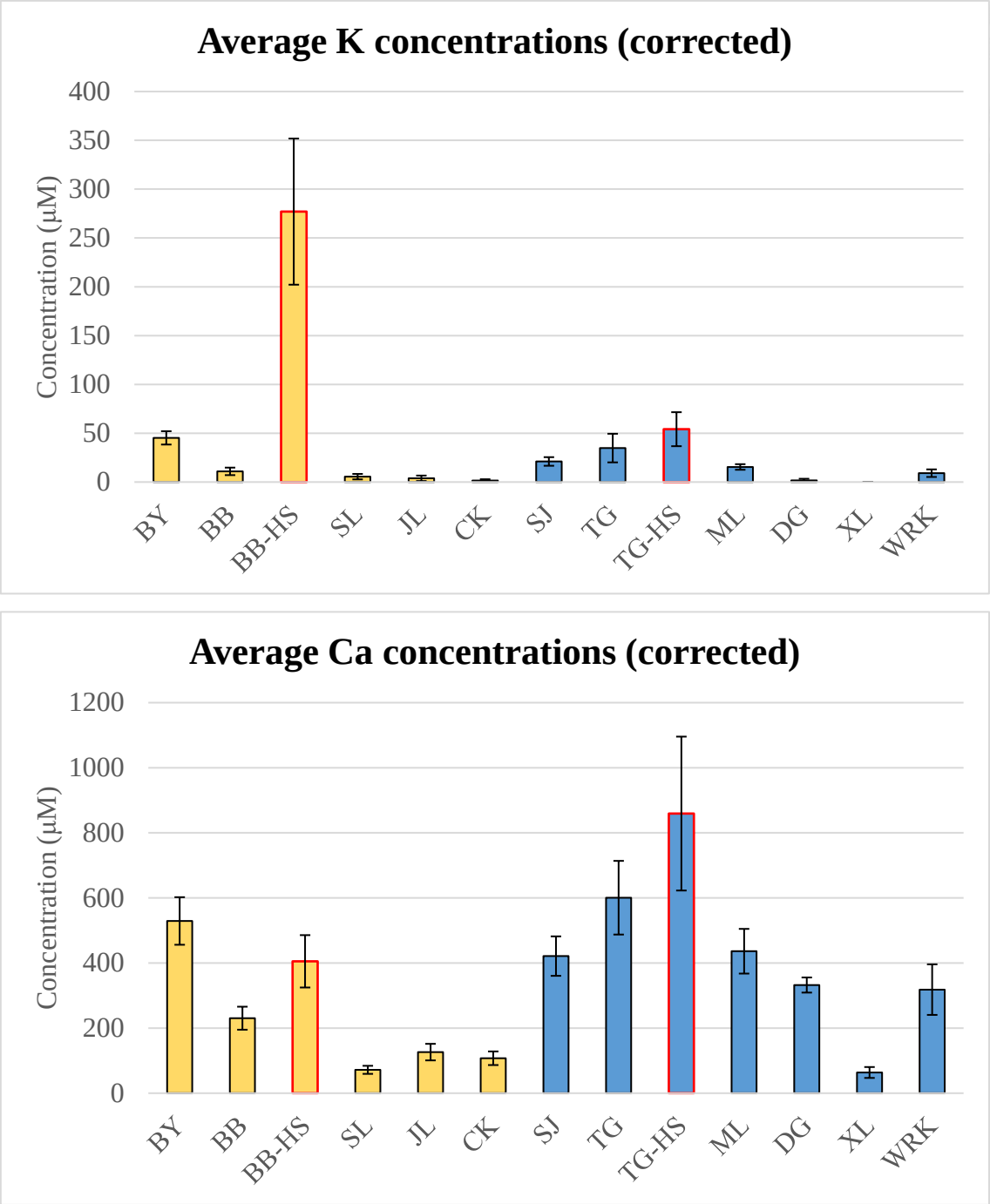


Figure 5.12 Average K and Ca concentrations of riverine and hot spring samples from this study (corrected). Yellow bars are sites in the Hsuehshan Range; blue bars are sites in the Central range. Hots spring samples are bars with red outlines. The bars are arranged in an eastward direction from left to right



doi:10.6342/NTU202500428

In the end-member weathering model (Figure 5.13), the Mg/Na and Ca/Na ratios of the BB hot spring samples (BB-HS) are one to two magnitudes smaller than riverine waters form the Hsuehshan Range. However, only two samples from the four TG hot spring (TG-HS) samples have a similar characteristic. Although cation concentrations are consistently higher in hot spring waters, the cation compositions may differ depending on the hot springs.

Based on the sulfate and cation concentrations, hot springs appears to play a role in chemical weathering and providing dissolved materials in the study area. Therefore, bedrock lithology is perhaps not the primary control of riverine chemical properties in the northern Central Range and the Hsuehshan Range.

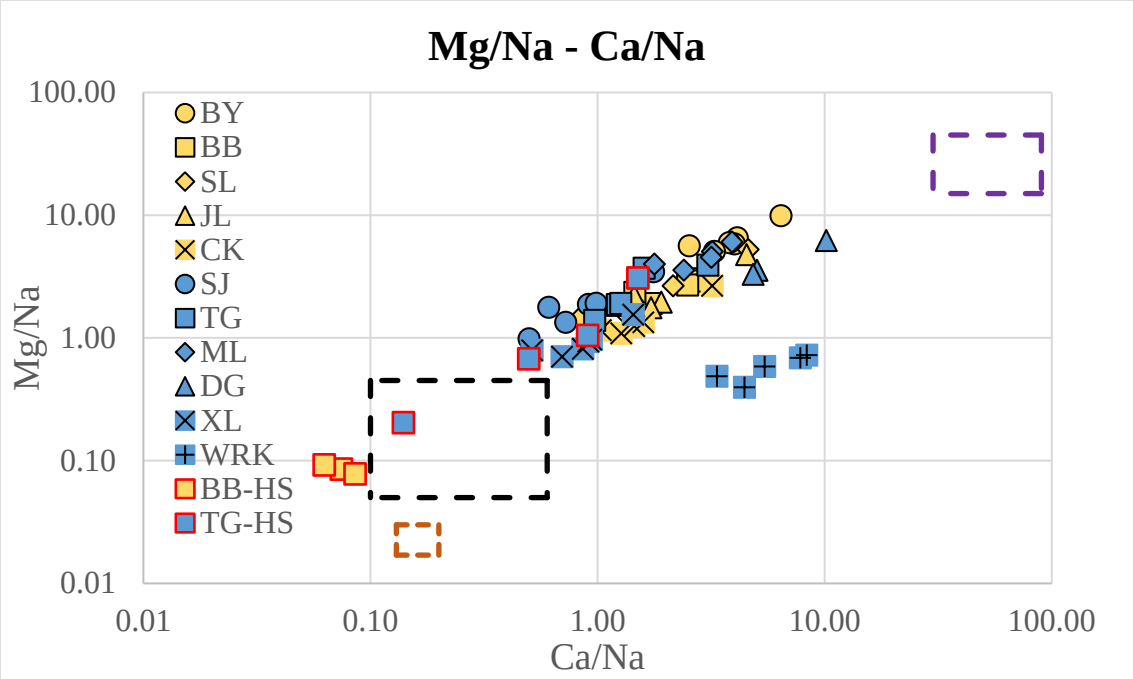


Figure 5.13 End-member model of riverine and hot spring data. Hot spring samples are highlighted with red outlines.



doi:10.6342/NTU202500428

## 5.3 Noticeable cases

### 5.3.1 BY

BY stands out from the other sites with its abnormally high sulfate concentrations, even higher than hot spring samples in the region (Figure 5.9). Although there is no documented hot spring in the BY region, it is still possible that some unknown hot springs affected the riverine chemical compositions of BY. Additionally, the Szeleng Sandstone is a major formation in the BY basin, which had been found with imbedded sulfide-bearing quartz veins (Yui et al., 1997). As a result, the Szeleng Sandstone could be a potential contributor of the riverine sulfate in BY.

The field observations at BY support this hypothesis. Large metasandstone boulders are common in the riverbed of BY (Figure 5.14). The boulders are mostly sub-angular with low sphericity, indicating that they are local deposits from the Szeleng Sandstone. There are yellowish-orange weathering marks on these boulders, which are indications of iron oxidation. Furthermore, the river water at the BY occasionally bears a faint, metallic smell, similar to the smell of iron oxide. These observations indicate that pyrite may be abundant in the rocks in the BY basin.



doi:10.6342/NTU202500428

Figure 5.14 Large metasandstone boulders in BY riverbed. The fresh surfaces reveal the natural gray of the sandstone rocks. There are orange to yellow colorations on the surfaces exposed to weathering.

However, there are still other possible processes that we have not considered the tributaries in this region. These processes may include effects of unfound hot springs or biochemical reactions driven by microorganisms (Wang et al., 2024) to produce such high sulfate concentrations in its river waters.



doi:10.6342/NTU202500428

### 5.3.2 WRK

WRK samples were measured to have high chloride concentrations and low sulfate concentrations. The high chloride concentrations at WRK is likely due to the shorter distance between the WRK site and the coastline, since chloride is mainly supplied by the sea through atmospheric deposition.

WRK samples display noteworthy cation characteristics. As shown in the end-member model (Figure 5.3), WRK samples have obviously high Ca ratio. This makes the WRK samples different enough to be separated from the other sites. This could be the result of the marbles in its basin. The WRK basin is the only basin to have higher-grade metamorphic rocks of the Tananao Schist in this study (Figure 2.4), which includes a variety of schists and marble. In-field observation shows that marble pebbles are only found at WRK amongst all the sites (Figure 4.6). The cation results at WRK indicate that when there is no hot spring presence, and the rock composition is distinctive enough, the influence of bedrock lithology on river chemistry is more prominent.



doi:10.6342/NTU202500428

# Chapter 6 Conclusions

In this study, we analyzed major chemical composition in river waters to investigate their possible geological controls. We took samples from 11 tributaries and 2 hot springs in the Lanyang River system. These tributaries originate from the Hsuehshan Range and the Central Range, and contain a variety of bedrock formations in their drainage basins.

Riverine chloride concentrations decrease when the distances between the sites and the coast increase. This suggests that riverine chloride is mainly supplied by the sea through atmospheric deposition. Thus, we performed atmospheric correction of sulfate, Na, Mg, K, and Ca based on riverine chloride and rainwater properties.

After correction, sulfate concentrations of some drainage basins, such as BY, BB, SJ, TG, ML, and DG, are higher than the world average, but the other basins are lower. Unlike chloride, sulfate concentrations are higher in the upstream regions in the Hsuehshan Range and the Central Range.

The cation end-member model was implemented to determine the weathering sources in the study area. The model confirms the lack of evaporites in the drainage basins. It indicates a mixture of carbonate and silicate weathering in the region. The data from this study is distinctive from the river systems in the southern Central Range in the end-member model. However, apart from WRK, the cation compositions do not display any



doi:10.6342/NTU202500428

pattern related to bedrock lithology.

The sulfate to Mg and Ca plot shows that sulfuric acid driven carbonate weathering is strong at BY and BB. The data of the other sites indicate weak carbonate weathering by sulfuric acid in the region, suggesting that some rivers can be distinguished from others by their carbonate weathering paths.

Hot spring samples produced higher concentrations in sulfate and cations compared to riverine results. Rivers that flow through hot springs also have higher sulfate and cation concentrations than the rivers that do not. Thus, hot springs could be a potential control of the chemical compositions of river waters in this region.

The highest sulfate concentrations were found in BY. Field observations suggest that this may be contributed by an abundance of sulfide-bearing Szeleng Sandstone in its drainage basin. The distinctive cation characteristics of WRK samples are likely due to the presence of the Tananao Schist bedrocks in this basin. In summary, it appears that when hot spring is absent and the local rock composition is different enough, bedrock lithology's influence on chemical properties of river waters could be more obvious.



doi:10.6342/NTU202500428

# References

Berner, R. A., Lasaga, A. C., & Garrels, R. M. (1983). The carbonate-silicate geochemical cycle and its effect on atmospheric carbon dioxide over the past 100 million years. *American Journal of Science*, 283(7), 641–683.

Blattmann, T. M., Wang, S. L., Lupker, M., Märki, L., Haghipour, N., Wacker, L., Chung, L. H., Bernasconi, S. M., Plötze, M., & Eglinton, T. I. (2019). Sulphuric acid-mediated weathering on Taiwan buffers geological atmospheric carbon sinks. *Scientific Reports*, 9(1), 2945.

Blum, J.D., Gazis, C.A., Jacobson, A.D., & Chamberlain, C.P. (1998). Carbonate versus silicate weathering in the Raikhot watershed within the High Himalayan Crystalline Series. *Geology*, 26(5), 411–414.

Bucher, K., Zhou, W. & Stober, I. (2017). Rocks control the chemical composition of surface water from the high Alpine Zermatt area (Swiss Alps). *Swiss Journal of Geosciences*, 110(3), 811–831.

Bufe, A., Hovius, N., Emberson, R., Caves Rugenstein, J., Galy, A., Hassenruck-Gudipati, H., & Chang, J. M. (2021). Co-variation of silicate, carbonate and sulfide weathering drives CO2 release with erosion. *Nature Geoscience*, 14(4), 211-216.

Burke, A., Present, T. M., Paris, G., Rae, E. C. M., Sandilands, B. H., Gaillardet, J.,



doi:10.6342/NTU202500428

Peucker-Ehrenbrink, B., Fischer, W. W., McClelleand, J. W., Spencer, G. M., Voss, B. M., & Adkins, J. F. (2018). Sulfur isotopes in rivers: Insights into global weathering budgets, pyrite oxidation, and the modern sulfur cycle. *Earth and Planetary Science Letters*, 496, 168-177.

Calmels, D., Gaillardet, J., Brenot, A., & France-Lanord, C. (2007). Sustained sulfide oxidation by physical erosion processes in the Mackenzie River basin: Climatic perspectives. *Geology*, 35(11), 1003-1006.

Calmels, D., Galy, A., Hovius, N., Bickle, M., West, A. J., Chen, M. C., & Chapman, H. (2011). Contribution of deep groundwater to the weathering budget in a rapidly eroding mountain belt, Taiwan. *Earth and Planetary Science Letters*, 303(1-2), 48-58.

Chen, C. (1985). Chemical Characteristics of thermal waters in the Central Range of Taiwan, R.O.C. *Chemical Geology*, 49(1), 303–317.

Chung, C. H., You, C. F., & Chu, H. Y. (2009). Weathering sources in the Gaoping (Kaoping) river catchments, southwestern Taiwan: Insights from major elements, Sr isotopes, and rare earth elements. *Journal of Marine Systems*, 76(4), 433-443.

Das, A., Chung, C. H., & You, C. F. (2012). Disproportionately high rates of sulfide oxidation from mountainous river basins of Taiwan orogeny: Sulfur isotope



doi:10.6342/NTU202500428

evidence. *Geophysical Research Letters*, 39(12), 6.

Emberson, R., Hovius, N., Galy, A., & Marc, O. (2016). Oxidation of sulfides and rapid weathering in recent landslides. *Earth Surface Dynamics*, 4(3), 727-742.

Emberson, R., Galy, A., & Hovius, N. (2018). Weathering of reactive mineral phases in landslides acts as a source of carbon dioxide in mountain belts. *Journal of Geophysical Research-Earth Surface*, 123(10), 2695-2713.

Francois, L.M. & Walker, J.C.G. (1992). Modelling the Phanerozoic carbon cycle and climate, constraints from the 87Sr/86Sr isotopic ratio of seawater. *American Journal of Science*, 292(2), 81-135.

Gaillardet, J., Dupre, B., Louvat, P., & Allegre, C. J. (1999). Global silicate weathering and CO2 consumption rates deduced from the chemistry of large rivers. *Chemical Geology*, 159(1-4), 3-30.

Galy, A. & France-Lanord, C. (1999). Weathering processes in the Ganges-Brahmaputra basin and the riverine alkalinity budget. *Chemical Geology*, 159(1-4), 31-60.

Graedel, T. E. & Keene, W. C. (1996). The Budget and Cycle of Earth's Natural Chlorine, *Pure and Applied Chemistry*, 68(9), 1689-1697.

Ho, C. S. (1975). An introduction to the geology of Taiwan: Explanatory text of the geologic map of Taiwan, 153, Ministry of Economic Affairs, Taipei.



doi:10.6342/NTU202500428

Horng, C. S., Huh, C. A., Chen, K. H., Lin, C. H., Shea, K. S., & Hsiung, K. H. (2012). Pyrrhotite as a tracer for denudation of the Taiwan orogen. *Geochemistry, Geophysics, Geosystems*, 13(8), Q08Z47.

Johnson, N. M., & Reynolds, R. C. (1972). Atmospheric Sulfur - Its Effect on Chemical Weathering of New England. *Science*, 177(4048), 514-516.

Lerman, A., Wu, L. L., & Mackenzie, F. T. (2007). CO2 and H2SO4 consumption in weathering and material transport to the ocean, and their role in the global carbon balance. *Marine Chemistry*, 106(1-2), 326-350.

Li, Y.H. (2000). *A Compendium of Geochemistry, from Solar Nebula to the Human Brain*. Princeton University Press, Princeton, N.J.

Li, Y. H., Chen, C. T. A. & Hung, J. J. (1997). Aquatic chemistry of lakes and reservoirs in Taiwan. *Terrestrial Atmospheric and Oceanic Sciences*, 8, 405–426.

Meybeck, M. (1987). Global Chemical-Weathering of Surficial Rocks Estimated from River Dissolved Loads. *American Journal of Science*, 287(5), 401-428.

Meyer, K. J., Carey, A. E., & You, C. F. (2017). Typhoon impacts on chemical weathering source provenance of a High Standing Island watershed, Taiwan. *Geochimica Et Cosmochimica Acta*, 215, 404-420.

Relph, K. E., Stevenson, E. I., Turchyn, A. V., Antler, G., Bickle, M. J., Baronas, J., J.



doi:10.6342/NTU202500428

Jotautas, Darby, S. E., Parsons, D. R., & Tipper, E. T. (2021). Partitioning riverine sulfate sources using oxygen and sulfur isotopes: Implications for carbon budgets of large rivers. *Earth and Planetary Science Letters*, 567(2), 116957

Siever, R. (1968), Sedimentological consequences of a steady-state ocean-atmosphere. *Sedimentology*, 11, 5-29.

Taylor, B. E., Wheeler, M. C., & Nordstrom, D. K. (1984). Stable Isotope Geochemistry of Acid-Mine Drainage - Experimental Oxidation of Pyrite. G*eochimica Et Cosmochimica Acta*, 48(12), 2669-2678.

Torres, M., West, A. & Li, G. (2014) Sulphide oxidation and carbonate dissolution as a source of CO2 over geological timescales. *Nature*, 507(7492), 346–349.

Walker, J. C. G., Hays, P. B., & Kasting, J. F. (1981). A Negative Feedback Mechanism for the Long-Term Stabilization of Earths Surface-Temperature. *Journal of Geophysical Research*, 86(C10), 9776-9782.

Wang, P. L., Tu, T. H., Lin, L. H. *et al*. (2024) Microbial communities modulate chemical weathering and carbon dioxide cycling in an active orogen in Taiwan. *Communications Earth & Environment*, 5(1), 174.

Wang, Y. J. (2019). The effect of chemical weathering on CO2 budget in the Beinan river system (In Chinses with English abstract). Graduate Institute of Oceanography,



doi:10.6342/NTU202500428

College of Science, National Taiwan University, Master's thesis, 88.

Yen, T. P. (1959). The stratigraphic distribution of the bedded cupriferous pyrite deposits and manganese deposits in Taiwan. *Mining Geology (Society of Mining Geologists Japan)*, 9(33), 19-24.

Yoshimura, K., Nakao, S., Noto, M., Inokura, Y., Urata, K., Chen, M., & Lin, P. W. (2001). Geochemical and stable isotope studies on natural water in the Taroko Gorge karst area, Taiwan - chemical weathering of carbonate rocks by deep source CO2 and sulfuric acid. *Chemical Geology*, 177(3-4), 415-430.

Yui, T. F., Chu, H. T., Wang, Y. H., & Yeh, T. H. (1997). Sulfide-bearing Quartz Veins in the Szeleng Sandstone, Chinmienshan, Northeastern Taiwan: A Preliminary Study on Fluid Inclusions and Stable Isotopes (In Chinses with English abstract). *Journal of the Geological Society of China*, 40(4), 723-742.

Encyclopaedia Britannica. https://www.britannica.com/science/water-cycle

First River Management Branch, Water Resources Agency, Ministry of Economic Affairs, https://www.wra01.gov.tw/Default.aspx .

Geological Survey and Mining Management Agency (formally Central Geological Survey, CGS), Ministry of Economic Affairs, Taiwan. https://twgeoref.gsmma.gov.tw/GipOpenWeb/wSite/lp?ctNode=339&mp=106



doi:10.6342/NTU202500428

Water Education Foundation. https://www.watereducation.org/

Water Resources Department, Yilan County.

https://wres.e-land.gov.tw/cp.aspx?n=79FB5DB9DC2E17BE



doi:10.6342/NTU202500428

# Appendix

Table A.1 Anion concentrations of rainwater samples.

| Sample name | Process date | $Cl^-$ (μM) | $SO_4^{2-}$ (μM) |
|---|---|---|---|
| 220223-RW | 2022/3/30 | 2.1 ± 0.4 | 2.8 ± 0.0 |
| *220303-RW* | *2022/3/30* | *18.2 ± 0.2* | *8.0 ± 0.1* |
| 220307-RW | 2022/3/30 | 7.9 ± 0.0 | 3.5 ± 0.2 |
| 2203021-RW | 2022/3/30 | 4.5 ± 0.3 | 2.7 ± 0.0 |
| 220323-RW | 2022/3/30 | - | 2.0 ± 0.3 |
| 220328-RW | 2022/3/30 | - | 1.5 ± 0.1 |
| 220503RW_1x | 2022/5/20 | 20.5 ± 0.6 | 5.7 ± 0.0 |
| 220504RW_1x | 2022/5/20 | 69.0 ± 0.1 | 12.9 ± 0.0 |
| 220506RW_1x | 2022/5/20 | 41.4 ± 0.1 | 9.0 ± 0.2 |
| 220509RW_1x | 2022/5/20 | 15.1 ± 0.2 | 6.3 ± 0.0 |
| 0517RW-B_1x | 2022/7/19 | 6.6 ± 0.1 | 3.6 ± 0.0 |
| 0519RW-B_1x | 2022/7/19 | 42.4 ± 0.1 | 12.5 ± 0.0 |
| 0531RW-C_1x | 2022/7/19 | 4.4 ± 0.1 | 4.8 ± 0.1 |
| 0531RW-ND_1x | 2022/7/19 | 2.9 ± 0.1 | 4.5 ± 0.0 |
| 0607RW-B_1x | 2022/7/27 | 22.4 ± 0.4 | - |
| 0608RW-B_1x | 2022/7/19 | 10.1 ± 0.1 | 7.1 ± 0.0 |
| 220803RW-A_1x | 2022/9/22 | 100.8 ± 0.2 | 16.0 ± 0.1 |
| 220905RW-B_1x | 2022/10/10 | 26.4 ± 0.2 | 3.0 ± 0.1 |
| 220906RW-ND-B_1x | 2022/10/10 | 5.9 ± 0.1 | 3.8 ± 0.1 |
| 220912RW-B_1x | 2022/10/10 | 57.1 ± 0.1 | 8.8 ± 0.1 |
| 220913RW-B_1x | 2022/10/10 | 33.2 ± 0.0 | 3.3 ± 0.0 |
| 220913RW-ZW-B_1x | 2022/10/10 | 68.0 ± 0.1 | 5.5 ± 0.0 |
| 220916RW-C_1x | 2022/10/10 | 24.3 ± 0.2 | 6.7 ± 0.1 |
| 220925RW-C_1x | 2022/10/10 | 25.7 ± 0.1 | 5.4 ± 0.0 |
| *220926RW-B_1x* | 2022/10/25 | *194.1 ± 0.2* | 16.9 ± 0.2 |

Sample 0607RW-B was determined to be invalid due to possible human error, highlighted in red. *Italic figures* are calculated outliers and thus were excluded from the calculations for average ion concentrations.



doi:10.6342/NTU202500428

Table A.1 (continued)

| Sample name | Process date | $Cl^-$ (μM) | $SO_4^{2-}$ (μM) |
|---|---|---|---|
| 221005RW-B_1x | 2022/10/25 | 94.5 ± 0.1 | 12.7 ± 0.1 |
| 221006RW-B_1x | 2022/10/25 | 44.6 ± 0.1 | 6.6 ± 0.0 |
| *221011RW-ZW-B_1x* | 2022/10/25 | *194.7 ± 0.4* | *17.8 ± 0.1* |
| 221018RW-B | 2023/4/12 | 21.9 ± 0.1 | 4.0 ± 0.0 |
| 221024RW-B | 2023/4/12 | 2.4 ± 0.1 | - |
| 221024RW-ND-B | 2023/4/12 | 7.3 ± 0.1 | 3.7 ± 0.2 |
| 221024RW-ZW-B | 2023/4/12 | 62.9 ± 0.3 | 7.0 ± 0.0 |
| *221031RW-B* | 2023/4/12 | *151.9 ± 0.2* | 12.8 ± 0.1 |
| 221031RW-C | 2023/4/12 | 9.2 ± 0.1 | 2.9 ± 0.1 |
| 221031RW-ZW-B | 2023/4/12 | 25.4 ± 0.2 | - |
| 221101RW-B | 2023/4/12 | 37.0 ± 0.1 | 9.0 ± 0.0 |
| 221101RW-C | 2023/4/12 | 16.8 ± 0.7 | 3.1 ± 0.0 |
| 221108RW-A | 2023/4/12 | 58.9 ± 0.3 | 6.9 ± 0.0 |
| 221118RW-C | 2023/4/12 | 100.9 ± 0.6 | 12.7 ± 0.6 |
| 221208RW-A | 2023/5/5 | 30.1 ± 0.3 | 3.9 ± 0.0 |
| 221229RW-C | 2023/5/5 | 16.9 ± 0.3 | 9.3 ± 0.1 |
| 230104RW-ZW | 2023/5/5 | 104.6 ± 0.8 | 13.7 ± 0.5 |
| 230105RW-B | 2023/5/5 | 27.2 ± 0.1 | 9.2 ± 0.1 |
| 230105RW-ND | 2023/5/5 | 20.9 ± 0.2 | 5.2 ± 0.1 |
| 230110RW-B | 2023/5/5 | 9.8 ± 0.5 | 3.1 ± 0.1 |

*Italic figures* are calculated outliers and thus were excluded from the calculations for average ion concentrations.

.



doi:10.6342/NTU202500428

Table A.2 Cation concentrations of rainwater samples.

| Sample name | Process date | Na (μM) | Mg (μM) | K (μM) | Ca (μM) |
|---|---|---|---|---|---|
| 220223RW-B | 2022/3/22 | 24.4 ± 0.6 | 2.1 ± 0.0 | 2.6 ± 0.1 | 5.5 ± 0.2 |
| *220303RW-B* | 2022/3/22 | *173.9 ± 0.6* | *24.6 ± 0.1* | *11.7 ± 0.1* | 12.4 ± 0.5 |
| 220307RW-B | 2022/3/22 | 84.3 ± 1.0 | 11.0 ± 0.1 | 6.3 ± 0.2 | 8.7 ± 0.1 |
| 220321RW-B | 2022/7/12 | 56.5 ± 0.6 | 9.6 ± 0.0 | 3.9 ± 0.1 | 4.3 ± 0.3 |
| 220323RW-B | 2022/7/12 | 35.5 ± 0.2 | 6.6 ± 0.0 | 3.2 ± 0.1 | 2.7 ± 0.2 |
| 220328RW-B | 2022/7/12 | 32.9 ± 0.4 | 6.1 ± 0.0 | 2.5 ± 0.2 | 1.6 ± 0.3 |
| 220503RW-B | 2022/7/12 | 46.6 ± 0.1 | 7.7 ± 0.0 | 5.1 ± 0.1 | 2.1 ± 0.2 |
| 220504RW-B | 2022/7/12 | 71.2 ± 0.4 | 11.6 ± 0.1 | 4.0 ± 0.1 | 2.9 ± 0.2 |
| 220506RW-B | 2022/7/12 | 56.6 ± 0.6 | 9.2 ± 0.0 | 4.8 ± 0.2 | 3.5 ± 0.1 |
| 220509RW-C | 2022/7/12 | 39.2 ± 0.2 | 7.3 ± 0.0 | 4.3 ± 0.0 | 1.7 ± 0.2 |
| 220517RW-B | 2022/7/12 | 23.8 ± 0.2 | 6.3 ± 0.0 | 3.0 ± 0.2 | 3.1 ± 0.4 |
| 220519RW-B | 2022/7/12 | 47.2 ± 0.4 | 9.4 ± 0.0 | 2.3 ± 0.1 | 2.0 ± 0.1 |
| 220531RW-C | 2022/7/12 | 22.0 ± 0.0 | 6.2 ± 0.0 | 2.6 ± 0.2 | 1.5 ± 0.2 |
| 220531RW-ND | 2022/7/12 | 28.4 ± 0.3 | 6.1 ± 0.0 | 1.7 ± 0.1 | 0.9 ± 0.1 |
| 220607RW-B | 2022/7/12 | 3012.1 ± 23.1 | 248.6 ± 3.3 | 477.2 ± 4.2 | 84.7 ± 1.7 |
| 220608RW-B | 2022/7/12 | 26.5 ± 0.2 | 6.9 ± 0.0 | 1.9 ± 0.1 | 1.5 ± 0.2 |
| *220803RW-A* | 2022/12/13 | 50.6 ± 0.3 | 14.8 ± 0.3 | 6.5 ± 0.1 | *30.1 ± 1.1* |
| 220905RW-B | 2022/12/13 | 41.4 ± 0.2 | 5.4 ± 0.1 | 1.9 ± 0.1 | 2.5 ± 0.2 |
| *220906RW-ND* | 2022/12/13 | 59.0 ± 0.3 | *29.5 ± 0.3* | 2.8 ± 0.1 | 11.3 ± 0.6 |
| *220912RW-B* | 2022/12/13 | 64.0 ± 0.1 | 5.4 ± 0.1 | *20.0 ± 0.3* | *14.7 ± 0.5* |
| 220913RW-B | 2022/12/13 | 38.6 ± 0.2 | 4.9 ± 0.1 | 1.7 ± 0.1 | 5.1 ± 0.2 |
| *220913RW-ZW* | 2022/12/13 | 73.7 ± 0.6 | 6.6 ± 0.1 | 7.3 ± 0.0 | *16.1 ± 0.7* |
| *220916RW-C* | 2022/12/13 | 53.4 ± 0.4 | *32.7 ± 0.3* | 2.4 ± 0.1 | *15.9 ± 0.3* |
| 220925RW-C | 2022/12/13 | 40.2 ± 0.4 | 2.7 ± 0.0 | 2.3 ± 0.1 | 2.4 ± 0.4 |
| *220926RW-B* | 2022/12/13 | *156.8 ± 0.7* | 16.5 ± 0.1 | 5.6 ± 0.1 | 8.7 ± 0.2 |

Sample 0607RW-B was determined to be invalid due to possible human error, highlighted in red. *Italic figures* are calculated outliers and thus were excluded from the calculations for average ion concentrations.



doi:10.6342/NTU202500428

Table A.2 (continued)

| Sample name | Process date | Na (μM) | Mg (μM) | K (μM) | Ca (μM) |
|---|---|---|---|---|---|
| *221005RW-B* | 2022/12/13 | 115.6 ± 1.1 | *33.6 ± 0.3* | 3.5 ± 0.1 | *13.9 ± 0.4* |
| *221006RW-B* | 2022/12/13 | 61.7 ± 0.5 | *25.6 ± 0.2* | 2.2 ± 0.1 | 10.3 ± 0.7 |
| *221011RW-ZW* | 2022/12/13 | *170.7 ± 1.4* | 17.3 ± 0.1 | 8.3 ± 0.1 | 2.7 ± 0.3 |
| 221018RW-B | 2023/5/2 | 39.8 ± 0.5 | 1.9 ± 0.0 | 2.1 ± 0.1 | 1.9 ± 0.3 |
| *221024RW-B* | 2023/5/2 | 54.4 ± 0.1 | *58.7 ± 0.5* | 3.4 ± 0.0 | *129.5 ± 1.8* |
| 221024RW-ND | 2023/5/2 | 35.8 ± 0.3 | 9.0 ± 0.1 | 1.8 ± 0.0 | 5.3 ± 0.3 |
| 221024RW-ZW | 2023/5/2 | 98.5 ± 0.7 | 7.1 ± 0.0 | 7.2 ± 0.0 | 3.6 ± 0.3 |
| *221031RW-B* | 2023/5/2 | *122.9 ± 1.0* | 12.0 ± 0.1 | 3.7 ± 0.0 | 3.5 ± 0.3 |
| 221031RW-C | 2023/5/2 | 21.7 ± 0.2 | 0.5 ± 0.0 | 1.3 ± 0.1 | 1.0 ± 0.2 |
| *221031RW-ZW* | 2023/5/2 | *271.0 ± 4.8* | *31.9 ± 0.2* | *9.2 ± 0.1* | 6.6 ± 0.2 |
| 221101RW-B | 2023/5/2 | 37.0 ± 0.3 | 1.2 ± 0.0 | 1.9 ± 0.1 | 1.8 ± 0.4 |
| 221101RW-C | 2023/5/2 | 50.5 ± 0.3 | 3.4 ± 0.0 | 2.3 ± 0.1 | 2.5 ± 0.3 |
| 221108RW-A | 2023/5/2 | 70.0 ± 0.3 | 7.3 ± 0.1 | 4.8 ± 0.1 | 4.1 ± 0.4 |
| 221118RW-C | 2023/5/2 | 94.7 ± 0.5 | 9.0 ± 0.0 | 3.5 ± 0.1 | 3.1 ± 0.4 |
| 221208-RW-A | 2023/5/2 | 45.7 ± 0.2 | 2.3 ± 0.1 | 2.1 ± 0.0 | 1.5 ± 0.3 |
| 221229RW-C | 2023/5/2 | 36.8 ± 0.4 | 1.2 ± 0.0 | 2.9 ± 0.1 | 2.2 ± 0.1 |
| 230104RW-ZW | 2023/5/2 | 88.8 ± 0.7 | 8.3 ± 0.0 | 3.7 ± 0.0 | 3.5 ± 0.4 |
| 230105RW-B | 2023/5/2 | 39.9 ± 0.5 | 2.6 ± 0.0 | 3.1 ± 0.1 | 4.6 ± 0.0 |
| 230105RW-ND | 2023/5/2 | 37.7 ± 0.4 | 1.8 ± 0.0 | 2.5 ± 0.0 | 1.9 ± 0.2 |
| 230110RW-B | 2023/5/2 | 32.4 ± 0.2 | 0.8 ± 0.0 | 2.7 ± 0.1 | 2.3 ± 0.2 |
| 230110RW-ZW | 2023/5/2 | 50.3 ± 0.2 | 2.9 ± 0.1 | 3.9 ± 0.0 | 5.8 ± 0.2 |

*Italic figures* are calculated outliers and thus were excluded from the calculations for average ion concentrations.



doi:10.6342/NTU202500428

Table A.3 Riverine anion concentrations by campaign.

| Sample site | Sample period | $Cl^-$ (μM) | $SO_4^{2-}$ (uncorrected) (μM) | $SO_4^{2-}$ (corrected) (μM) |
|---|---|---|---|---|
| BY | 22-Feb | 20.8 ± 1.8 | 1270.4 ± 8.1 | 1266.9 ± 8.2 |
| | 22-Jul | 15.2 ± 0.2 | 1408.7 ± 1.6 | 1406.1 ± 1.6 |
| | 22-Sep | 21.6 ± 0.6 | 1444.6 ± 4.7 | 1441.0 ± 4.7 |
| | 23-Apr | 15.7 ± 1.7 | 1534.7 ± 39.1 | 1532.0 ± 39.1 |
| | 23-Jun | 12.4 ± 0.1 | 1374.5 ± 46.1 | 1372.4 ± 46.1 |
| | 23-Sep | 29.8 ± 0.8 | 1192.6 ± 25.7 | 1187.6 ± 25.7 |
| BB | 22-Feb | 36.9 ± 2.1 | 390.0 ± 3.2 | 383.7 ± 3.4 |
| | 22-Jul | 26.4 ± 0.6 | 478.4 ± 1.9 | 473.9 ± 2.0 |
| | 22-Sep | 47.1 ± 1.3 | 467.5 ± 3.0 | 459.5 ± 3.4 |
| | 23-Apr | 29.3 ± 1.4 | 556.0 ± 12.1 | 551.0 ± 12.2 |
| | 23-Jun | 24.9 ± 0.6 | 505.7 ± 9.9 | 501.4 ± 9.9 |
| | 23-Sep | 55.8 ± 8.7 | 404.6 ± 5.6 | 395.2 ± 6.1 |
| SL | 22-Feb | 46.3 ± 3.6 | 108.8 ± 1.1 | 100.9 ± 1.9 |
| | 22-Jul | 31.9 ± 1.3 | 116.7 ± 0.1 | 111.2 ± 1.0 |
| | 22-Sep | 38.9 ± 0.6 | 83.3 ± 0.6 | 76.7 ± 1.3 |
| | 23-Apr | 33.4 ± 3.4 | 113.6 ± 14.9 | 107.9 ± 15.0 |
| | 23-Jun | 32.7 ± 0.4 | 131.5 ± 1.2 | 126.0 ± 1.5 |
| | 23-Sep | 53.9 ± 1.6 | 139.9 ± 2.1 | 130.7 ± 2.7 |
| JL | 22-Feb | - | - | - |
| | 22-Jul | - | - | - |
| | 22-Sep | 52.5 ± 1.3 | 136.1 ± 1.6 | 127.1 ± 2.2 |
| | 23-Apr | 43.6 ± 2.8 | 174.0 ± 8.6 | 166.6 ± 8.7 |
| | 23-Jun | 57.1 ± 1.1 | 166.2 ± 3.6 | 156.4 ± 4.0 |
| | 23-Sep | 64.0 ± 2.1 | 144.7 ± 1.5 | 133.8 ± 2.5 |
| CK | 22-Feb | 71.8 ± 5.3 | 89.9 ± 5.4 | 77.6 ± 5.9 |
| | 22-Jul | 60.7 ± 3.0 | 111.0 ± 0.9 | 100.6 ± 2.1 |
| | 22-Sep | 70.1 ± 2.2 | 105.5 ± 1.2 | 93.6 ± 2.4 |
| | 23-Apr | - | - | - |
| | 23-Jun | 94.7 ± 4.3 | 118.1 ± 5.3 | 102.0 ± 6.1 |
| | 23-Sep | 84.2 ± 1.8 | 89.7 ± 2.1 | 75.4 ± 3.3 |

Concentration results of chloride ($Cl^-$) and sulfate ($SO_4^{2-}$) across 6 campaigns. Dashed lines signify the lack of sample; due to reasons such as river water absence, inaccessibility resulted from typhoons events, and planning.



doi:10.6342/NTU202500428

Table A.3 (continued)

| Sample site | Sample period | $Cl^-$ (μM) | $SO_4^{2-}$ (uncorrected) (μM) | $SO_4^{2-}$ (corrected) (μM) |
|---|---|---|---|---|
| SJ | 22-Feb | 23.6 ± 2.6 | 607.1 ± 7.5 | 603.1 ± 7.5 |
| | 22-Jul | 18.2 ± 2.3 | 653.1 ± 20.4 | 650.0 ± 20.4 |
| | 22-Sep | 24.1 ± 3.2 | 514.2 ± 4.3 | 510.1 ± 4.4 |
| | 23-Apr | 18.6 ± 1.9 | 696.7 ± 11.6 | 693.6 ± 11.6 |
| | 23-Jun | 14.5 ± 0.4 | 572.1 ± 6.6 | 569.6 ± 6.6 |
| | 23-Sep | 30.4 ± 0.6 | 499.8 ± 12.0 | 494.6 ± 12.0 |
| TG | 22-Feb | 38.6 ± 2.2 | 789.9 ± 2.8 | 783.4 ± 3.1 |
| | 22-Jul | 13.5 ± 1.4 | 702.6 ± 12.9 | 700.3 ± 12.9 |
| | 22-Sep | 28.6 ± 1.1 | 817.8 ± 4.2 | 813.0 ± 4.3 |
| | 23-Apr | 22.9 ± 1.7 | 885.7 ± 25.1 | 881.8 ± 25.1 |
| | 23-Jun | 16.6 ± 0.5 | 824.9 ± 18.3 | 822.1 ± 18.3 |
| | 23-Sep | 37.4 ± 0.7 | 683.2 ± 17.7 | 676.9 ± 17.8 |
| ML | 22-Feb | 43.6 ± 5.5 | 594.8 ± 3.5 | 587.4 ± 3.8 |
| | 22-Jul | 24.4 ± 2.5 | 545.8 ± 16.0 | 541.7 ± 16.0 |
| | 22-Sep | - | - | - |
| | 23-Apr | 26.2 ± 2.0 | 776.3 ± 67.9 | 771.9 ± 67.9 |
| | 23-Jun | 26.4 ± 0.8 | 681.4 ± 19.8 | 676.9 ± 19.8 |
| | 23-Sep | 46.0 ± 1.1 | 525.7 ± 5.6 | 517.8 ± 5.7 |
| DG | 22-Feb | 74.2 ± 3.8 | 281.0 ± 1.6 | 268.4 ± 2.8 |
| | 22-Jul | - | - | - |
| | 22-Sep | 83.9 ± 2.6 | 352.9 ± 0.2 | 338.6 ± 2.6 |
| | 23-Apr | - | - | - |
| | 23-Jun | - | - | - |
| | 23-Sep | 91.5 ± 4.6 | 377.6 ± 3.8 | 362.0 ± 4.8 |
| XL | 22-Feb | 87.8 ± 2.2 | 70.0 ± 2.5 | 55.0 ± 3.6 |
| | 22-Jul | 76.0 ± 2.1 | 94.1 ± 2.7 | 81.2 ± 3.6 |
| | 22-Sep | 90.8 ± 2.3 | 65.5 ± 0.3 | 50.0 ± 2.8 |
| | 23-Apr | 80.9 ± 7.6 | 97.6 ± 3.4 | 83.9 ± 4.4 |
| | 23-Jun | 74.4 ± 1.8 | 98.1 ± 0.8 | 85.4 ± 2.4 |
| | 23-Sep | 97.8 ± 1.4 | 90.2 ± 4.5 | 73.5 ± 5.4 |
| WRK | 22-Feb | 103.6 ± 4.1 | 76.0 ± 1.4 | 58.4 ± 3.5 |
| | 22-Jul | 104.2 ± 4.7 | 115.7 ± 3.5 | 98.0 ± 4.8 |
| | 22-Sep | 100.5 ± 3.8 | 80.9 ± 0.3 | 63.8 ± 3.1 |
| | 23-Apr | 94.1 ± 3.7 | 105.9 ± 2.4 | 89.9 ± 3.8 |
| | 23-Jun | 91.3 ± 1.7 | 108.8 ± 0.8 | 93.3 ± 2.9 |
| | 23-Sep | 128.3 ± 3.2 | 110.7 ± 5.6 | 88.9 ± 6.9 |



doi:10.6342/NTU202500428

Table A.4 Riverine cation concentrations by campaign. (uncorrected).

| Sample site | Sample period | Na (μM) | Mg (μM) | K (μM) | Ca (μM) |
|---|---|---|---|---|---|
| BY | 22-Feb | 153.1 ± 1.6 | 851.0 ± 9.1 | 45.5 ± 0.4 | 539.4 ± 2.5 |
| | 22-Jul | 158.0 ± 0.4 | 824.6 ± 0.7 | 57.2 ± 1.3 | 567.2 ± 2.2 |
| | 22-Sep | 172.3 ± 1.7 | 886.5 ± 14.8 | 46.6 ± 0.4 | 567.5 ± 5.7 |
| | 23-Apr | 207.9 ± 0.7 | 965.1 ± 2.5 | 54.4 ± 1.0 | 625.7 ± 9.3 |
| | 23-Jun | 167.4 ± 2.3 | 864.6 ± 5.5 | 44.6 ± 0.9 | 391.6 ± 2.6 |
| | 23-Sep | 110.4 ± 3.6 | 764.4 ± 6.4 | 38.4 ± 1.0 | 499.6 ± 5.8 |
| BB | 22-Feb | 124.2 ± 1.4 | 256.1 ± 3.1 | 13.2 ± 0.1 | 228.3 ± 5.7 |
| | 22-Jul | 122.6 ± 1.5 | 273.6 ± 2.7 | 17.0 ± 0.2 | 263.0 ± 7.7 |
| | 22-Sep | 830.5 ± 6.0 | 259.8 ± 2.0 | 50.5 ± 0.5 | 251.2 ± 3.2 |
| | 23-Apr | 194.6 ± 0.7 | 311.6 ± 0.5 | 20.4 ± 0.1 | 283.0 ± 3.2 |
| | 23-Jun | 150.2 ± 0.7 | 290.7 ± 2.8 | 14.1 ± 0.3 | 182.2 ± 2.8 |
| | 23-Sep | 147.5 ± 1.2 | 236.9 ± 2.3 | 12.9 ± 0.6 | 219.5 ± 5.8 |
| SL | 22-Feb | 83.1 ± 0.1 | 89.5 ± 0.5 | 10.2 ± 0.2 | 73.3 ± 0.9 |
| | 22-Jul | 98.4 ± 0.2 | 108.2 ± 1.1 | 13.4 ± 0.3 | 88.2 ± 2.0 |
| | 22-Sep | 79.1 ± 0.7 | 69.9 ± 0.9 | 11.1 ± 0.2 | 58.6 ± 1.1 |
| | 23-Apr | 104.5 ± 0.6 | 112.8 ± 0.6 | 12.3 ± 0.1 | 92.4 ± 2.5 |
| | 23-Jun | 110.1 ± 0.4 | 110.8 ± 0.7 | 10.0 ± 0.4 | 65.6 ± 1.9 |
| | 23-Sep | 77.4 ± 1.1 | 96.9 ± 0.8 | 7.5 ± 0.4 | 85.5 ± 1.2 |

Dashed lines signify the lack of sample; due to reasons such as river water absence, inaccessibility resulted from typhoons events, and planning.



doi:10.6342/NTU202500428

Table A.4 (continued)

| Sample site | Sample period | Na (μM) | Mg (μM) | K (μM) | Ca (μM) |
|---|---|---|---|---|---|
| JL | 22-Feb | - | - | - | - |
| | 22-Jul | - | - | - | - |
| | 22-Sep | 121.9 ± 0.6 | 131.1 ± 1.1 | 13.3 ± 0.2 | 127.4 ± 5.4 |
| | 23-Apr | 146.9 ± 1.5 | 179.1 ± 0.6 | 12.4 ± 0.1 | 174.4 ± 6.0 |
| | 23-Jun | 133.3 ± 2.4 | 161.6 ± 2.0 | 9.9 ± 0.3 | 108.3 ± 1.9 |
| | 23-Sep | 97.5 ± 1.4 | 131.9 ± 1.1 | 7.9 ± 0.2 | 124.8 ± 1.8 |
| CK | 22-Feb | 146.7 ± 1.2 | 99.2 ± 1.8 | 8.9 ± 0.2 | 115.2 ± 1.3 |
| | 22-Jul | 164.8 ± 0.7 | 129.5 ± 0.6 | 11.2 ± 0.2 | 148.5 ± 3.8 |
| | 22-Sep | 173.3 ± 2.3 | 113.4 ± 1.5 | 10.7 ± 0.2 | 130.0 ± 1.7 |
| | 23-Apr | - | - | - | - |
| | 23-Jun | 188.5 ± 3.2 | 109.1 ± 0.3 | 7.9 ± 0.3 | 98.0 ± 1.0 |
| | 23-Sep | 121.6 ± 0.2 | 84.5 ± 0.9 | 6.7 ± 0.2 | 98.1 ± 2.4 |



doi:10.6342/NTU202500428

Table A.4 (continued)

| Sample site | Sample period | Na (μM) | Mg (μM) | K (μM) | Ca (μM) |
|---|---|---|---|---|---|
| SJ | 22-Feb | 525.0 ± 4.3 | 935.9 ± 1.9 | 22.9 ± 0.3 | 458.6 ± 3.0 |
| | 22-Jul | 669.3 ± 4.8 | 869.8 ± 10.7 | 30.9 ± 0.8 | 473.1 ± 4.3 |
| | 22-Sep | 448.1 ± 4.9 | 809.2 ± 9.7 | 22.1 ± 0.6 | 419.2 ± 3.8 |
| | 23-Apr | 995.5 ± 10.7 | 958.6 ± 17.9 | 26.4 ± 0.2 | 490.1 ± 4.6 |
| | 23-Jun | 517.8 ± 3.0 | 892.8 ± 3.3 | 23.1 ± 0.2 | 308.6 ± 4.2 |
| | 23-Sep | 255.6 ± 2.6 | 768.7 ± 7.4 | 18.2 ± 0.4 | 395.7 ± 10.1 |
| TG | 22-Feb | 605.6 ± 8.6 | 1039.7 ± 13.3 | 30.2 ± 0.1 | 693.1 ± 9.4 |
| | 22-Jul | 167.1 ± 1.3 | 595.4 ± 3.0 | 67.8 ± 0.2 | 467.6 ± 6.3 |
| | 22-Sep | 574.4 ± 2.8 | 1015.6 ± 8.6 | 36.5 ± 0.4 | 668.7 ± 7.2 |
| | 23-Apr | 785.2 ± 6.1 | 1057.9 ± 7.4 | 33.9 ± 0.4 | 742.5 ± 1.5 |
| | 23-Jun | 289.1 ± 1.1 | 1000.8 ± 11.5 | 23.1 ± 0.3 | 436.7 ± 9.6 |
| | 23-Sep | 524.1 ± 2.9 | 926.1 ± 3.8 | 38.3 ± 0.8 | 616.6 ± 7.7 |
| ML | 22-Feb | 195.1 ± 1.9 | 746.9 ± 6.3 | 18.5 ± 0.3 | 473.9 ± 3.3 |
| | 22-Jul | 156.0 ± 1.0 | 588.3 ± 10.0 | 21.1 ± 0.5 | 411.5 ± 6.9 |
| | 22-Sep | - | - | - | - |
| | 23-Apr | 256.5 ± 1.1 | 814.0 ± 6.2 | 22.0 ± 0.5 | 548.4 ± 4.5 |
| | 23-Jun | 218.9 ± 4.2 | 761.0 ± 8.1 | 20.2 ± 0.4 | 340.6 ± 2.0 |
| | 23-Sep | 159.9 ± 3.0 | 662.4 ± 7.4 | 17.5 ± 0.4 | 429.5 ± 2.7 |



doi:10.6342/NTU202500428

Table A.4 (continued)

| Sample site | Sample period | Na (μM) | Mg (μM) | K (μM) | Ca (μM) |
|---|---|---|---|---|---|
| DG | 22-Feb | 142.8 ± 0.9 | 222.9 ± 1.0 | 7.9 ± 0.0 | 309.8 ± 1.1 |
| | 22-Jul | - | - | - | - |
| | 22-Sep | 166.3 ± 2.6 | 250.7 ± 0.8 | 14.4 ± 0.1 | 360.5 ± 4.9 |
| | 23-Apr | - | - | - | - |
| | 23-Jun | - | - | - | - |
| | 23-Sep | 137.1 ± 1.5 | 227.5 ± 1.0 | 8.2 ± 0.3 | 361.5 ± 13.5 |
| XL | 22-Feb | 157.3 ± 1.3 | 68.0 ± 0.9 | 4.3 ± 0.2 | 65.7 ± 0.6 |
| | 22-Jul | 179.3 ± 1.4 | 102.4 ± 0.6 | 5.9 ± 0.2 | 98.8 ± 0.0 |
| | 22-Sep | 168.3 ± 1.7 | 60.2 ± 0.2 | 7.0 ± 0.1 | 58.9 ± 2.3 |
| | 23-Apr | 190.3 ± 1.1 | 93.1 ± 0.5 | 6.4 ± 0.1 | 96.9 ± 3.7 |
| | 23-Jun | 185.9 ± 0.7 | 92.3 ± 0.7 | 3.5 ± 0.3 | 63.1 ± 0.6 |
| | 23-Sep | 148.4 ± 1.6 | 74.2 ± 0.7 | 1.5 ± 0.0 | 69.0 ± 1.3 |
| WRK | 22-Feb | 146.7 ± 1.4 | 36.3 ± 0.3 | 15.4 ± 0.2 | 251.8 ± 3.0 |
| | 22-Jul | 190.0 ± 2.3 | 60.2 ± 0.7 | 24.1 ± 0.1 | 435.1 ± 2.6 |
| | 22-Sep | 146.0 ± 1.4 | 38.9 ± 0.3 | 25.7 ± 0.5 | 290.0 ± 1.8 |
| | 23-Apr | 201.9 ± 1.4 | 52.1 ± 0.5 | 25.6 ± 0.3 | 439.9 ± 5.1 |
| | 23-Jun | 175.7 ± 3.1 | 49.2 ± 0.7 | 21.3 ± 0.1 | 258.2 ± 2.2 |
| | 23-Sep | 147.1 ± 0.8 | 44.3 ± 1.0 | 23.9 ± 0.3 | 320.4 ± 8.4 |



doi:10.6342/NTU202500428

Table A.5 Riverine cation concentrations by campaign (corrected).

| Sample site | Sample period | Na (μM) | Mg (μM) | K (μM) | Ca (μM) |
|---|---|---|---|---|---|
| BY | 22-Feb | 129.8 ± 4.9 | 848.0 ± 9.1 | 42.8 ± 0.7 | 536.5 ± 2.6 |
| | 22-Jul | 140.9 ± 3.1 | 822.3 ± 0.9 | 55.2 ± 1.4 | 565.0 ± 2.3 |
| | 22-Sep | 148.1 ± 4.8 | 883.3 ± 14.8 | 43.7 ± 0.7 | 564.5 ± 5.8 |
| | 23-Apr | 190.3 ± 3.5 | 962.8 ± 2.5 | 52.3 ± 1.1 | 623.5 ± 9.3 |
| | 23-Jun | 153.5 ± 3.4 | 862.8 ± 5.6 | 43.0 ± 0.9 | 389.8 ± 2.7 |
| | 23-Sep | 77.0 ± 7.1 | 760.0 ± 6.4 | 34.4 ± 1.2 | 495.4 ± 5.9 |
| BB | 22-Feb | 82.7 ± 8.0 | 250.6 ± 3.3 | 8.3 ± 0.9 | 223.2 ± 5.7 |
| | 22-Jul | 92.9 ± 5.6 | 269.7 ± 2.9 | 13.5 ± 0.7 | 259.3 ± 7.8 |
| | 22-Sep | 777.6 ± 11.4 | 252.8 ± 2.5 | 44.3 ± 1.2 | 244.7 ± 3.4 |
| | 23-Apr | 161.7 ± 6.2 | 307.3 ± 1.1 | 16.5 ± 0.7 | 278.9 ± 3.3 |
| | 23-Jun | 122.2 ± 5.2 | 287.0 ± 2.9 | 10.8 ± 0.7 | 178.8 ± 2.9 |
| | 23-Sep | 84.8 ± 15.0 | 228.7 ± 3.2 | 5.5 ± 1.9 | 211.8 ± 6.1 |
| SL | 22-Feb | 31.1 ± 10.2 | 82.6 ± 1.7 | 4.1 ± 1.2 | 66.8 ± 1.6 |
| | 22-Jul | 62.6 ± 6.6 | 103.4 ± 1.5 | 9.2 ± 0.8 | 83.8 ± 2.2 |
| | 22-Sep | 35.5 ± 8.0 | 64.2 ± 1.5 | 6.0 ± 0.9 | 53.1 ± 1.5 |
| | 23-Apr | 66.9 ± 7.8 | 107.8 ± 1.3 | 7.9 ± 0.9 | 87.8 ± 2.7 |
| | 23-Jun | 73.4 ± 6.7 | 106.0 ± 1.3 | 5.7 ± 0.9 | 61.0 ± 2.1 |
| | 23-Sep | 16.9 ± 11.2 | 88.9 ± 1.9 | 0.4 ± 1.3 | 78.0 ± 1.9 |

Results have been corrected with atmospheric input. Dashed lines signify the lack of sample; due to reasons such as river water absence, inaccessibility resulted from typhoons events, and planning.



doi:10.6342/NTU202500428

Table A.5 (continued).

| Sample site | Sample period | Na (μM) | Mg (μM) | K (μM) | Ca (μM) |
|---|---|---|---|---|---|
| JL | 22-Feb | - | - | - | - |
| | 22-Jul | - | - | - | - |
| | 22-Sep | 63.0 ± 10.9 | 123.4 ± 2.0 | 6.4 ± 1.3 | 120.1 ± 5.6 |
| | 23-Apr | 97.9 ± 9.5 | 172.7 ± 1.6 | 6.7 ± 1.1 | 168.4 ± 6.2 |
| | 23-Jun | 69.2 ± 11.9 | 153.1 ± 2.7 | 2.4 ± 1.4 | 100.4 ± 2.5 |
| | 23-Sep | 25.6 ± 13.3 | 122.3 ± 2.4 | 0.0 | 115.9 ± 2.5 |
| CK | 22-Feb | 66.1 ± 15.8 | 88.6 ± 3.0 | 0.0 | 105.2 ± 2.4 |
| | 22-Jul | 96.6 ± 12.8 | 120.5 ± 2.1 | 3.2 ± 1.5 | 140.1 ± 4.2 |
| | 22-Sep | 94.6 ± 14.6 | 103.0 ± 2.7 | 1.5 ± 1.7 | 120.3 ± 2.5 |
| | 23-Apr | - | - | - | - |
| | 23-Jun | 82.1 ± 20.1 | 95.0 ± 3.1 | 0.0 | 84.9 ± 2.8 |
| | 23-Sep | 27.0 ± 17.2 | 72.0 ± 2.8 | 0.0 | 86.3 ± 3.3 |



doi:10.6342/NTU202500428

Table A.5 (continued).

| Sample site | Sample period | Na (μM) | Mg (μM) | K (μM) | Ca (μM) |
|---|---|---|---|---|---|
| SJ | 22-Feb | 498.5 ± 7.1 | 932.4 ± 2.1 | 19.8 ± 0.7 | 455.4 ± 3.1 |
| | 22-Jul | 648.9 ± 6.6 | 867.1 ± 10.7 | 28.5 ± 0.9 | 470.6 ± 4.4 |
| | 22-Sep | 421.1 ± 7.8 | 805.7 ± 9.8 | 18.9 ± 1.0 | 415.8 ± 3.9 |
| | 23-Apr | 974.7 ± 11.6 | 955.9 ± 17.9 | 24.0 ± 0.6 | 487.5 ± 4.6 |
| | 23-Jun | 501.5 ± 4.2 | 890.7 ± 3.4 | 21.2 ± 0.4 | 306.5 ± 4.2 |
| | 23-Sep | 221.4 ± 6.7 | 764.2 ± 7.5 | 14.2 ± 0.8 | 391.4 ± 10.2 |
| TG | 22-Feb | 562.3 ± 11.9 | 1033.9 ± 13.4 | 25.1 ± 1.0 | 687.8 ± 9.4 |
| | 22-Jul | 151.9 ± 3.4 | 593.4 ± 3.0 | 66.1 ± 0.4 | 465.8 ± 6.3 |
| | 22-Sep | 542.3 ± 6.6 | 1011.3 ± 8.6 | 32.7 ± 0.8 | 664.7 ± 7.3 |
| | 23-Apr | 759.5 ± 7.9 | 1054.5 ± 7.4 | 30.8 ± 0.7 | 739.3 ± 1.7 |
| | 23-Jun | 270.4 ± 3.6 | 998.3 ± 11.5 | 20.9 ± 0.5 | 434.4 ± 9.6 |
| | 23-Sep | 482.1 ± 8.2 | 920.6 ± 4.0 | 33.3 ± 1.2 | 611.4 ± 7.8 |
| ML | 22-Feb | 146.2 ± 11.0 | 740.4 ± 6.5 | 12.7 ± 1.3 | 467.9 ± 3.6 |
| | 22-Jul | 128.6 ± 5.8 | 584.6 ± 10.1 | 17.9 ± 0.8 | 408.1 ± 7.0 |
| | 22-Sep | - | - | - | - |
| | 23-Apr | 227.1 ± 5.9 | 810.1 ± 6.2 | 18.5 ± 0.9 | 544.7 ± 4.6 |
| | 23-Jun | 189.3 ± 6.9 | 757.0 ± 8.1 | 16.7 ± 0.7 | 337.0 ± 2.1 |
| | 23-Sep | 108.2 ± 9.9 | 655.6 ± 7.6 | 11.4 ± 1.2 | 423.1 ± 3.0 |



doi:10.6342/NTU202500428

Table A.5 (continued).

| Sample site | Sample period | Na (μM) | Mg (μM) | K (μM) | Ca (μM) |
|---|---|---|---|---|---|
| DG | 22-Feb | 59.5 ± 15.7 | 211.9 ± 2.6 | 0.0 | 299.5 ± 2.3 |
| | 22-Jul | - | - | - | - |
| | 22-Sep | 72.0 ± 17.5 | 238.2 ± 2.8 | 3.4 ± 2.0 | 348.8 ± 5.4 |
| | 23-Apr | - | - | - | - |
| | 23-Jun | - | - | - | - |
| | 23-Sep | 34.3 ± 19.4 | 213.9 ± 3.2 | 0.0 | 348.8 ± 13.8 |
| XL | 22-Feb | 58.7 ± 18.1 | 55.0 ± 3.0 | 0.0 | 53.5 ± 2.4 |
| | 22-Jul | 94.0 ± 15.7 | 91.1 ± 2.5 | 0.0 | 88.2 ± 2.0 |
| | 22-Sep | 66.3 ± 18.7 | 46.7 ± 2.9 | 0.0 | 46.3 ± 3.4 |
| | 23-Apr | 99.4 ± 18.6 | 81.1 ± 2.9 | 0.0 | 85.7 ± 4.4 |
| | 23-Jun | 102.3 ± 15.3 | 81.3 ± 2.5 | 0.0 | 52.7 ± 2.1 |
| | 23-Sep | 38.6 ± 20.0 | 59.7 ± 3.2 | 0.0 | 55.3 ± 2.9 |
| WRK | 22-Feb | 30.3 ± 21.6 | 20.9 ± 3.4 | 1.8 ± 2.5 | 237.3 ± 4.1 |
| | 22-Jul | 77.4 ± 21.2 | 45.3 ± 3.4 | 10.9 ± 2.4 | 421.2 ± 3.8 |
| | 22-Sep | 33.1 ± 20.9 | 24.0 ± 3.3 | 12.5 ± 2.5 | 276.0 ± 3.3 |
| | 23-Apr | 96.2 ± 19.6 | 38.1 ± 3.1 | 13.2 ± 2.3 | 426.8 ± 5.7 |
| | 23-Jun | 73.1 ± 18.9 | 35.6 ± 3.0 | 9.3 ± 2.2 | 245.4 ± 3.3 |
| | 23-Sep | 3.0 ± 26.3 | 25.2 ± 4.3 | 7.0 ± 3.1 | 302.6 ± 9.0 |



doi:10.6342/NTU202500428

Table. A.6 Hot spring anion concentrations by campaign.

| Sample site | Sample period | $Cl^-$ (μM) | | $SO_4^{2-}$ (μM) (uncorrected) | | $SO_4^{2-}$ (μM) (corrected) | |
|---|---|---|---|---|---|---|---|
| BB - HS | 22-Feb | - | | - | | - | |
| | 22-Jul | 125.4 | ± 14.1 | 607.3 | ± 5.6 | 586.0 | ± 7.2 |
| | 22-Sep | 184.9 | ± 12.3 | 497.4 | ± 5.4 | 465.9 | ± 8.1 |
| | 23-Apr | 110.8 | ± 6.6 | 645.3 | ± 25.3 | 626.5 | ± 25.5 |
| | 23-Jun | 99.9 | ± 2.9 | 718.9 | ± 4.9 | 701.9 | ± 5.8 |
| | 23-Sep | - | | - | | - | |
| TG - HS | 22-Feb | - | | - | | - | |
| | 22-Jul | 134.6 | ± 14.9 | 908.0 | ± 20.5 | 885.1 | ± 21.0 |
| | 22-Sep | 161.9 | ± 3.6 | 889.3 | ± 11.8 | 861.8 | ± 12.8 |
| | 23-Apr | 98.4 | ± 28.4 | 1084.5 | ± 46.4 | 1067.7 | ± 46.8 |
| | 23-Jun | 66.9 | ± 2.7 | 979.8 | ± 3.4 | 968.4 | ± 3.9 |
| | 23-Sep | - | | - | | - | |



doi:10.6342/NTU202500428

Table. A.7 Hot spring cation concentrations by campaign.

| Sample site | Sample period | Na (μM) | Mg (μM) | K (μM) | Ca (μM) |
|---|---|---|---|---|---|
| BB-HS | 22-Feb | - | - | - | - |
| | 22-Jul | 6342.4 ± 89.4 | 547.4 ± 2.5 | 387.6 ± 9.1 | 480.2 ± 25.7 |
| | 22-Sep | 864.1 ± 15.3 | 267.3 ± 1.5 | 60.8 ± 2.6 | 247.1 ± 20.1 |
| | 23-Apr | 5492.2 ± 80.8 | 433.4 ± 7.7 | 284.9 ± 3.3 | 475.0 ± 15.5 |
| | 23-Jun | 4759.5 ± 12.4 | 442.9 ± 6.6 | 201.1 ± 4.8 | 305.3 ± 12.1 |
| | 23-Sep | - | - | - | - |
| TG-HS | 22-Feb | - | - | - | - |
| | 22-Jul | 6101.7 ± 17.6 | 1232.1 ± 0.7 | 96.5 ± 0.8 | 852.3 ± 51.1 |
| | 22-Sep | 1826.1 ± 17.2 | 1132.3 ± 6.7 | 63.7 ± 2.0 | 842.4 ± 9.4 |
| | 23-Apr | 1473.3 ± 21.6 | 1426.2 ± 9.9 | 56.0 ± 0.9 | 1238.3 ± 20.4 |
| | 23-Jun | 446.5 ± 0.6 | 1151.1 ± 2.7 | 3.8 ± 4.9 | 569.8 ± 25.7 |
| | 23-Sep | - | - | - | - |



doi:10.6342/NTU202500428